Electrochemical Capacitors with Confined Redox Electrolytes and Porous Electrodes

Nianjun Yang, Siyu Yu, Wenjun Zhang, Hui-ming Cheng, Patrice Simon, Xin Jiang

ADVANCED MATERIALS
www.advmat.de

Electrochemical Capacitors with Confined Redox Electrolytes and Porous Electrodes

Nianjun Yang, Siyu Yu,* Wenjun Zhang, Hui-Ming Cheng, Patrice Simon, and Xin Jiang**

Electrochemical capacitors (ECs), including electrical-double-layer capacitors and pseudocapacitors, feature high power densities but low energy densities. To improve the energy densities of ECs, redox electrolyte-enhanced ECs (R-ECs) or supercapbatteries are designed through employing confined soluble redox electrolytes and porous electrodes. In R-ECs the energy storage is based on diffusion-controlled faradaic processes of confined redox electrolytes at the surface of a porous electrode, which thus take the merits of high power densities of ECs and high energy densities of batteries. In the past few years, there has been great progress in the development of this energy storage technology, particularly in the design and synthesis of novel redox electrolytes and porous electrodes, as well as the configurations of new devices. Herein, a full-screen picture of the fundamentals and the state-of-art progress of R-ECs are given together with a discussion and outlines about the challenges and future perspectives of R-ECs. The strategies to improve the performance of R-ECs are highlighted from the aspects of their capacitances and capacitance retention, power densities, and energy densities. The insight into the philosophies behind these strategies will be favorable to promote the R-EC technology toward practical applications of supercapacitors in different fields.

1. Introduction

Electrochemical energy storage systems (EESSs) are becoming one of the leading energy storage technologies and have attained growing interests in recent years.[1] The investigated electrochemical EESSs mainly cover batteries and supercapacitors (SCs), which have been applied in various areas, including hybrid electric vehicles, portable and multifunctional electronics, microgrid, as well as industrial equipment.

Electrochemical capacitor (EC) or SC can be generally divided into two categories: electrical double layer capacitor (EDLC) and psuedocapacitors (PCs), based on the involvement of non faradaic and faradaic charge storage processes, respectively.[2] An EDLC stores charges electrostatically via charge adsorption/accumulation (non faradaic reactions) at an electrode/electrolyte interface, allowing fast charging/discharging rates. By contrast, a

N. Yang, X. Jiang
Institute of Materials Engineering
University of Siegen
Siegen 57076, Germany
E mail: nianjun.yang@uni siegen.de; xin.jiang@uni siegen.de

S. Yu
School of Chemistry and Chemical Engineering
Southwest University
Chongqing 400715, China
E-mail: yusiyu@swu.edu.cn

W. Zhang
Center of Super-Diamond and Advanced Films
Department of Materials Science and Engineering
City University of Hong Kong
Tat Chee Avenue, Kowloon, Hong Kong, China

The ORCID identification number(s) for the author(s) of this article can be found under https://doi.org/10.1002/adma.202202380.

DOI: 10.1002/adma.202202380

W. Zhang
City University of Hong Kong Shenzhen Research Institute
Shenzhen 518057, China

H. M. Cheng
Shenyang National Laboratory for Materials Science
Institute of Metal Research
Chinese Academy of Sciences
Shenyang 110016, China

H. M. Cheng
Faculty of Materials Science and Engineering/Institute of Technology for Carbon Neutrality
Shenzhen Institute of Advanced Technology
Chinese Academy of Sciences
Shenzhen 518055, China

H.-M. Cheng
Advanced Technology Institute
University of Surrey
Guildford, Surrey GU2 7XH, UK

P. Simon
CIRIMAT, UMR CNRS 5085
Université Toulouse III Paul Sabatier
Toulouse 31062, France

X. Jiang
Institute of Oceanographic Instrumentation
Qilu University of Technology (Shandong Academy of Science)
Qingdao 266001, China

PC is based on surface controlled faradaic reactions of redox active materials occurring at the electrode/electrolyte interface. The additional charge transfer brought from these redox reactions results in pseudocapacitances. Therefore, PCs can generally provide higher capacitances and higher energy densities than EDLCs. Compared to rechargeable batteries, both EDLCs and PCs feature much higher power densities (up to 10 kW kg^{-1}), faster charging/discharging rates (a few seconds), and long cycle life expectancy (up to 1 000 000 charging/discharging cycles).[3] However, the major bottleneck of SCs is their relatively low energy densities (less than 10 Wh kg^{-1} for SCs vs. up to 200 Wh kg^{-1} for batteries).[4] Other shortcomings of SCs cover their linear changing/discharging voltages, high self-discharge rates, and high energy storage costs per kilowatt hour. All these shortcomings hinder practical applications of SCs in diverse fields.

Nowadays, extensive efforts have been thus devoted to combining the advantages of SCs and batteries, namely to achieve electrochemical EESSs that feature energy densities of batteries and meanwhile maintain power densities and excellent cycling stability of ECs. Recently appeared redox electrolyte enhanced EC (R EC) is such a kind of electrochemical EESSs.[5] In contrast to EDLCs and PCs that use inert electrolytes, R ECs employ soluble redox electrolytes. To construct this new type of ECs, porous electrodes are generally utilized, enabling diffusion controlled faradaic reactions of redox electrolytes confined inside the electrodes. The enlarged surface areas of these porous electrodes also result in bigger double layer capacitances. Note that the energy storage mechanism of R ECs is different from that of conventional PCs. For PCs, the surface controlled faradaic reactions occur at the interface between redox active species coated electrodes and inert electrolytes. For R ECs, the energy storage is based on diffusion controlled faradaic processes of soluble redox electrolytes at the electrode surface, especially those confined inside the porous electrodes. In these regards, high capacitances with increased charge/discharge rates are achieved by R ECs. The energy storage mechanism of R ECs is also different from that of batteries. For batteries, the slow solid state diffusion processes occur within the bulk electrode materials, resulting in much longer charging/discharging times than SCs and thus limited power capability.[6] Consequently, R ECs exhibit intermediate electrochemical behavior between SCs and batteries. Moreover, the composition and amounts/concentrations of added soluble redox electrolytes are ready to be changed as required. With the utilization of confined redox electrolytes or entrapped redox electrolytes inside the pores of electrodes, the shortcomings of PCs can be avoided, where surface controlled redox reactions determine the PC performance. For example, the production and immobilization of some pseudocapacitive materials on the PC electrodes need complicated synthesis processes. These pseudocapacitive materials exhibit low conductivities, poor stability, and low performance/price ratios.[7] Therefore, R ECs are possible to fully use the advantages of capacitor electrodes as well as fast and stable charge/electron transfer during charging/discharging processes of soluble redox electrolytes. To further improve the performance of R-ECs, there exist different strategies such as introduction of extra reactive sites, rational design of electrode configuration to enhance the surface areas of capacitor electrodes, and an increase of ionic conductivity of the electrolytes. Eventually, the R EC is expected to feature energy densities at the battery level as well as power densities and cycling stability at the SC level. Nevertheless, R ECs might have short charge storage lives, stemming from their increased self-discharge rates that are caused by the diffusion of added soluble redox species.

Compared to the well developed EDLCs[8] and PCs,[9] the research on R ECs was only initialized at the beginning of this century (**Figure 1**). The first R EC was reported in 2005. It was constructed using activated carbon fiber/cloth as the electrodes and $AgNO_3$ dissolved in an aqueous H_2SO_4 solution as the redox electrolyte. The redox reaction of the Ag^+/Ag couple led to an increase of about 300% times of the achieved capacitance, compared to that of the EDLC using the same electrodes in H_2SO_4 solution.[10] In 2009 the combination of a pseudocapacitive electrode of a metal derived compound of Co–Al layered double hydroxide with redox electrolyte of $Fe(CN)_6^{3-/4-}$ in aqueous KOH solution was reported to form an R EC.[11] In 2010 and 2011, redox active ionic liquid (IL) of Cu(II) containing

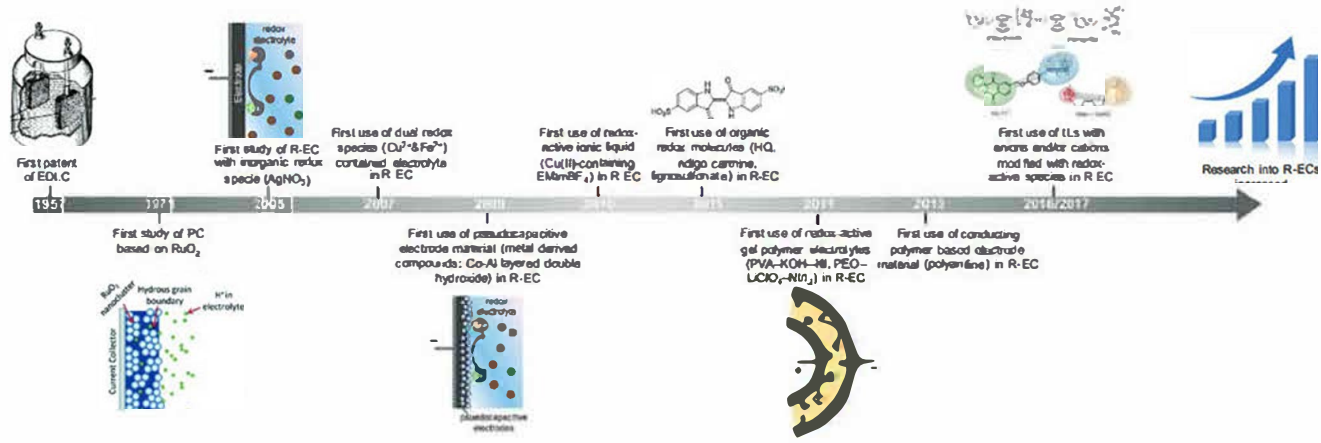

Figure 1. Timeline of major developments in the field of R ECs. Illustration of the first patented EDLC: Reproduced with permission.[8] Copyright 1957, General Electric Co. Schematic of the first reported PC: Reproduced with permission.[9] Copyright 2014, Royal Society of Chemistry. Illustrations of modified ILs: Top: Reproduced with permission.[18a] Copyright 2016, Elsevier B.V.; Bottom: Reproduced with permission.[18b] Copyright 2017, Springer Nature.

ionic liquid (namely, 1 ethyl 3 methylmidazolium tetrafluorobo rate ($EMImBF_4$)[12]) and several organic redox molecules (e.g., hydroquinone,[5a] indigo carmine,[13] and lignosulfonate[14]) were employed for the R EC fabrication, respectively. In 2011, redox electrolytes in the form of quasi solid gels such as poly(vinyl alcohol) (PVA) KOH KI[15] and poly(ethylene oxide) (PEO)/ $LiClO_4/NI/I_2$[16] redox-active gel polymer electrolytes (GPEs) were employed to assemble flexible R ECs. In 2013, a pseudoca pacitive electrode of conducting polyaniline was utilized for the R EC fabrication.[17] The performance of these R ECs was found to be superior to that of EDLCs and PCs. In 2016 and 2017, redox active ILs have been developed by modifying the cations and/or anions with redox active species and used for the forma tion of R ECs.[18] Triggered by these activities, redox electrolytes have been designed and synthesized in different forms to con struct R ECs together with newly developed capacitor electrode materials. The practical applications of these performance-improved R-ECs were then expanded in diverse fields.

This review article starts from the fundamentals of R ECs, namely, their working mechanism and performance evaluation, followed by their state of the art achievements, where reported redox electrolytes and used electrodes are summarized. The performance of these R ECs is then detailed in terms of their capacitances, capacitance retention, power densities, and energy densities. In the subsequent section, future perspectives of R ECs are discussed and outlined with respect to design and synthesis of capacitor electrodes and redox electrolytes, perfor mance evaluation of R ECs, formation of novel R-EC devices, and their potential applications.

2. Fundamentals of R-ECs

2.1. Working Mechanism of R-ECs

An R EC is constructed using porous capacitor electrodes and soluble redox-active electrolytes. It combines two kinds of charge storage mechanisms (Figure 2): the formation of an electric double layer with dissolved ions at the electrolyte/elec trode interface and the occurrence of a faradaic redox reaction on a high surface area (or a porous) electrode.[19] The former stores the charges in the same way as an EDLC, the latter is supposed to contribute the majority of the total charge storage capacity of an R EC. To distinguish two capacitances, the one derived from the faradaic reactions(s) of redox species dissolved in the electrolyte is described as redox electrolyte induced capacitance (R capacitance) in this review. During the charging process of an R EC (Figure 2A), the oxidation reaction of a redox active catholyte and the reduction reaction of a redox active anolyte occur at the positive and negative electrodes, respectively. During the discharging process, the reverse reac tions occur on both electrodes (Figure 2B).[19c] Electrons are then transferred at the electrode/electrolyte interface during these processes. Namely, they are given to or obtained from the redox species dissolved in the electrolyte, leading to the cur rent flow in and out of porous electrodes. More specifically, the redox species either in an oxidized (O_{bulk}) or a reduced (R_{bulk}) state in the bulk solution is first entrapped inside the pores of the electrode (O_{pore} or R_{pore}) (Figure 2C). Once they reach the transition states (O^* or R^*), their conversion into their adsorbed states (O_{ads} and R_{ads}) happens. The electron transfer reactions of these confined/adsorbed redox species ultimately lead to enhanced charge storage capacity of porous electrodes.[5c] Note that electron transfer reactions of redox species in transition states (O^* or R^*) may also occur even without their adsorption. Meanwhile, electron transfer reactions of soluble redox electrolytes can take place on the outer electrode surface, although the contribution of these reactions into the total capacitance is expected to be very small. More importantly, adsorbed redox species are easily converted to soluble states of O_{pore} or R_{pore} (e.g., 5 or 5′ process) and subsequently diffuse to the bulk solu tion, resulting in short lived charge storage processes of R ECs.

The redox kinetic, ion adsorption, and diffusion of redox electrolytes inside the electrode pores are different from those on bulk materials. A concept of thin layer electrochemistry (TLE) has been proposed to describe the faradaic reactions inside the pores, which can be induced under the conditions of smaller pore diameter compared to the equivalent diffusion layer thick ness.[20] With the absence of diffusion inside the porous space, superior kinetic is expected. Therefore, the peak current of an R EC obtained by general cyclic voltametric measurements is the sum of a capacitive current of the formed double layer (i_{EDL}), a planar diffusion limited redox current at the top of the electrode (i_{diff}), and a TLE based redox current (i_{TLE})[20,21]

$$i_p = i_{EDL} + i_{diff} + i_{TLE} = i_{EDL} + nFAc\left(\frac{\pi DnF\nu}{RT}\right)^{1/2}\chi\left(\frac{nF\nu t}{RT}\right) + nFV_{pore}c\frac{nF\nu}{RT}\frac{\xi}{(1+\xi)^2} \quad (1)$$

where n is the number of transferred electrons, F is the faraday constant, A is the geometric area of the electrode, c is the bulk concentration, D is the diffusion coefficient, ν is the scan rate, R is the gas constant, T is the temperature, V_{pore} is the porous volume, the function χ is the normalized current for a reversible reaction under planar diffusion, and $\xi = \exp\left[\left(\frac{nF}{RT}\right)(E - E^0)\right]$ with E the applied voltage, and E^0 the formal potential of the redox couple. Obviously, at a very high scan rate, i_{diff} proportional to the square root of the scan rate plays the dominant role, while i_{TLE} proportional to the scan rate shows major contribution at a very low scan rate.

In addition to porous capacitor electrodes and soluble redox electrolytes, separators or membranes are required for the R EC construction. They are placed between two electrodes to insulate ion transfer but maintain ionic conductivity. In most cases, the electrolyte is homogeneous in the discharged state, with the anolyte and catholyte fully miscible throughout the cell.[19c] With the confinement of soluble ions in the pores of a porous electrode, rapid charge transfer reaction of a redox electrolyte occurs, leading to superior performance of an R EC (e.g., high power densities, high charge/discharge rates). For example, R ECs can deliver energy densities of up to ≈200 Wh kg^{-1} as well as power densities higher than 1 kW kg^{-1}.[21a]

It has to point out that an R EC is different from a flow battery. In a flow battery, redox electrolytes introduced in the positive and negative cell compartments are separately stored in external reservoirs.[22] During the charging/discharging

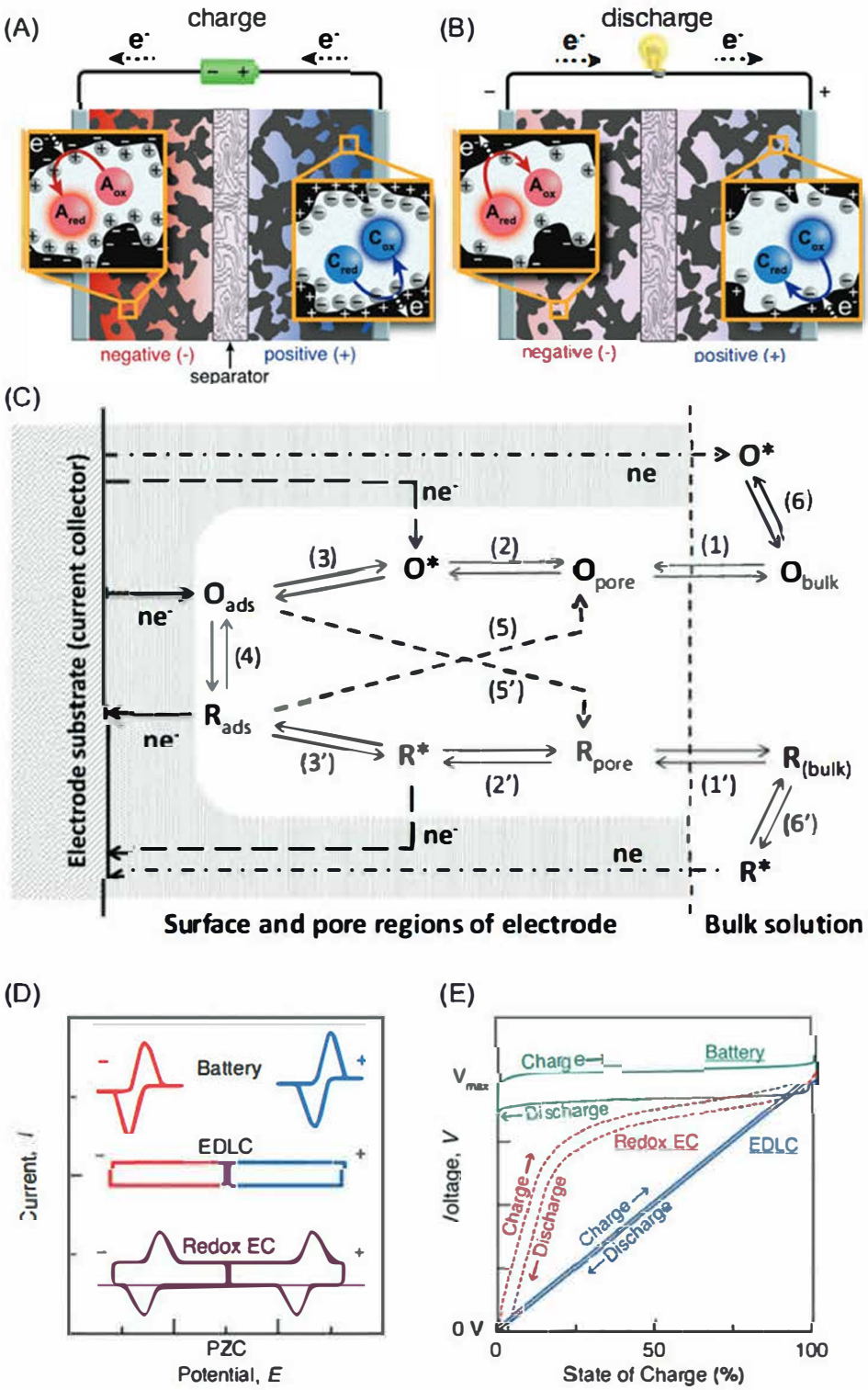

Figure 2. A,B) Energy storage mechanisms in an R EC under charging (A) and discharging (B) conditions utilizing the electric double layer for capacitive charge storage, as well as reduction and oxidation of the anolyte and catholyte redox couples in the electrolyte for faradaic charge storage. C) Illustration of charge storage mechanisms in a porous electrode of an R EC. The letters O and R refer to the oxidized and reduced states of the used redox species in the electrolyte, respectively. D,E) Comparison of the theoretical three-electrode CVs (D) and two-electrode GCD (E) voltage profiles of a battery, an EDLC, and an R EC. The term of PZC in (D) stands for point of zero charge. A,B,D,E) Reproduced with permission.[19c] Copyright 2017, American Chemical Society. C) Reproduced under the terms of the CC BY Creative Commons Attribution 4.0 License (http://creativecommons.org/licenses/by/4.0/).[5c] Copyright 2015, The Authors, published by IOP Science.

processes they are respectively pumped through corresponded compartments divided by a membrane. As the charge carriers, they participate in redox reactions and energy storage processes. A hydraulic pressure drop exists over the porous electrode when filled with redox electrolyte during the circulation of the electrolyte in a flow mode.[23] Flow batteries thus feature the advantage of facile adjustability toward energy and power storage capability, simply by adjusting the amounts of stored electrolytes in the reservoirs and the scale of the cell stack. However, they suffer from lower energy densities when compared to batteries and meanwhile lower power densities when compared to SCs.[24]

2.2. Performance Evaluation of R-ECs

The performance of an EC is generally qualified by its (specific) capacitance (C) or capacity, cycling stability or cycle life described as capacitance retention in this review, energy density (E), power density (P), coulombic efficiency (η_C) or energy efficiency (η_E), and self-discharge rate. A three electrode configuration is often applied for the characterization of capacitive behavior (namely, C, and cycling stability) of a single capacitor electrode. A two electrode configuration is usually utilized to evaluate the E and P values of an assembled full cell or an EC device.

To estimate the electrochemical performance of ECs, cyclic voltammetry, galvanostatic charging/discharging (GCD) method, and electrochemical impedance spectroscopy are frequently applied techniques. An EDLC has similar cyclic voltammogram (CV, Figure 2D) and GCD curve (Figure 2E) as those of PCs, in spite of their different charge storage mechanisms. Due to the occurrence of faradaic reactions in a PC, redox peaks in its CVs and plateaus in its GCDs have also been observed. Differently, an R EC integrates the features of both an EDLC and a battery. The peaks in its CVs and the plateaus in its GCD curves correspond to the diffusion controlled redox reactions that occur inside porous electrodes. Therefore, an R EC is also called a battery like SC or a supercapbattery in some cases.[25]

2.2.1. Capacity and Capacitance

From the nonlinear GCD curve of an R EC and the active mass (m) of the used capacitor electrode, a specific charge/discharge capacity (Q_{GCD}, mA h g^{-1}) can be calculated from[26]

$$Q_{GCD} = \frac{I \times \Delta t}{m} \tag{2}$$

where I is the discharging current, Δt is the discharging time obtained from the GCD curve.

The capacitance is commonly used for to evaluate R ECs in literature and is estimated by dividing transferred charges (Q) during the charging/discharging processes when the potential or cell voltage (V), namely, $\Delta Q/\Delta V$ is altered. Similarly, the capacitance of an R EC can be evaluated using the following equations[27]

$$C = \frac{\int I dV}{v \times \Delta V} \tag{3}$$

$$C = \frac{I \times \Delta t}{\Delta V} \tag{4}$$

$$C = \frac{I}{dV/dt} \tag{5}$$

where ΔV is the scanned potential range or the applied cell voltage, v is the scan rate used for recording CVs. In case of a full cell test or an R EC device, the capacitance can be also normalized by the effective area, volume or mass of the active material of a single capacitor electrode or both capacitor electrodes. Such a geometric, volumetric or gravimetric capacitance allows direct comparison between different ECs. Meanwhile, the capacitance of an R EC can be calculated from its GCD curves using the equation of[28]

$$C = \frac{2I \int V dt}{V^2 \left| \begin{matrix} V_f \\ V_i \end{matrix} \right.} \tag{6}$$

where V_i and V_f refer to the initial and final values of the scanned potential range or cell voltage, respectively.

Since each electrode/electrolyte interface is an individual R EC, a full cell R EC can be considered as two R ECs in series. The total cell capacitance of a full cell R EC is then determined by the following equation

$$\frac{1}{C} = \frac{1}{C_+} + \frac{1}{C_-} \tag{7}$$

where $C+$ and C represent the capacitances of the positive and the negative electrodes, respectively.[29] Obviously, the cell capacitance of an R EC is dominated by the capacitor electrode with a lower capacitance. For a symmetrical R EC, the specific capacitance of a single capacitor electrode is expected to be four times of the specific cell capacitance.

Note that the capacitance evaluation based on the ratio of $\Delta Q/\Delta V$ may lead to over or underestimation of the capacitance of an R EC. Moreover, the charge storage via redox reactions is not totally capacitive since redox reactions do not necessarily exhibit true capacitive response (e.g., linear galvanostatic discharge slopes or box like voltammograms) in nature. The use of capacitance might be problematic for the R ECs, although there is wide spread practice in the literature.[30] Therefore, it is actually better and even more precisely to use Q_{GCD} rather than C for the R ECs.

2.2.2. Capacitance Retention

Cycle life or cycling stability of an R EC refers to capacitance variation during the application of many charging/discharging cycles under given conditions. The cycling stability of an R EC is determined by the stability of the whole system, including the elements of capacitor electrode(s), added electrolyte(s), formed electrode/electrolyte interfaces, and used membrane. Consequently, the reversibility of redox reactions that occur during the charging/discharging cycles plays a critical role in the fabrication of a high performance R EC.

2.2.3. Energy Density and Power Density

To calculate energy density of an EC, a full cell test is generally carried out by means of the GCD technique in a two electrode system. The gravimetric/volumetric energy density of an R EC can be integrated from a GCD profile using the equation

$$E = \frac{\int IVdt}{X} \tag{8}$$

where I is the applied discharging current, V is the voltage that varies with the discharging time, X represents the total mass or total volume of the used active capacitor elec trode materials. In this way, the gravimetric or volumetric E of an R EC can be calculated. To obtain more precise E values, the mass or volume of involved redox electrolytes needs to be counted into the total mass or volume during the calculation.[5c,31]

The power density of an R EC is calculated by dividing its massive or volumetric E value by Δt at the corresponding cur rent density[19a,31]

$$P = \frac{E}{\Delta t} \tag{9}$$

To achieve high E and P values for an R-EC, the key is to increase the cell voltage, which is closely related with the elec trochemical potential window of both the electrolytes and the electrode. Therefore, by increasing the cell voltage, or an elec trochemical potential window of the electrolyte, the energy den sity of the formed R EC can be improved significantly. Aqueous electrolytes exhibit higher ionic conductivity (up to 1 S cm ^{1}) than that of organic and IL electrolytes, resulting probably in a lower resistance and hence a better power output.[1b] On con trary, the main advantage of nonaqueous electrolytes is their wider electrochemical potential windows over those of aqueous solutions. Organic electrolytes provide electrochemical potential windows wider than 2.5 V.[32] With such wider electrochemical potential windows, the cell voltages of R EC can be enhanced, leading to significantly improved energy and power densities of R EC devices. Therefore, organic electrolytes, for example, qua ternary ammonium salts (e.g., tetraethylammonium tetrafluor oborate) dissolved into an aprotic solvent (typically acetonitrile and propylene carbonate), have been widely used for commer cial EC devices currently.

2.2.4. Coulombic Efficiency and Energy Efficiency

The coulombic efficiency (η_C) and energy efficiency (η_E) have been utilized to characterize the efficiency of an EC.[26] The term of η_C is defined as the ratio of the charge transferred in the discharging step (Q_{dc}) to that in the charging process (Q_c). The term of η_E is determined through dividing the energy released during the discharging process (E_{dc}) with the energy stored during the charging step (E_c). The transferred charges can be obtained from the integration of related GCD curves. For EDLCs, the η_C and η_E values are generally same. However, they are different for R ECs.

2.2.5. Self-Discharge Rate

The self-discharge rate of an EC demonstrates the ability of an R EC to preserve the stored energy. Unfortunately, such rates have not been frequently measured during the self-discharge processes (SDPs) of ECs. To evaluate the self-discharge rate of an R EC, it needs to be charged to a set voltage and then left at open circuit. During the open circuit period, the voltage decay is recorded as a function of time. The slope of such a plot dem onstrates the self-discharge rate of an R EC.[19b,33] Alternatively, considering the nonlinear relationship of the voltage with the charge or stored energy in an R EC, energy retentions after the application of different open circuit durations have been used to describe the SDP (or to calculate the self-discharge rate).[31,34] In this way, the change of stored energy in an R EC during the SDP can be directly revealed.

3. Progress of R-ECs

It is quite clear that the overall performance of an R EC is mainly dependent on i) type, pH, concentration of redox active electrolytes,[35] ii) surface area, pore size, wettability of porous electrodes, iii) composition,[36] pH,[35a,37] concentration[38] of supporting electrolytes, iv) the interactions between these electrodes and electrolytes/solvent, and v) operating condi tions (e.g., applied voltage,[39] temperature[35c,40]). To ensemble an R EC with high C, E, P, and long term cycling stability, a proper concentration of the used redox electrolyte needs to be first considered. This is because when the concentration of the used redox electrolyte is too low, the contribution of redox electrolyte to the overall performance of an R EC is relatively small. By contrast, a too high concentration of redox electrolyte leads to high electrode polarization, a low charging rate, and relatively poor electrochemical reversibility of related faradaic reactions.[35b–d] Second, the pH value of the electrolyte must be suitable because it influences the activities of redox electrolytes. Taking an R EC constructed using hydroquinone (HQ) as redox electrolyte as an example, its high capacitances were achieved in alkaline and acidic electrolytes, due to the facile accessibility of protons in an acidic medium and self-protonation process of HQ in an alkaline solution, respectively. These capacitances were about two times higher than those achieved in inert elec trolytes. Differently, the addition of HQ into a neutral Li_2SO_4 solution did not significantly alter related capacitances.[35a] Third, the performance of an R EC is affected by the proper ties of the used supporting electrolyte (e.g., aqueous/organic solutions, ionic liquids), originating from varied electrochem ical potential windows of the capacitor electrodes and the electrolytes, ionic conductivities/ion sizes/solubility of redox electrolytes, operating temperature ranges, and viscosity of the solutions.[21a,41]

This section summarizes utilized redox electrolytes and porous electrodes for the R EC fabrication. The redox electro lytes include those dissolved in the aqueous and organic solu tions, ionic liquids as well as gel-polymer redox electrolytes. Various carbon materials, metal derived compounds, and other materials that have been applied as porous electrodes for the R EC are then shown. Subsequently, the performance of these

reported R ECs is overviewed in terms of their capacitances, capacitance retention, power densities, and energy densi ties. The *E* and *P* values of R ECs in the gravimetric or volu metric units with those of EDLCs, PCs, and batteries are also compared.

3.1. Redox Electrolytes

In addition to the used porous electrode(s), the selected redox electrolyte(s) will dramatically and eventually determine the performance of as ensembled R ECs. A suitable redox elec trolyte that is used to fabricate an R EC featuring high *P* and high *E* must possess a high ionic conductivity, a wide electro chemical potential window, and a high solubility in the applied solvent.[3c,31,42] Moreover, the electrolyte itself and its oxidation/ reduction products need to be stable. Namely, no side reactions occur when the electrolyte is in contact with other SC compo nents, including capacitor electrodes, solvent, and supporting electrolyte. The faradaic reactions of the selected redox elec trolytes are better to be reversible. When the diffusion kinetics and electron transfer kinetics of the selected redox electrolytes are fast, a minimized voltage loss can be achieved during the charging/discharging processes. Particularly, the redox potential of the selected redox electrolyte needs to match with or be located within the electrochemical potential windows of both the solvent and the capacitor electrode. Only under such condi tions, a high cell voltage of an R EC is expected. In addition, the selected redox electrolyte is better to be easily accessible, envi ronmentally friendly, cheap, safety, and abundant.

Numbers of redox species (**Figure 3**) from inorganic compounds, organic molecules, and redox active gel polymer electrolytes have been used for the construction of R ECs.[11,28c,d,31,34,36,43] They feature varied redox potentials, ionic conduc tivity, electron mobility, redox activity, and reversibility. Therefore, these redox electrolytes actually determined the operating

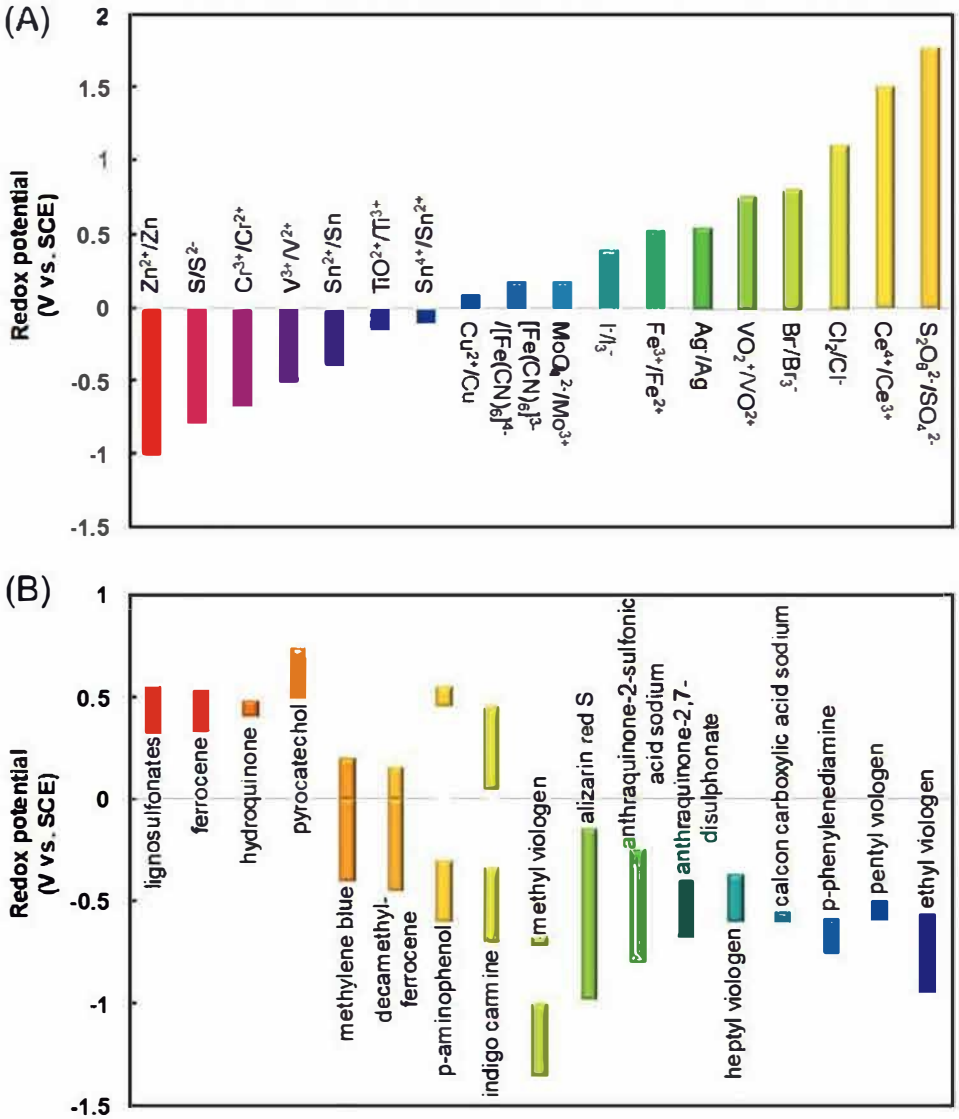

Figure 3. A,B) Redox potentials of various inorganic (A) and organic (B) redox electrolytes used for the construction of R-ECs.

conditions of an R EC (e.g., operating voltage, temperature, and pH of the electrolyte) and eventually the performance of an R EC (e.g., *C*, *E*, *P*, and stability). In general, redox electrolytes are prepared by dissolving redox active additives in supporting electrolytes. Redox species dissolved directly in solvents that are capable of undergoing redox reactions have also been utilized as the redox electrolytes.[5b]

3.1.1. Inorganic Compounds

The inorganic redox species used for the R EC fabrication mainly cover halogen ions (e.g., iodide, bromide),[37b,40e] metal ions (e.g., Cu^{2+}/Fe^{2+} and Ce^{3+}),[39a,44] and metal complexation (e.g., $Fe(CN)_6^{3-}$, $Fe(CN)_6^{4-}$, VO_3^-/VO^{2+}, and VO^{2+}/VO_2^+).[20a,45] Electrolytes with individual or dual/multiple inorganic redox species as well as inorganic redox species with multiple redox centers have been applied. As for an individual inorganic redox electrolyte, the iodide aqueous solution (e.g., KI) has been widely applied for the R EC construction.[46] This is because iodide ions have a variety of oxidation states (e.g., $3I^- \leftrightarrow I_3^- + 2e^-$, $2I^- \leftrightarrow I_2 + 2e^-$, $2I_3^- \leftrightarrow 3I_2 + 2e^-$, and $I_2 + 6H_2O \leftrightarrow 2IO_3^- + 12H^+ + 10e^-$) at different potentials. These states are further varied with the pH values of the electrolyte. The addition of KI reduces the diffusive resistance of the electrolytes and the charge transfer at electrolyte/electrode interface. To match the capacitance of a positive electrode with that of a negative electrode, and eventually to achieve a high-performance R-EC, redox electrolytes with dual/multiple redox sources were utilized for both positive and negative electrodes during the R EC construction.[46b,47] The reported redox mixtures included KI + Na_2MoO_4,[48] KI + $VOSO_4$,[49] $SnSO_4$ + $VOSO_4$,[19a] $Fe^{2+/3+}$,[50] Cu^{2+} + Fe^{2+},[44a] and $Fe(CN)_6^{3-/4-}$.[9,25c,d,43m,51] The usage of these mixed redox electrolytes has efficiently improved the performance of as fabricated R ECs. This is because the synergistic effect exists within different redox additives in the electrolytes.[37a,43f] When the concentration of one redox electrolyte reaches its maximal value, the dissolution of another redox electrolyte is still possible, leading to a higher concentration of redox additives and thus higher pseudocapacitive contribution to the whole performance (e.g., capacitance) of an R EC. Moreover, different redox species have varied redox peak potentials (Figure 3). In other words, the mixtures of various redox species widen the operating voltages of the R ECs.

Taking the mixture of Na_2MoO_4 + KI in 0.1 M H_2SO_4 as an example, the synergistic effect of these redox additives has been proved in the constructed R-ECs (**Figure 4**).[48] The promoted redox reactions of Mo^{n+} and I^n at the electrode surfaces was proposed, and further explained by the overlapped redox peak potentials of faradaic reactions of Na_2MoO_4 and KI as well as the formation of a complex substance $[(Mo_xI_yO_{4x})^n C_z]$. After the addition of equal molar concentration of Na_2MoO_4 and KI into 0.1 M H_2SO_4, the capacitance of the used carbon electrode was 17.4 times higher than that acquired in H_2SO_4, which was even bigger than the sum of theoretical capacitances of two individual systems.[48] In some cases the redox additives were restricted only to a positive or negative compartment and separated by a membrane (denoted as a vertical line),

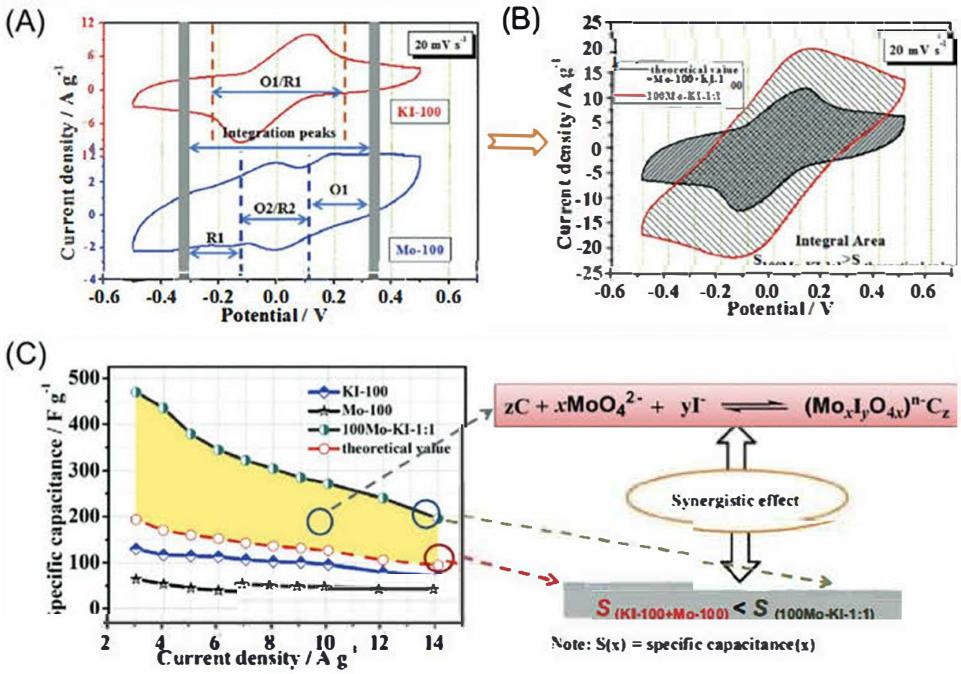

Figure 4. A,B) The synergistic effect of KI and Na_2MoO_4 inside an R EC: CVs at a scan rate of 20 mV s^{-1} of: A) Mo(Na_2MoO_4) 100 and KI 100 samples, B) 100Mo KI 1:1 sample and the theoretical value with the sum of current intensities in CVs of KI 100 and Mo 100. C) The specific capacitances of the Mo 100, KI 100, and 100Mo KI 1:1 samples obtained from the GCD curves with different current densities at a cell voltage of 1 V. The theoretical value shows the summed capacitances of the Mo 100 and KI 100 samples. The possible faradaic reaction mechanism of the synergistic effects is shown. A C) Reproduced with permission.[48] Copyright 2016, Elsevier.

such as KI | $VOSO_4$,[32] $SnSO_4$ | $VOSO_4$,[19a] SnF_2 | $VOSO_4$.[23a] For example, in a KI (1 M) | $VOSO_4$ (1 M) cell where a Nafion membrane separated two cells, the capacitances of the positive and negative AC electrodes were over 1200 and about 670 F g^{-1}, respectively. As for an R-EC cell, a *C* of as high as 500 F g^{-1} was achieved at 0.5 A g^{-1}, along with an *E* of ≈20 Wh kg^{-1} and a maxima *P* of 2 kW kg^{-1}.[32]

Single inorganic redox species containing dual redox active ions have been utilized for the R-EC construction. These redox species are different from the addition of dual/multiple redox species into the solutions since they simultaneously deliver reversible faradic reactions at both electrodes. For example, iron bromide ($FeBr_3$) has been introduced in the H_2SO_4 solution to build R-ECs.[52] Using a mesoporous carbon as the capacitor electrode, as-built R-EC exhibited a *C* of 885 F g^{-1} at 2 A g^{-1}, much higher than that obtained using the electrolytes of H_2SO_4, H_2SO_4 + Br^-, or H_2SO_4 + Fe^{2+}. The superior performance of this R-EC originated from the simultaneous occurrence of redox reactions of Br^-/Br_3^- and Fe^{3+}/Fe^{2+} at the positive and negative electrodes, respectively. This R-EC also showed excellent cycling stability (105.2% of the initial capacitance after 10 000 cycles at a current density of 10 A g^{-1}), probably due to increased amount of redox active material adsorbed on the electrode.

3.1.2. Organic Molecules

Many soluble organic substances, especially those containing hydroxyl and/or amine groups have been used as aqueous and organic redox electrolytes for the development of various R-ECs. In aqueous solutions, the frequently reported individual redox species cover HQ,[5a,47a,53] pyrocatechol,[43d] methylene blue (MB),[43g] p-hydroxyaniline,[40a] p-phenylenediamine (PPD),[38b,43j] m-phenylenediamine (MPD),[39b] p-nitroaniline,[28b] dibromodihydroxybenzene,[35a,38a] and calcon carboxylic acid sodium salt.[28c] Meanwhile, the dual redox species of HQ-PPD,[37a] HQ-benzoquinone (BQ),[54] and alizarin red S-bromoamine acid[55] have been utilized for R-ECs.

To dissolve these redox electrolytes, acidic, alkaline, and neutral solutions have been applied. For example, HQ is usually dissolved in an acidic supporting electrolyte (e.g., H_2SO_4). Using an AC electrode and the aqueous electrolyte of HQ + H_2SO_4, the constructed R-EC exhibited an *E* of as high as 31.3 Wh kg^{-1}.[5a] The energy storage mechanism of HQ was proposed in the following way (Figure 5A).[47a] The redox reaction of HQ/BQ took place at the positive electrode in acidic solutions, resulting in battery-like behavior of this electrode. The negative electrode exhibited its capacitor-type behavior, accompanied with a pseudocapacitive hydrogen-electrosorption process.[47a] Highly reversible and diffusion-controlled redox reactions of organic redox species (e.g., MB (Figure 5B)[43g] and indigo carmine (Figure 5C)[11]) are responsible for the superior performance of as-constructed R-ECs, compared to that of related EDLCs or PCs. Meanwhile, numerous R-ECs have been fabricated using redox species (e.g., bromine derivatives of dihydroxybenzenes,[35a] calcon carboxylic acid,[28c] KI,[40b] MPD,[39b] PPD[38b,43k]) dissolved in alkaline media. For example, to clarify the effects of amine/nitro/hydroxyl groups

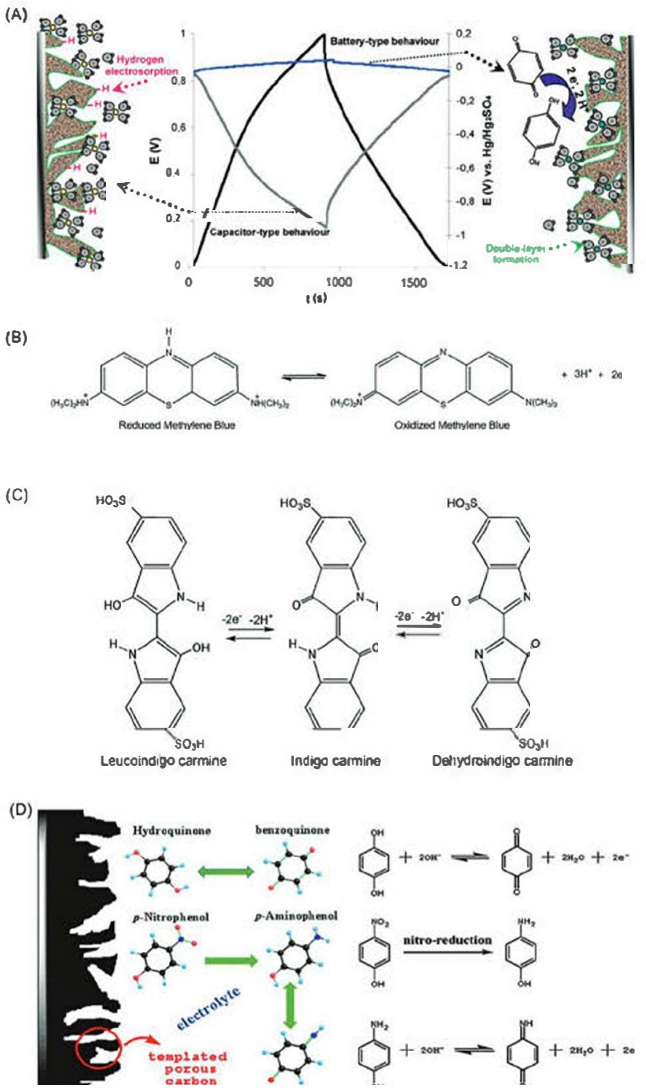

Figure 5. A) Energy storage mechanism at the positive and negative electrodes of an R-EC in HQ contained redox electrolyte. Reproduced with permission.[47a] Copyright 2011, American Chemical Society. B) Redox reaction of MB in the H_2SO_4 solution. Reproduced with permission.[43g] Copyright 2012, Elsevier. C) Redox reaction of indigo carmine occurred in the R-EC system. Reproduced with permission.[11] Copyright 2010, Elsevier. D) Electrochemical redox mechanisms of HQ, PNP, and PAP associated with the related oxidative and reductive reactions at the carbon electrode surface in KOH supporting electrolyte. Reproduced with permission.[28d] Copyright 2016, PCCP Owner Societies, published by Royal Society of Chemistry.

within the benzene rings on the obtained R-capacitances, the battery-like behavior of HQ, p-aminophenol (PAP), and p-nitrophenol (PNP) have been studied in the alkaline solutions.[28d] The irreversible reduction of the nitro group led to the formation of amine group, while the reversible redox reactions of amine/imine and hydroxyl/quinone group highly enhanced the R-capacitances (Figure 5D).[28d] In the neutral solutions (e.g., KNO_3 solution), anthraquinone-2,7-disulphonate (AQDS) has been dissolved and further used as the redox electrolytes.[43e] Stemming from the involvement of two electrons and two

protons during the quasi-reversible reaction of AQDS, as-constructed R-EC exhibited a C of 225 F g^{-1}, an E of 21.2 Wh kg^{-1}, and a P of 412 W kg^{-1} when a cell voltage of 1.8 V and a current density of 1 A g^{-1} were applied.

Similar as those conducted for inorganic redox electrolytes, multiple organic redox additives (e.g., HQ + PPD[37a]) and organic species with multiple redox centers have been added in aqueous solutions for the R-EC construction. The latter redox species include 1,1′-bis[3-(trimethylammonio)-propyl]-4,4′-bipyridinium tetrabromide ($NVBr_4$),[56] ethyl viologen dibromide ($EVBr_2$),[43v] methyl viologen dibromide ($MVBr_2$),[31] heptyl viologen dibromide ($HVBr_2$),[31] pentyl viologen dibromide,[43y] etc. For instance, $EVBr_2$ possesses redox-active bipyridinium cation and bromide anion, its redox reactions can thus occur at the negative and positive electrodes, respectively. Combined $EVBr_2$ with activated charcoal, the fabricated R-EC exhibited a specific C of as high as 408.0 F g^{-1} and an E of 23.0 Wh kg^{-1} at 0.25 A g^{-1}. A 30% increase of the initial capacitance was observed after 1000 GCD cycles at 2.50 A g^{-1}. Such high-performance of this R-EC was explained by the adsorption of bipyridinium cations on the electrode surface, caused by the π-π interaction between the carbon electrode and viologen electrolyte.[43v]

The main bottleneck of using aqueous electrolytes for the R-EC construction is their narrow electrochemical potential windows (<1.23 V), which is constricted by the water decomposition. To widen the electrochemical potential window of the capacitor electrode(s) and eventually the cell voltage of an R-EC, nonaqueous electrolytes such as organic solutions have been utilized to dissolve organic redox electrolytes.[57] To date, various redox-active organic compounds such as ferrocene (Fc),[43m,58] decamethylferrocene (DmFc),[42a] PPD,[59] 4-oxo-2,2,6,6-tetramethylpiperidinooxy (4-oxo TEMPO),[58] and ethyl viologen[60] have been dissolved in organic solvents. The used organic solvents mainly cover acetonitrile, tetrahydrofuran, and propylene carbonate. For example, three phenylenediamine molecules, namely, o-phenylenediamine (OPD), PPD, and MPD have been introduced into the triethylmethylammonium tetrafluoroborate ($MeEt_3NBF_4$) + acetonitrile solutions for the fabrication of graphene hydrogel-based R-ECs (**Figure 6A**).[59b] Compared to MPD and OPD, the R-EC in the PPD-contained electrolyte exhibited significantly enhanced performance. It delivered a cell voltage of as large as 2.7 V, an E of 143 Wh kg^{-1} at a P of 1.11 kW kg^{-1}, and an excellent cycling stability (93.8% of initial capacitance after 5000 GCD cycles at 2 A g^{-1}). Dual organic redox species (e.g., HQ + BQ) dissolved in organic solvents have been utilized to construct R-ECs based on polyaniline emeraldine-salt modified electrodes (Figure 6B), achieving excellent cycling stability with an increase of capacitance after long-term cycling.[54] The increased capacitance obtained during this cycling test was attributed to the adsorption of more quinones at the electrode, the ratio change of BQ to HQ redox states at the electrodes, and the prevented unfavorable redox reactions in these polyaniline electrodes. As-obtained performance was much better than that of R-ECs when individual HQ or BQ redox states were applied as the redox sources.

In addition to organic solvents, numerous ILs have been applied as the solvents to dissolve redox species or directly as the redox-active electrolytes (without the use of any additional solvents). The reported IL solvents mainly include triethylammonium bis(trifluoromethane)sulfonimide (TEATFSI),[61] *N*-butyl-*N*-methylpyrrolidinium bis(trifluoromethane-sulfonyl) imide ($PYR_{14}TFSI$),[62] $EMImBF_4$,[63] and 1-ethyl-3-methylimidazolium bis(trifluoromethyl sulfonyl)imide (EMImTFSI).[64] Some examples of redox-active species in ILs are Cu(II),[10] HQ,[61] and para-BQ.[62,65] For example, in a protic IL of TEATFSI + HQ, as-formed R-EC exhibited a C of 72 F g^{-1} and an E of 31.22 Wh kg^{-1}. While in the TEATFSI, they were only 42 F g^{-1} and 18.4 Wh kg^{-1}, respectively.[61] In terms of redox-active ILs, EMIm halide (EMIm-X, X = Br, I),[63,64,66] EMIm ferrocenylsulfonyl-(trifluoromethylsulfonyl)-imide (EMImFcNTf)[16a] and biredox IL composed of a perfluorosulfonate anion bearing anthraquinone and a methyl imidazolium cation bearing TEMPO[16b] have been applied to construct R-ECs. When both EMImI and EMImBr were added into the EMImTFSI, the capacitance of a porous carbon-based R-EC was enhanced, attributed to the redox reactions of different halide ions and size effect of these redox molecules (Figure 6C).[64] The charging/discharging behavior of a full R-EC cell is different from that of an individual AC electrode in the EMImFcNTf + acetonitrile solution (Figure 6D). On this R-EC, an E of 23.7 Wh kg^{-1} was obtained when a cell voltage of 2.5 V was applied. Meanwhile, the utilization of EMImFcNTf resulted in full suppression of the self-discharge at the positive electrode since a thin film was formed during the oxidation reaction between $[FcNTf]^-$ and $[Fc^+NTf^-]^0$.[16a] Despite the enlarged voltage was achieved by nonaqueous electrolytes compared to aqueous electrolytes, the lower conductivity, higher viscosity, larger ion size, and more complicated preparation procedure of organic electrolytes and ILs unfortunately hinder their electrochemical performance and mass-scale synthesis, which need to be taken into account for their application in R-ECs.

3.1.3. Redox Active Gel-Polymer Electrolytes

Quasi-solid-state GPEs that have been frequently utilized in recent years to ensemble solid-state SCs, especially portable, wearable, and flexible EC devices[67] have been explored for the R-EC formation. Typically, a GPE consists of a host polymeric framework/matric, a supporting electrolytic compound, and an organic or an aqueous solvent. The reported host polymeric frameworks/matrices include PVA, polyvinylpyrrolidone (PVP), PEO, poly(vinylidene fluoride) (PVDF), and poly(methyl methacrylate) (PMMA), poly([2-(methacryloyloxy)ethyl]dimethyl-(3-sulfopropyl)ammonium hydroxide) (PPDE)[14,67b,68] as well as the polymer mixture such as poly(vinylidene-fluoride-*co*-hexafluoropropylene) (PVDF-HFP).[69] The supporting electrolytic compound can be a salt, an acid, or an alkali. Once redox additives are incorporated into these GPEs, they can be employed for the R-EC construction. The reported GPEs include PVA–H_2SO_4–$VOSO_4$,[45b] PVA–H_2SO_4–NH_4VO_3,[45c] PVA–H_2SO_4–KI,[40e] PVA–H_2SO_4–bromamine acid sodium (BAAS),[68] PVA-H_2SO_4-*p*-benzenediol,[70] PVA–H_2SO_4–HQ,[71] PVA–KOH–KI,[13] PVA–KOH–PPD,[72] PVA–KOH–alizarin red S,[43q] PMMA–tetraethylammonium tetrafluoroborate ($TEABF_4$)–Fc,[58] poly(2-acrylamido-2-methyl-1-propanesulfonic acid)–$(NH_4)_2MoO_4$.[73] These GPEs actually overcame the

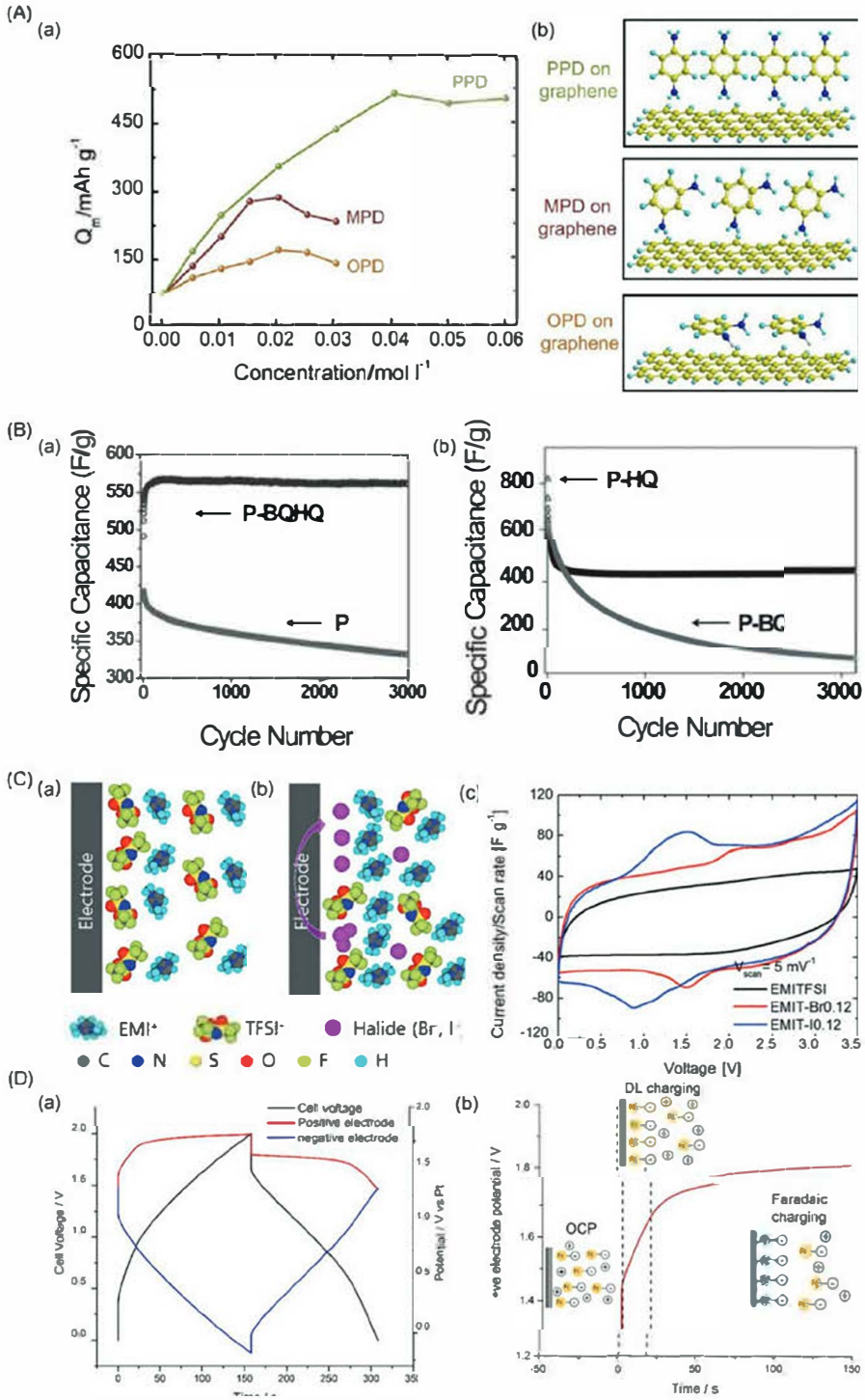

Figure 6. A) a) The electrode specific capacity of the R-ECs in a $MeEt_3NBF_4/CH_3CN$ organic electrolyte after adding OPD, MPD, or PPD with different concentrations. The current density was 1 A g^{-1}. b) Hypothetical images illustrating the interaction between different phenylenediamine molecules and the graphene surface. A) Reproduced with permission.[59b] Copyright 2018, Elsevier. B) The specific electrode capacitance of various polyaniline SCs as a function of cycling numbers in different electrolytes of: a) H_2SO_4/AcOH (acetic acid) (P, gray curve), HQ + BQ in H_2SO_4/AcOH (P-BQHQ, black curve) and b) HQ in H_2SO_4/AcOH (P-HQ, black curve), BQ in H_2SO_4/AcOH (P-BQ, gray curve). All the capacitances were recorded at a current density of 12.5 mA cm^{-2} using the GCD technique. B) Reproduced with permission.[54] Copyright 2014, Wiley-VCH. C) Charge storage mechanisms of SCs using: a) EMImTFSI and b) a mixture of EMImTFSI and EMI-halide as the electrolytes, respectively. c) CVs of a carbon-based R-EC at a scan rate of 5 mV s^{-1} in the electrolytes of EMImTFSI, EImTFSI + EMIml, and EMImTFSI + EMImBr. C) Reproduced with permission.[64] Copyright 2017, The Royal Society of Chemistry. D) Electrochemical performance of an R-EC with 80 wt% of [EMIm][FcNTf] in acetonitrile at 25 °C and a current of 2 mA: a) GCD curves of the full-cell and the individual electrode, b) the charging potential curve of the positive electrode associated with the processes during a charging process. D) Reproduced with permission.[16a] Copyright 2016, Elsevier.

shortcomings of liquid electrolytes, such as the difficulty to be packed, leakage, and leakage-caused corrosion. Moreover, they possess the advantages of high flexibility, reliability, and ease of design. Furthermore, they can be behaved as the separators. Meanwhile, the GPEs containing dual redox sources have also been utilized for the R-EC fabrication, such as PVA–H_2SO_4–KI–$VOSO_4$,[49a] PVA–H_2SO_4–HQ | PVA–H_2SO_4–MB,[74] PVA–H_2SO_4–$VOSO_4$ | PVA–H_2SO_4–Na_2MoO_4,[75] and PVA–H_2SO_4–$FeBr_3$,[52] PPDE–LiCl–$EVBr_2$.[76] For example, KI and $VOSO_4$ have been added into a PVA–H_2SO_4 GPE. Compared with those fabricated using the electrolytes of PVA–H_2SO_4, PVA–H_2SO_4–KI, and PVA–H_2SO_4–$VOSO_4$, the R-EC with the PVA–H_2SO_4–KI–$VOSO_4$ GPE exhibited better performance.[49a] It showed a C of 1232.8 F g^{-1} at 0.5 A g^{-1}, an E of 25.4 Wh kg^{-1}, and good cycling stability. The additional R-capacitances from the redox reactions of iodine at the positive electrode and V-based ions at the negative electrode were interpreted as the sources for better performance of this R-EC.

Unfortunately, a GPE has relatively low ionic mobility. Its full contact with the electrode surface is actually impossible. Compared to those using liquid electrolytes, the R-ECs constructed using GPEs feature inferior performance. For example, a reduced graphene oxide (rGO)-based R-EC fabricated using a GPE of PVA–KOH–KI then had a lower specific C than that fabricated using a KOH–KI aqueous electrolyte.[77] The performance of an R-EC formed with a GPE of PVA–H_2SO_4–$VOSO_4$ was worse than that formed using an aqueous electrolyte of $VOSO_4$ + H_2SO_4.[45b] One proposed approach to solve these challenges of the GPEs was to add an optimal amount of redox species.[75,78] Alternatively, the addition of other conductive materials like CNTs into GPEs effectively enhanced the ionic conductivity of GPEs.[79] Another problem to utilize GPEs for the R-EC fabrication is their poor mechanical strength.[13b,80] To solve this problem, GPEs containing redox species that can also act as plasticizers have been developed. They include BMIMBr,[79] indigo carmine,[81] alizarin red S,[82] and BAAS.[68] The strong plasticizing effect of these GPEs resulted in their reinforced mechanical performance. The introduction of BMIMI into the PVA–Li_2SO_4 GPE generated more amorphous regions and improved its elasticity.[83] The AC-based R-EC using a GPE of PVA–H_2SO_4–1-anthraquinone sulfonic acid showed small capacitance deviation under various stretching, folding, and compressing strain conditions.[84]

3.2. Porous Electrodes

To achieve a high-performance R-EC with high E and P as well as excellent stability, its electrode materials or capacitor electrodes must feature high specific surface areas (SSAs), high porosities with proper pore sizes and distribution, high stability, and high conductivities, similar as those for conventional ECs. In these regards, a great variety of functional materials have been designed and utilized directly as electrodes or as the active components of electrodes to fabricate R-ECs (**Figure 7**). They mainly include carbon materials, metal-based materials, conducting polymers, and different composite materials.

3.2.1. Carbon Materials

As one of the most attractive electrode materials for ECs, various carbon materials have been used as the capacitor electrodes to construct R-ECs, including AC,[38a,43e,46b] CNT,[11,20a,42a,43g,100] graphene,[59b,101] and conductive diamond.[25d,51a,b] Meanwhile, hybrid carbon materials (e.g., CNT/mesoporous carbon hybrid fibers[102]) have been utilized as the capacitor electrodes to fabricate R-ECs. They show the features of different hybridization of atomic orbitals (e.g., sp^2 or sp^3) and dimensionalities (e.g., 0D to 3D), high electrical conductivity, easily tunable surface chemistry and surface terminations, and abundant synthesis technologies with high and controlled porosity, offering more opportunities for the fabrication of R-ECs with high performance.

Among those porous carbon materials, AC has been the most frequently used as the base or the support to fabricate the R-EC electrodes since it can be easily produced from biomasses and their derivatives[37b,40a,71,103] as well as from carbonaceous compounds.[28c,d,39a,43j,48,66f] For example, the R-EC using ACs derived from *Eichhornia crassipes* as the capacitor electrodes (**Figure 8A**) showed capacitances of 912, 572, and 604 F g^{-1} at 2 mA cm^{-2} when the redox electrolytes of KI + H_2SO_4, KBr + H_2SO_4, and KI + Na_2SO_4 were utilized, respectively. Their energy densities were 19.04, 11.6, and 12.3 Wh kg^{-1}, respectively.[37b] Moreover, AC materials can be activated (e.g., in the KOH solutions) to further enhance their surface areas.[5a] They can be also doped (e.g., with nitrogen) to vary their properties such as ion and electron transfer ability, porous structure, SSA, and electrical conductivity.[35d,43d,k,55,104] Meanwhile, these doped AC materials can be obtained via thermal treatment of nitrogen-rich carbon precursors or the mixtures of carbon precursors and nitrogen-contained reagents.

The secondly frequently applied R-EC capacitor electrodes are from CNTs.[20a,43a,47b,100] For example, the R-EC using the capacitor electrode of vertically aligned CNTs (**Figure 8B**) that were grown in a thermal CVD reactor showed a capacity of 26 mA h cm^{-3} or 0.28 mA h cm^{-2} in a $K_3Fe(CN)_6$ contained redox electrolyte.[20a] In a PPD + KOH electrolyte, a CNT-based R-EC showed a C of 162.66 F g^{-1}, an E of 4.23 Wh kg^{-1}, a P of 2.79 kW kg^{-1}.[100] Once CNTs were treated in alkali media or acidic mixtures, their specific surface areas and wettability can be further varied. Meanwhile, different surface oxygen-containing functional groups (e.g., hydroxyl, carboxyl, carbonyl, and epoxy groups) can be introduced during wet-chemical treatment.[43a,47b] These introduced surface functionalities led to the occurrence of faradaic redox reactions and thus additional pseudocapacitances were obtained on these wet-chemically treated CNTs.

Conductive diamond is known as a promising electrode material, stemming from its unique advantages over other sp^2 carbon and classical metal electrodes, such as a wide electrochemical potential window, excellent chemical inertness and stability. Conductive diamond films and their nanostructures have been applied as the R-EC capacitor electrodes. They include boron-doped diamond (BDD),[25d] BDD networks (**Figure 8C**),[25d] carbon nanofiber (CNF)-coated BDD hybrid film (CNF/BDD) (**Figure 8D**),[25c] phosphorus-doped nanocrystalline diamond,[51a] graphite@nitrogen-doped diamond nanoneedle

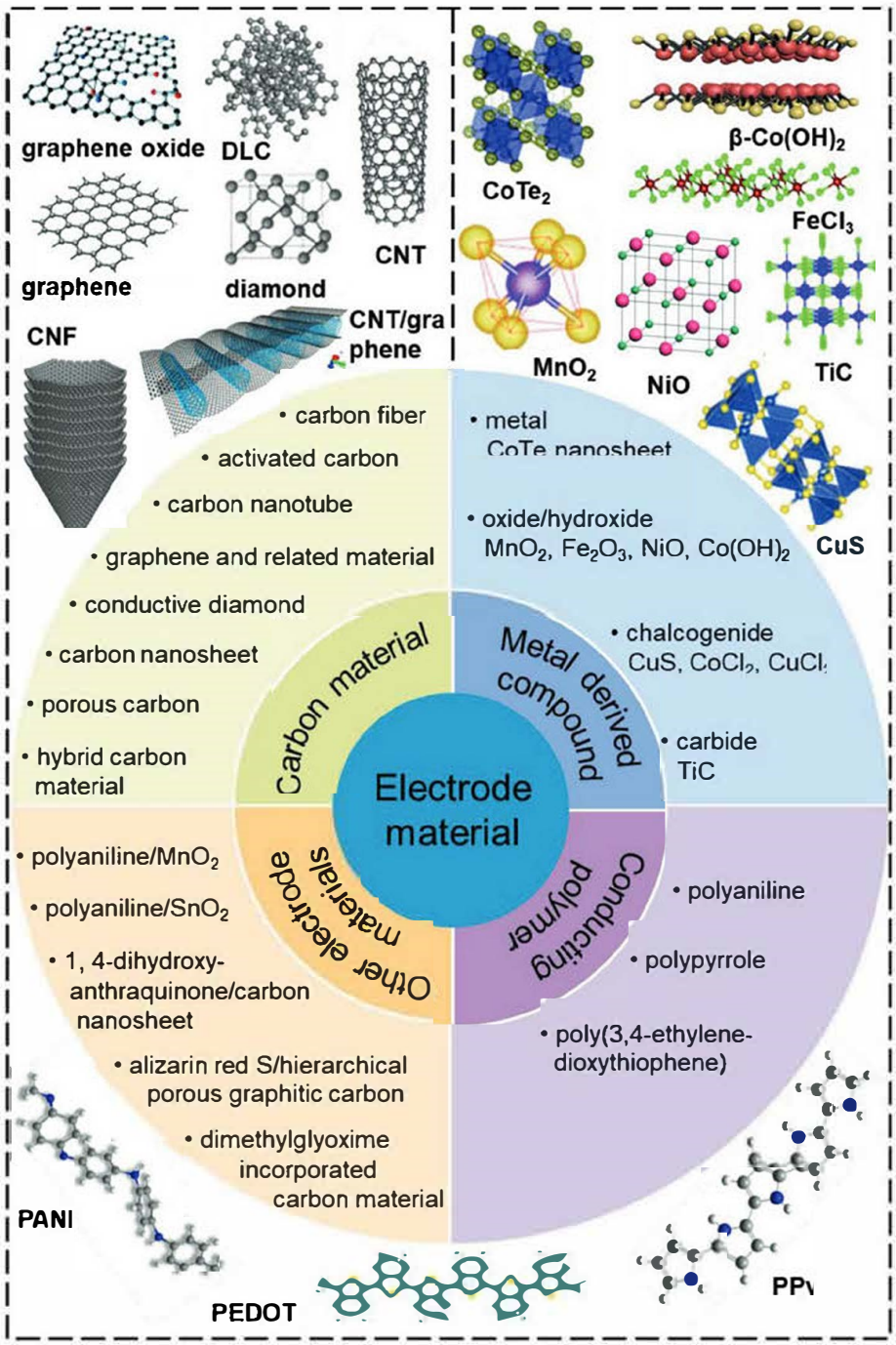

Figure 7. Summary of electrode materials designed for the construction of R-ECs. The inset example images illustrate the structures of different materials of graphene oxide,[85] graphene,[86] carbon nanofiber (CNF),[87] carbon nanotube (CNT),[86] diamond,[86] diamond-like carbon (DLC),[88] CNT/graphene,[89] $CoTe_2$,[90] β-$Co(OH)_2$,[91] $FeCl_3$,[92] MnO_2,[93] NiO,[94] TiC,[95] CuS,[96] polyaniline (PANI),[97] poly(3,4-ethylenedioxythiophene) (PEDOT),[98] and polypyrrole (PPy).[99] Image for graphene oxide: Reproduced with permission.[85] Copyright 2016, Elsevier. Images for graphene, carbon nanotube, and diamond: Reproduced under the terms of the CC-BY Creative Commons Attribution 4.0 International license (https://creativecommons.org/licenses/by/4.0).[86] Copyright 2015, The Author, published by Wiley-VCH. Image for carbon nanofiber: Reproduced with permission.[87] Copyright 2020, Elsevier. Image for diamond-like carbon: Reproduced under the terms of the CC-BY Creative Commons Attribution 4.0 International license (https://creativecommons.org/licenses/by/4.0).[88] Copyright 2019, The Authors, published by AIP Publishing. Image for CNT/graphene: Reproduced with permission.[89] Copyright 2017, Elsevier. Image for $CoTe_2$: Reproduced with permission.[90] Copyright 2015, Royal Society of Chemistry. Image for β-$Co(OH)_2$: Reproduced with permission.[91] Copyright 2019, Elsevier. Image for $FeCl_3$: Reproduced with permission.[92] Copyright 2018, Royal Society of Chemistry. Image for MnO_2: Reproduced with permission.[93] Copyright 2020, Royal Society of Chemistry. Image for NiO: Reproduced with permission.[94] Copyright 2014, Elsevier. Image for TiC: Reproduced with permission.[95] Copyright 2018, Royal Society of Chemistry. Image for CuS: Reproduced with permission.[96] Copyright 2021, American Chemical Society. Image for PANI: Reproduced with permission.[97] Copyright 2019, American Chemical Society. Image for PEDOT: Reproduced with permission.[98] Copyright 2021, American Chemical Society. Image for PPy: Reproduced with permission.[99] Copyright 2018, Springer Nature.

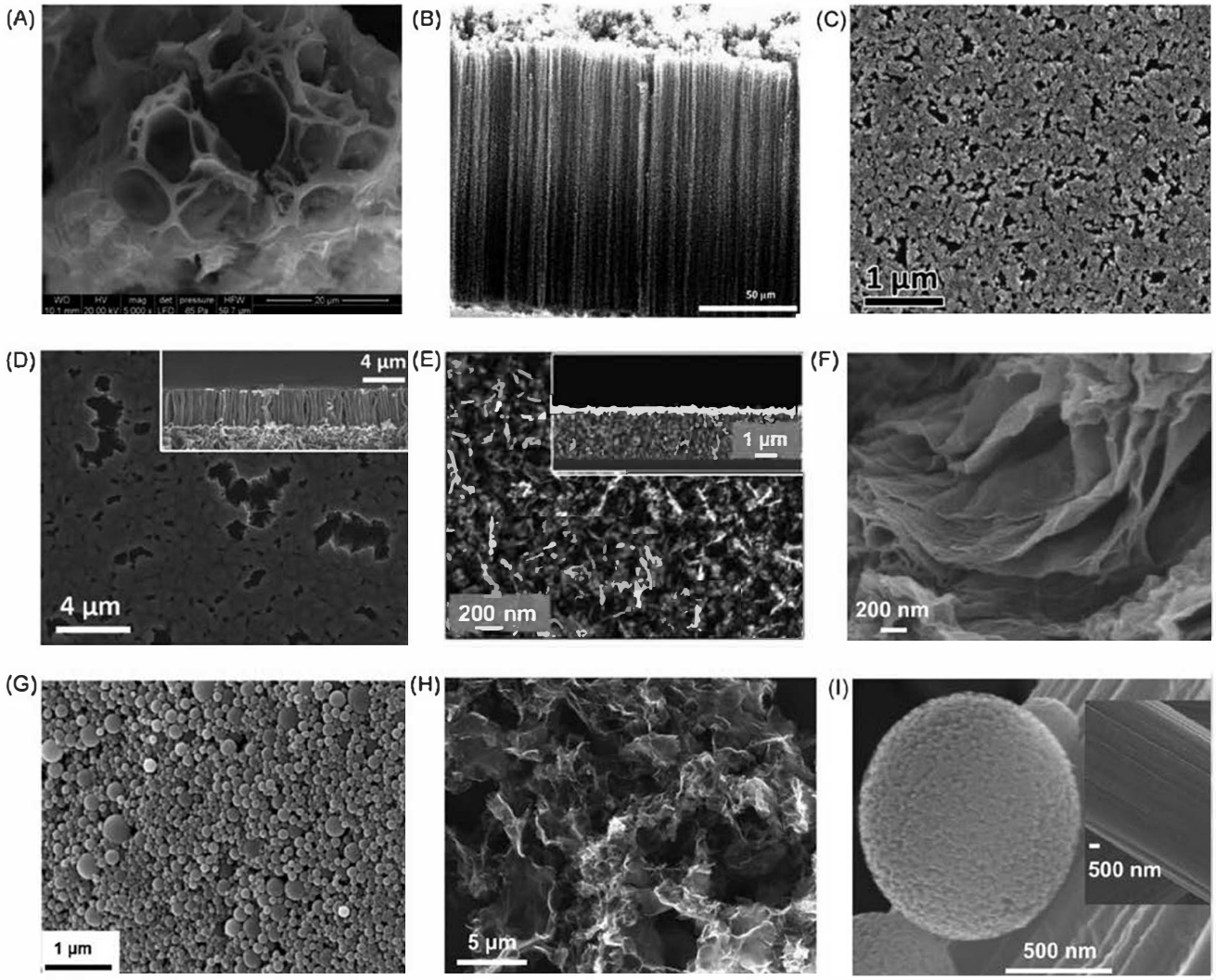

Figure 8. SEM images of different carbon materials: A) AC derived from biomass (*Eichhornia crassipes*) with a carbonization temperature of 900 °C; B) vertically aligned CNT array; C) a diamond network; D) a CNF-coated BDD film; E) graphite@diamond nanoneedles; F) rGO nanosheets; G) carbon beans; H) NC-TEG; I) PCMSs anchored on microfiber carbon paper (the inset is the SEM image of a microwire in pristine microfiber carbon paper). A) Reproduced with permission.[37b] Copyright 2013, Royal Society of Chemistry. B) Reproduced with permission.[20a] Copyright 2015, The Electrochemical Society, published by IOP Science. C) Reproduced with permission.[25d] Copyright 2017, Royal Society of Chemistry. D) Reproduced with permission.[25c] Copyright 2018, Wiley-VCH. E) Reproduced with permission.[51b] Copyright 2019, Royal Society of Chemistry. F) Reproduced with permission.[101] Copyright 2016, Elsevier. G) Reproduced with permission.[108] Copyright 2016, Elsevier. H) Reproduced with permission.[38c] Copyright 2014, Elsevier. I) Reproduced with permission.[28a] Copyright 2013, Springer Nature.

(Figure 8E),[51b] boron and nitrogen bielement incorporated diamond,[105] and pours TiC/BDD composite film.[43m] For example, an R-EC using a BDD capacitor electrode showed a C of 41.51 mF cm^{-2} in 1 0.05 M $Fe(CN)_6^{3-/4-}$ + 1 M Na_2SO_4 aqueous solution at 10 mV s^{-1}.[25d] This capacitance was several magnitudes higher than that (3.6–7 μF cm^{-2}) of a BDD-based EDLC in 1 M Na_2SO_4 aqueous solution.[106] By applying the porous and binder-free CNF/BDD as the capacitor electrode, the fabricated R-EC revealed a C of 232.01 mF cm^{-2} at 2 mA cm^{-2}.[25c] This high capacitance resulted from the unique structure of the CNF/BDD and the involvement of redox reaction of $[Fe(CN)_6]^{3-} + e^- \leftrightarrow [Fe(CN)_6]^{4-}$. When the capacitor electrodes of BDD,[25d] BDD networks,[25d] CNF/BDD,[25c] and graphite@diamond nanoneedles[51b] were applied, related R-EC devices delivered energy densities of 46.96, 56.50, 44.1, and 10.40 Wh kg^{-1}, respectively. Their power densities were 9.87, 13.7, 25.3, and 6.96 kW kg^{-1}, respectively.[25c,d,51b]

Graphene, rGO, holey graphene, and doped graphene have been utilized as the active materials to fabricate R-EC capacitor electrodes.[38c,43d,45c,77,101,107] For example, a fiber/cable type R-EC, formed using hydrothermally synthesized rGO nanosheets (Figure 8F) as the capacitor electrodes and a GPE redox electrolyte of PVA–H_3PO_4–Na_2MoO_4, exhibited a C of 18.75 mF cm^{-1} or 38.2 mF cm^{-2} and an E of 6 μWh cm^{-1} or 5.3 μWh cm^{-2}.[101]

Other carbon forms have been applied as the R-EC capacitor electrodes. They include carbon beans,[108] activated carbon fiber cloth,[109] functionalized carbons, and carbon composites. For example, the R-EC capacitor electrode of carbon beans

(Figure 8G), which were synthesized in a self-emulsifying novolac–ethanol–water system, followed by an activation process in CO_2 atmosphere, provided a cell voltage of 1.4 V, an E of 32.6 Wh kg^{-1}, and a P of 5.7 kW kg^{-1} in a KI redox electrolyte.[108]

Meanwhile, functionalized carbon materials, especially those doped with various heteroatoms (e.g., nitrogen, boron, phosphorus, and sulphur)[51a,b,104] have been utilized as the R-EC capacitor electrodes. This is because the incorporation of these heteroatoms into carbon skeletons varies the wettability, conductivity, surface area, reactivity, pore structure and distribution, and surface chemistry of related carbon materials. For example, an R-EC capacitor electrode of thermally exfoliated graphene (TEG) coated with a 6.1% nitrogen-doped carbon layer (NC-TEG) (Figure 8H) showed a C of 635 F g^{-1} at 10 mV s^{-1} in the PPD + KOH redox electrolyte.[38c] Another R-EC capacitor electrode of S-doped graphene with a 5 wt% S-content exhibited a C of 364 F g^{-1}, an E of 32 Wh kg^{-1}, and a P of 2.37 kW kg^{-1} at 3 A g^{-1} in H_2SO_4 + NH_4VO_3 redox electrolyte.[45c] Such improved R-EC performance was believed to be contributed by N-functionalities and dopants (e.g., the electron-donor features of pyridinic-N atoms). An R-EC capacitor electrode of a surface-functionalized carbon (Figure 8I), prepared by coating porous carbon microspheres (PCMSs) onto a piece of microfiber carbon paper, exhibited a C of 4 700 F g^{-1} at 5 mV s^{-1} in a redox electrolyte of $CuCl_2$ + HNO_3.[28a] The synergistic effect between carbonyl groups on the surface of PCMSs and $CuCl_2$ in the redox-active electrolyte was proposed to be responsible for this big C in that a reversible redox CuCl surface layer was formed.

3.2.2. Metal-Derived Compounds

Pseudocapacitive electrodes derived from metal oxides, conducting polymers, and redox-active compounds generally feature bigger capacitances than traditional EDLC electrodes, stemming from the involvement of their surface-controlled faradaic reactions.[110] Recently, these pseudocapacitive materials have also been employed as the R-EC capacitor electrodes, where R-capacitances stemmed from the redox species dissolved in the electrolyte and pseudocapacitances from the electrode themselves are simultaneously obtained. Using these pseudocapacitive materials, for the fabricated R-ECs then exhibit much enhanced energy densities.

Numerous pseudocapacitive metals and metal-derived compounds (e.g., metal oxide and hydroxides, metal chalcogenides, and metal carbides) have been reported as the capacitor electrodes for the R-EC construction. The examples of metal oxides are MnO_2,[40c,111] ZrO_2,[40d,112] WO_3,[40d,112] Fe_3O_4,[113] and $BiMn_2O_5$.[114] For example, in a KOH + PPD electrolyte, an R-EC capacitor electrode of a ball-milled MnO_2-electrode exhibited a C of 325.24 F g^{-1} and an E of 10.12 Wh kg^{-1}. They were six- and tenfold higher when compared with those obtained in the KOH electrolyte without the addition of PPD, respectively.[111a] The example of R-EC capacitor electrodes of metal chalcogenides is CuS.[115] An R-EC capacitor electrode of polycrystalline and porous hollow CuS nanotubes (NTs), composed of CuS nanoparticles (**Figure 9**A) provided a C of as high as 2393 F g^{-1} at 10 mV s^{-1} in a NaOH solution containing the redox powders of Na_2S and S.[115] This C was much higher than that obtained in a NaOH electrolyte without these redox powders because it was arisen from both redox reaction of CuS NTs and faradaic reaction of polysulfide.[115] Highly electroactive metal chlorides[116] and fluorides[117] have been combined with redox electrolytes to construct R-ECs. The reported metal chlorides cover $CuCl_2$, $FeCl_3$, and $NiCl_2$. On these R-EC capacitor electrodes, the R-capacitances of redox species in the electrolytes were integrated with the pseudocapacitances of these pseudocapacitive

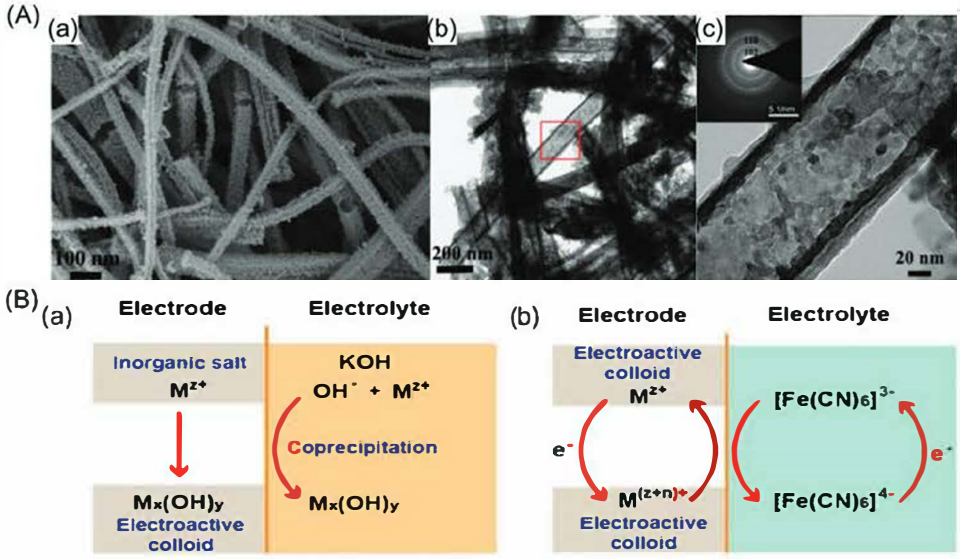

Figure 9. A) a) SEM and b) TEM images of CuS NTs with 1D structure, c) high-resolution TEM image related to the marked area in (b). The inset in (c) shows the selected-area electron diffraction (SAED) pattern of CuS. A) Reproduced with permission.[115] Copyright 2013, Royal Society of Chemistry. B) Illustration of charge storage mechanism of SC systems using electroactive inorganic salts as electrodes, and KOH in the absence (a) and presence (b) of redox-active $K_3Fe(CN)_6$ as the electrolytes. The R-EC system in (b) combines two types of ionic-state redox species in the electrode and electrolyte, respectively. B) Reproduced with permission.[116] Copyright 2014, Royal Society of Chemistry.

electrodes themselves (Figure 9B).[116] A porous titanium carbide/BDD (TiC/BDD) composite material has been used as the R-EC capacitor electrode. In an $Fe(CN)_6^{3-/4-}$ + Na_2SO_4 aqueous electrolyte, it delivered a *C* of 46.30 mF cm^{-2} at 1 mA cm^{-2}, an *E* of 47.4 Wh kg^{-1} and a *P* of 21 918 W kg^{-1}. Such performance was attributed to wide pore-size distribution of this composite material since it was beneficial not only to the transfer of charges/ions, but also the encapsulation of redox ions.[43m]

Conducting polymers are promising R-EC capacitor electrodes in that they feature high-redox active capacitances, ease of preparation, lightweight, high intrinsic flexibility, and environmental compatibility.[118] The reported R-EC capacitor electrodes from conducting polymers include polyaniline (PANI),[15.50a.54.119] polypyrrole (PPy),[119a.120] and poly(3,4-ethylenedioxythiophene) (PEDOT).[58,119a] For example, using the PANI nanospheres or nanotubes (Figure 10A) that showed a porous nature and enlarged surface areas as the capacitor electrode, the formed R-EC provided a *C* of 896 F g^{-1} at 1 A g^{-1}.[15b] An R-EC capacitor electrode of a drop-cast and porous polymer film based on doped PANI emeraldine-di-hydrogensulfate showed a *C* of 2646 F g^{-1}.[54] The synergistic effect of the redox species on the electrode and in the electrolyte was proposed to be responsible for the superior performance of this R-EC (Figure 10B). For an R-EC formed using the capacitor electrode of a CNT-PPy nanocomposite fiber and the redox electrolyte of an HQ-filled GPE (Figure 10C), HQ was generated from the reduction of BQ by accepting hydrogen ions and electrons at the positive electrode in the course of the discharging process. Meanwhile, dedropped PPy was dropped by the anions from the electrolyte and generated electrons to balance the circuit on the negative electrode. Consequently, the redox reactions HQ/BQ and PPy happened simultaneously and synergistically, leading to improved performance of the formed R-EC.[120] Conducting polymers have been further incorporated with metal oxides to construct R-ECs. This is because these composites (e.g., PANI/SnO_2,[50b,119c] PANI/MnO_2[121]) coupled the unique advantages of pseudocapacitive metal oxides with those of conducting polymers. Meanwhile, the disadvantages of conducing polymers such as their relatively poor cycling ability were overcome. The cooperation of these composites with redox electrolytes thus enabled the construction of high-performance R-ECs. For example, an R-EC capacitor electrode of a PANI/SnO_2 composite possessed a *C* of 857 F g^{-1} in the HQ + H_2SO_4 solution.[119c]

3.3. Performance of R-ECs

3.3.1. Capacitance and Capacitance Retention

The performance of some example R-ECs are summarized using the inorganic redox electrolytes (**Table 1**), organic redox electrolytes (**Table 2**), and redox-active GPEs (**Table 3**). The capacitances of reported R-ECs were obtained under different conditions (e.g., current densities, scan rates, and solutions). These capacitances are then compared at different current densities and in different redox electrolytes (**Figure 11**A). They are varied in a wide range. For example, the capacitances increase from 30 to 1600 F g^{-1} when inorganic redox electrolytes are used. When GPEs are applied, the obtained capacitances are

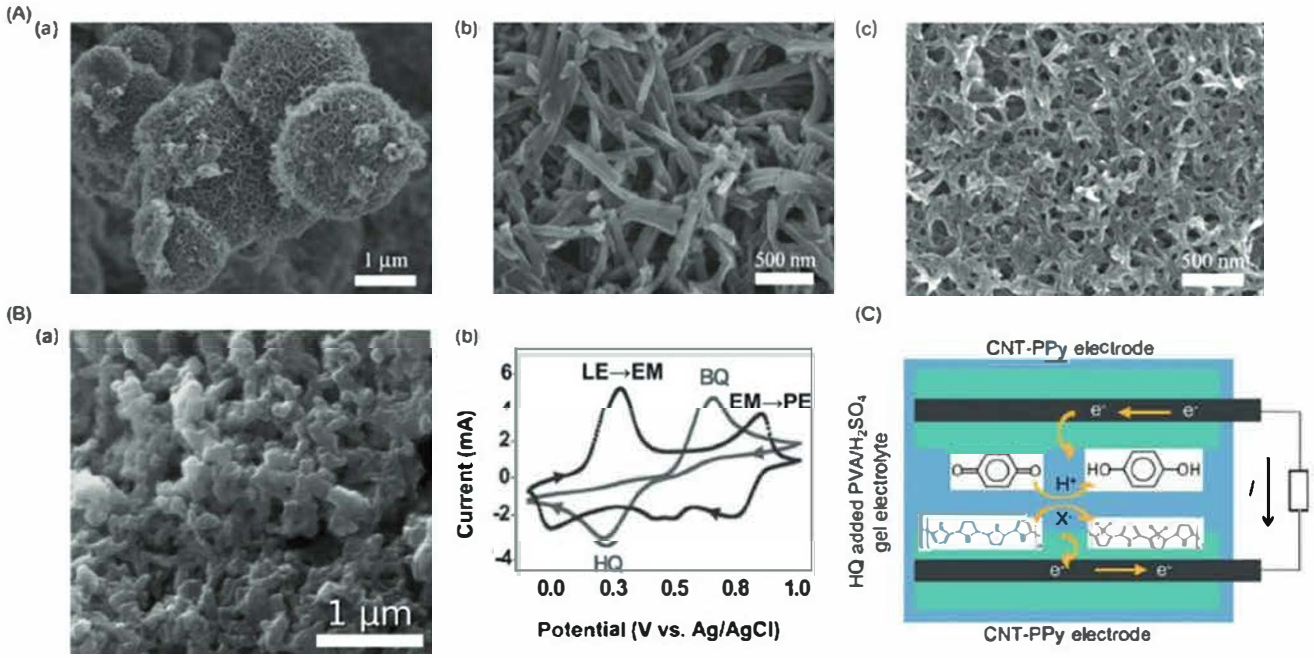

Figure 10. A) SEM images of PANI nanosphere (a), nanotubes (b), and nanofibers (c). A) Reproduced with permission.[15b] Copyright 2013, American Chemical Society. B) a) SEM images of the drop-cast film of doped PANI emeraldine-di-hydrogensulfate. b) CVs of a single polyaniline-modified electrode in H_2SO_4 + AcOH (30%) solution without (the black curve) and with (the gray curve) the incorporation of HQ-BQ. B) Reproduced with permission.[54] Copyright 2014, Wiley-VCH. C) Schematic illustration of the working mechanism at the discharging process for an R-EC based on a CNT-PPY nanocomposite fiber and an HQ contained GPE. C) Reproduced with permission.[120] Copyright 2015, Royal Society of Chemistry.

Table 1. Performance of R-ECs with inorganic redox electrolytes (III: three-electrode configuration, @: the *P*-value is related to *E*; max.: maximum).

Electrode materials	Electrolytes	C [F g^{-1} or mF cm^{-2}]	E [Wh kg^{-1}]	P [W kg^{-1}]	Cycling stability	Ref.
Porous carbon	KI	271 F g^{-1} (0.2 A g^{-1})	–	–	127.7% (10 000 cycles, 1 A g^{-1})	[46a]
Carbon beads	KI	493 F g^{-1}	32.6	@17	–	[108]
			29.5	@33		
			13.3	@5700		
			4.6	@12 300		
rGO	KOH–KI	500 F g^{-1} (0.83 A g^{-1})	11	@208	–	[77]
Activated carbon fiber	KOH–KI	–	7.1	@291	93% (14 000 cycles, 1 A g^{-1})	[40b]
			1.1	@6221		
AC	KI | KOH	56 F g^{-1} (5 mV s^{-1})	17.5	–	80% (16 000 cycles, 1 A g^{-1})	[46c]
AC	Na_2SO_4–KI	604 F g^{-1} (2 mA cm^{-2})	12.3	–	–	[37b]
α-Bi_2O_3//AC	Li_2SO_4–KI	99.5 F g^{-1} (1.5 mA cm^{-2})	35.4	@497.4	≈72% (1000 cycles, 4 mA cm^{-2})	[122]
MWCNTs/ZrO_2// MWCNTs/WO_3	Li_2SO_4–KI	198 F g^{-1} (1 A g^{-1})	133	@898	85.3% (3000 cycles, 2 A g^{-1})	[112]
			75	@10036		
Carbon nanosheets	KNO_3–KI	26 F g^{-1} (2 A g^{-1})	19.35	@1000	–	[43t]
AC	H_2SO_4–KI	912 F g^{-1} (2 mA cm^{-2})	19.04	@224.43	135.6% (4000 cycles, 5 mA cm^{-2})	[37b]
Nitrogen-doped porous carbons	H_2SO_4–KI	616 F g^{-1} (1 A g^{-1})	–	–	102% (5000 cycles, 4 A g^{-1})	[35d]
Nanoporous carbon	H_2SO_4–KI	–	8.9	@1500	78.6% (5000 cycles, 8 A g^{-1})	[48]
PANI/MnO_2	H_2SO_4–KI	1580 F g^{-1} (0.5 A g^{-1}) (III)	–	–	90% (500 cycles, 2 A g^{-1}) (III)	[121]
Nitrogen-doped AC	H_2SO_4–Na_2MoO_4	841 F g^{-1} (15 A g^{-1}) (III)	–	–	88.2% (1000 cycles, 20 A g^{-1})	[104]
Nanoporous carbon	H_2SO_4–Na_2MoO_4	–	18	@1500	67.2% (5000 cycles, 8 A g^{-1})	[48]
AC	H_2SO_4–$VOSO_4$	630.6 F g^{-1} (1 mA cm^{-2})	13.7	@325	97.57% (4000 cycle, 5 mA cm^{-2})	[45b]
AC//MWCNT	H_2SO_4–$Ce_2(SO_4)_3$	–	5.08	–	–	[44b]
AC//graphite felt	H_2SO_4–$Ce_2(SO_4)_3$	–	13.84	–	–	[44b]
AC	KBr	92 F g^{-1} (1 A g^{-1})	12	15×10^3 (max.)	111% (10 000 cycles, 1 A g^{-1})	[123]
CNT	Na_2SO_4–KBr	92.12 F g^{-1} (0.5 A g^{-1})	28.3	@372.1	86.3% (10 000 cycles, 10 A g^{-1})	[47b]
			11.7	@35.8×10^3		
AC	H_2SO_4–KBr	572 F g^{-1} (2 mA cm^{-2})	11.6	–	–	[37b]
Pretreated activated CF//non-treated activated CF	NaBr	74 F g^{-1} (0.5A g^{-1})	–	–	90.4% (100 000 cycles, 5 A g^{-1})	[109]
Pretreated activated CF//non-treated activated CF	NaI	58.2 F g^{-1} (0.5 A g^{-1})	–	–	94.9% (100 000 cycles, 5 A g^{-1})	[109]
AC	$K_4Fe(CN)_6$	272 F g^{-1} (0.25 A g^{-1})	–	–	–	[45a]
CoTe nanosheets//AC	KOH–$K_4Fe(CN)_6$	192.1 F g^{-1} (1 A g^{-1})	67.0	@793.5	80.7% (3000 cycles, 1 A g^{-1})	[124]
Co–Al layered double hydroxide	KOH–$K_4Fe(CN)_6$	317 F g^{-1} (2 A g^{-1}) (III)	–	–	95.9% (200 cycles, 2 A g^{-1}) (III)	[9]
Co–Al layered double hydroxide	KOH–$K_3Fe(CN)_6$	712 F g^{-1} (2 A g^{-1}) (III)	–	–	67% (200 cycles, 2 A g^{-1}) (III)	[9]
$Co(OH)_2$/graphene nanosheets	KOH–$K_3Fe(CN)_6$	7514.2 F g^{-1} (16 A g^{-1}) (III)	–	–	91.1% (20 00 cycles, 80 A g^{-1}) (III) 75% (20 000 cycles, 80 A g^{-1}) (III)	[35b]
$CoCl_2$	KOH–$K_3Fe(CN)_6$	12 658 mF cm^{-2} (20 mA cm^{-2}) (III)	–	–	–	[116]
$CuCl_2$	KOH–$K_3Fe(CN)_6$	25 253 mF cm^{-2} (20 mA cm^{-2}) (III)	–	–	–	[116]
$FeCl_3$	KOH–$K_3Fe(CN)_6$	12 680 mF cm^{-2} (20 mA cm^{-2}) (III)	–	–	–	[116]
$NiCl_2$	KOH–$K_3Fe(CN)_6$	12 569 mF cm^{-2} (20 mA cm^{-2}) (III)	–	–	–	[116]
MWCNTs/MnO_2//Fe_2O_3	Na_2SO_4–$K_3Fe(CN)_6$	226 F g^{-1} (5 mV s^{-1})	54.39	@667	83% (500 cycles, 200 mV s^{-1})	[111b]
AC	Na_2SO_4–$K_3Fe(CN)_6$	137 F g^{-1} (10 mA g^{-1})	28.3	–	80% (9000 cycles, 1 A g^{-1})	[19b]
			1.9	@7.14×10^3		
PANI	H_2SO_4–$K_3Fe(CN)_6$	228 F g^{-1} (1 mA cm^{-2})	20.34	@121.69	100% (100 cycles, 5 mA cm^{-2})	[119f]
			19.09	@545.59		

Table 1. Continued.

Electrode materials	Electrolytes	C [F g^{-1} or mF cm^{-2}]	E [Wh kg^{-1}]	P [W kg^{-1}]	Cycling stability	Ref.
Porous carbon microspheres coated microfiber carbon paper	HNO_3–$CuCl_2$	294 F g^{-1} (15 A g^{-1})	73	@7.5 × 10^3	99.1% (1000 cycles)	[28a]
Graphene hydrogel	H_2SO_4–$CuSO_4$	113 F g^{-1} (2.1 A g^{-1})	–	–	–	[33]
NiO	KOH–$Na_2S_2O_8$	6317.5 F g^{-1} (0.5 A g^{-1}) (III)	–	–	–	[35c]
BDD	Na_2SO_4–$Fe(CN)_6^{3-/4-}$	41.51 mF cm^{-2} (10 mV s^{-1}) (III)	46.96	9.87 × 10^3 (max.)	100% (6000 cycles, 5 mA cm^{-2}) (III)	[25d]
BDD network	Na_2SO_4–$Fe(CN)_6^{3-/4-}$	73.42 mF cm^{-2} (1 mA cm^{-2}) (III)	56.50	13.7 × 10^3 (max.)		[25d]
Carbon nanofiber/BDD	Na_2SO_4–$Fe(CN)_6^{3-/4-}$	232.01 mF cm^{-2} (2 mA cm^{-2}) (III)	44.1	25.3 × 10^3 (max.)	100% (10 000 cycles, 10 mA cm^{-2})	[25c]
Phosphorus-doped nanocrystalline diamond	Na_2SO_4–$Fe(CN)_6^{3-/4-}$	63.56 mF cm^{-2} (20 mV s^{-1}) (III)	–	–	–	[51a]
Graphite@nitrogen-doped diamond nanoneedle	Na_2SO_4–$Fe(CN)_6^{3-/4-}$	66.65 mF cm^{-2} (10 mV s^{-1}) (III)	10.40	6.96 × 10^3 (max.)	100% (10 000 cycles, 10 mA cm^{-2}) (III)	[51b]
TiC/BDD	Na_2SO_4–$Fe(CN)_6^{3-/4-}$	46.30 mF cm^{-2} (1 mA cm^{-2}) (III)	47.4	@2236	92% (10 000 cycles, 20 mA cm^{-2}) (III)	[43m]
			5.7	@21 918		
rGO	Na_2SO_4–$Fe(CN)_6^{3-/4-}$	101.25 F g^{-1} (5 A g^{-1})	56.25	35.83 × 10^3 (max.)	98% (5000 cycles, 10 A g^{-1})	[107]
Laser-scribed graphene/Fe_3O_4	Na_2SO_4–$Fe(CN)_6^{3-/4-}$	716 F g^{-1} (20mV s^{-1})	121	–	90% (5000 cycles, 12 mA m^{-2})	[113]
			93.2	@55.9 × 10^3		
CuS nanotubes	NaOH–Na_2S–S powder	2393 F g^{-1} (10 mV s^{-1}) (III)	–	–	≈ 80% (1000 cycles, 20 mV s^{-1}) (III)	[115]
PANI nanoflower	H_2SO_4–$Fe^{2+/3+}$	1062 F g^{-1} (2A g^{-1})	22.1	@774	93% (10 000 cycles, 5 A g^{-1})	[50a]
PANI/SnO_2	H_2SO_4–$Fe^{2+/3+}$	1172 F g^{-1} (1 A g^{-1})	–	–	88% (2000 cycles, 1 A g^{-1})	[50b]
Nanoporous carbon	H_2SO_4–KI–Na_2MoO_4	470 F g^{-1} (3 A g^{-1})	65.3	@1500	64.6% (5000 cycles, 8 A g^{-1})	[48]
			27.2	@7000		
AC	H_2SO_4–$VOSO_4$–$SnSO_4$	–	75	1.5 × 10^3 (max.)	85% (4500 cycles, 1 A g^{-1})	[19a]
AC	KI|$VOSO_4$	500 F g^{-1} (0.5 A g^{-1})	20	2 × 10^3 (max.)	–	[32]
AC	SnF_2|$VOSO_4$ in H_2SO_4		58.4	3.8 × 10^3 (max.)	80% (6500 cycles, 1 A g^{-1})	[23a]
Mesoporous few-layer carbon	H_2SO_4–$FeBr_3$	885 F g^{-1} (2 A g^{-1})	33.9	@430	105.2% (10 000 cycles, 10A g^{-1})	[52]
			8	@4.7 × 10^3		
Mesoporous few-layer carbon	Na_2SO_4–$FeBr_3$	519 F g^{-1} (2 A g^{-1})	40.4	@750	–	[52]
			8.24	@3.3 × 10^3		

changed from ≈40 to 1300 F g^{-1}. However, when organic redox electrolytes are applied, as-obtained capacitances are in the range of 40 to 900 F g^{-1}, generally smaller than those when inorganic and gel polymer redox electrolytes are utilized. On the other hand, these capacitances are generally higher than those obtained without the utilization of redox species, namely, those of EDLCs and PCs. Obviously, the capacitance of an R-EC is determined by the adopted electrodes, redox electrolytes, and the charging/discharging conditions. The varied ion/electron transfer ability inside the electrolytes and through the electrolyte/electrode interfaces alter the capacitances of a capacitor electrode in different redox electrolytes. Higher capacitances are thus expected to be achieved by further optimizing the art and properties of suitable redox species as well as their interactions with the selected electrode materials.

The capacitance retention of as-reported R-ECs is varied under different situations (Figure 11B), determined by the used capacitor electrodes, redox electrolytes, and cycling conditions. When the organic redox electrolytes were applied, the capacitance of these R-ECs was found to be altered from ≈30% to 120%, which was ≈60% to 110% and ≈70% to 100% in the inorganic redox electrolytes and redox active GPEs, respectively. Note here that as-constructed R-ECs exhibited different stability. This is because the stability of these R-ECs is actually determined by reversibility and stability of adopted redox electrolyte, stability of the used electrode materials, and stability of the interaction between the electrode materials and the electrolytes. It is also affected by the applied operation conditions (e.g., the current density or scan rates). On the other hand, several R-ECs showed capacitance retention of over 100% during the long-term cycling tests.[43,52,54] It mainly stems from varied properties of electrode materials and electrolytes as well as their interactions during such tests (e.g., enhanced amount or adsorption of redox electrolytes on the electrodes). Consequently, to achieve high and stable capacitances of R-ECs, selected redox electrolytes need possess the features of high ionic conductivities, wide potential windows, high solubility, high reversibility, and high stability.[21a,31] There should be no side reaction occurring

Table 2. Performance of R-ECs with organic redox electrolytes (III: three-electrode configuration, @: the *P*-value is related to *E*; max.: maximum).

Electrode materials	Electrolytes	*C* [F g^{-1} or mF cm^{-2}]	*E* [Wh kg^{-1}]	*P* [W kg^{-1}]	Cycling stability	Ref.
Nanoporous carbon	H_2SO_4–FAS	1499 F g^{-1} (10 A g^{-1})	58.70	@4.5 × 10^3	93.8% (10 000 cycles, 100 A g^{-1})	[39a]
			9.25	@60 × 10^3		
AC	H_2SO_4–HQ	901 F g^{-1} (2.65 mA cm^{-2})	31.3	–	35% (4000 cycles, 4.42 mA cm^{-2})	[5a]
PANI nanofibers	H_2SO_4–HQ	692 F g^{-1} (3 A g^{-1})	–	–	52% (10 000 cycles, 10 A g^{-1})	[119a]
PPy nanofibers	H_2SO_4–HQ	431 F g^{-1} (3 A g^{-1})	–	–	–	[119a]
PEDOT nanofibers	H_2SO_4–HQ	130 F g^{-1} (3 A g^{-1})	–	–	–	[119a]
PANI	H_2SO_4–HQ	584 F g^{-1} (0.5 A g^{-1})	–	–	67% (5000 cycles, 0.5 A g^{-1})	[119b]
Curved graphene–polyaniline	H_2SO_4–HQ	553 F g^{-1} (1 A g^{-1})	–	–	64% (50 000 cycles, 10 A g^{-1})	[15a]
PANI nanosphere	H_2SO_4–HQ	619 F g^{-1} (1 A g^{-1})	–	–	–	[15b]
PANI nanotube	H_2SO_4–HQ	896 F g^{-1} (1 A g^{-1})	–	–	61.8% (5000 cycles, 10 A g^{-1})	[15b]
PANI nanofiber	H_2SO_4–HQ	690 F g^{-1} (1 A g^{-1})	–	–	–	[15b]
1,4-Dihydroxyanthraquinone (DQ)/carbon nanosheets	H_2SO_4–HQ	138 F g^{-1} (2 A g^{-1})	21.1	@500	90.1% (5000 cycles, 4 A g^{-1})	[53]
Graphene hydrogel	H_2SO_4–HQ	100.2 F g^{-1} (1.3 A g^{-1})	–	–	–	[33]
CNT	H_2SO_4–HQ	3199 F g^{-1} (5 mV s^{-1})	–	–	70.3% (350 cycles, 5 mV s^{-1})	[43a]
Porous carbon	KOH–HQ	240 F g^{-1} (2 A g^{-1}) (III)	7.5	@0.5 × 10^3	113.5% (5000 cycles, 10 A g^{-1}) (III)	[28d]
AC	KOH–dibromodihydroxy-benzene	255 F g^{-1} (2 A g^{-1})	–	–	83% (5000 cycles, 2 A g^{-1})	[35a]
AC	KOH–dibromodihydroxy-benzene	314 F g^{-1} (5 mV s^{-1})	13	–	75–94% (5000 cycles, 2 A g^{-1})	[38a]
AC	KNO_3–AQDS	225 F g^{-1} (1 A g^{-1})	21.2	@412	–	[43e]
MWCNT	H_2SO_4–3,9-bis(dimethylamino) phenazothionium chloride–MB	23 F g^{-1} (0.88 mA cm^{-2})	–	–	88% (6000 cycles, 8.84 mA cm^{-2})	[43g]
MWCNT	H_2SO_4–indigo carmine	50 F g^{-1}	1.7	–	70% (10 000 cycles, 8.84 mA cm^{-2})	[11]
AC	KOH–MPD	78.01 F g^{-1} (0.5 A g^{-1})	9.99	5.78 × 10^3 (max.)	90.68% (10 000 cycles, 2 A g^{-1})	[39b]
AC	KOH–PPD	605. F g^{-1} (1 A g^{-1})	19.862	@16 999	94.53% (4000 cycles, 1 A g^{-1})	[38b]
Nanoporous carbon	KOH–PPD	501.4. F g^{-1} (3 A g^{-1}) (III)	–	–	85.2% (5000 cycles, 20 A g^{-1}) (III)	[43j]
NC-TEG	KOH–PPD	635.6 F g^{-1} (10 mV s^{-1}) (III)	–	–	87.4% (10 000 cycles (III)	[38c]
N-doped nanoporous carbon	KOH–PPD	587.7 F g^{-1} (5 A g^{-1}) (III)	–	–	83.7% (5000 cycles, 10A g^{-1}) (III)	[43k]
MnO_2 nanorod	KOH–PPD	156 F g^{-1} (2A g^{-1}) (III)	–	–	84% (600 cycles, 2 A g^{-1}) (III)	[40c]
MnO_2	KOH–PPD	325.24 F g^{-1} (1 A g^{-1})	10.12	@455	75% (5000 cycles, 1 A g^{-1})	[111a]
SWCNT	KOH–PPD	162.66 F g^{-1} (1 A g^{-1})	4.23	@2.79 × 10^3	96.51% (4000 cycles, 1 A g^{-1})	[100]
Graphene-hydrogel	Acetonitrile–$MeEt_3NBF_4$–PPD	516 mA h g^{-1} (1 A g^{-1})	143	@1.11 × 10^3	93.8% (5000 cycles, 2 A g^{-1})	[59b]
AC	Acetonitrile–$LiClO_4$–PPD	68.59 F g^{-1} (0.5 A g^{-1})	54.46	@13.11 × 10^3	93% (5000 cycles, 0.5 A g^{-1})	[59a]
Porous carbon	KOH–PAP	184 F g^{-1} (2 A g^{-1}) (III)	6.1	@0.5 × 10^3	111.7% (5000 cycles, 10A g^{-1}) (III)	[28d]
Porous carbon	KOH–PNP	153 F g^{-1} (3 A g^{-1}) (III)	7.3	@0.5 × 10^3	101% (5000 cycles, 10 A g^{-1}) (III)	[28d]
Dimethylglyoxime (DMG) incorporated carbon materials	KOH–p-nitroaniline	386.1 F g^{-1} (3 A g^{-1}) (III)	–	–	113% (5000 cycles, 10 A g^{-1}) (III)	[28b]
Nanoporous carbon	KOH–calcon carboxylic acid sodium salt	82 F g^{-1} (3 A g^{-1})	11.4	@1.5 × 10^3	91% (5000 cycles, 10 A g^{-1})	[28c]
AC	H_2SO_4–p-hydroxyaniline	587.1. F g^{-1} (1 A g^{-1})	34.3	–	85.3% (5000 cycles, 100 mV s^{-1})	[40a]
AC	H_2SO_4–lignosulfonates	181 F g^{-1} (1 mV s^{-1})	–	–	102.2% (5000 cycles, 1 A g^{-1})	[12]
Graphene incorporated, N-doped AC	H_2SO_4–pyrocatechol	628 F g^{-1} (0.5 A g^{-1})	–	–	113.5% (6000 cycles, 5 A g^{-1})	[43d]
TiC/BDD	acetonitrile–$TBABF_4$–Fc	22.7 mF cm^{-2} (0.8 mA cm^{-2}) (III)	–	–	16% (10 000 cycles, 20 mA cm^{-2})	[43m]

Table 2. Continued.

Electrode materials	Electrolytes	C [F g^{-1} or mF cm^{-2}]	E [Wh kg^{-1}]	P [W kg^{-1}]	Cycling stability	Ref.
SWCNT	Tetrahydrofuran–tetrabutylammonium perchlorate–DmFc	61.3 F g^{-1} (1 A g^{-1})	36.76	@1.04 × 10^3	88.4% (10 000 cycles, 5 A g^{-1})	[42a]
			27.0	@2.56 × 10^3		
Nitrogen-doped AC	H_2SO_4–alizarin red	224.0 F g^{-1} (0.5 A g^{-1})	15.2	@360	–	[55]
Nitrogen-doped AC	H_2SO_4–bromoamine acid	205.2 F g^{-1} (0.5 A g^{-1})	14.0	@360	–	[55]
Activated charcoal	H_2SO_4–$N_{2224}Br$	254.0 F g^{-1} (0.25 A g^{-1})	14.3	–	109.5% (1000 cycles, 2.5 A g^{-1})	[43v]
Carbon nanosheets	KNO_3– AQSA–Na	43 F g^{-1} (2 A g^{-1})	11.55	@1000	–	[43t]
Carbon nanosheets	KNO_3–AQSA–Na–KI	75 F g^{-1} (2 A g^{-1})	33.81	@1000	95.2% (5000 cycles, 10 A g^{-1})	[43t]
			17.33	@10 000		
AC	H_2SO_4–PDD–HQ	116.23 F g^{-1} (2 A g^{-1})	1.85	@150	78.8% (2000 cycles)	[37a]
			1.42	@920		
Polyaniline emeraldine-salt modified electrode mateirla	Acetonitrile–H_2SO_4–BQ–HQ	2646 F g^{-1} (0.5 mA cm^{-2})	–	–	133% (50 000 cycles, 12.5 mA cm^{-2})	[54]
Nitrogen-doped AC	H_2SO_4–alizarin red–bromoamine acid	260.8 F g^{-1} (0.5 A g^{-1})	17.8	@360	87% (1000 cycles, 1.0 A g^{-1})	[55]
Activated charcoal	H_2SO_4–$EVBr_2$	408.0 F g^{-1} (0.25 A g^{-1})	23	–	130% (1000 cycles, 2.5 A g^{-1})	[43v]
AC	KBr–$MVCl_2$	48.8 mA h g^{-1} (0.5 A g^{-1})	51.0	@521	–	[31]
	KBr–$HVBr_2$	44 mA h g^{-1} (0.5 A g^{-1})	39.3	@447	–	[31]
AC	NaBr–TBABr–$EVBr_2$	–	64	–	90% (5000 cycles, 2 A g^{-1})	[34]
AC	NaBr–pentyl viologen dibromide	–	48.5	@440	97% (10 000 cycles, 2.5 A g^{-1})	[43y]
			–	4.2 × 10^3 (max.)		
AC	Cu(II)-containing $EMImBF_4$	225 F g^{-1} (1 mA cm^{-2})	46.6	@52	91% (500 cycles)	[10]
			32.8	@222		
Activated carbon fiber cloth	$EMImBF_4$–EMImBr	59.0 F g^{-1} (0.1 A g^{-1})	–	–	98% (10 000 cycles, 0.5 A g^{-1})	[63]
Porous carbon	EMImTFSI–EMImBr	171.8 F g^{-1} (5 mV s^{-1})	161.2	@5267	–	[64]
Microporou s-mesoporous carbon	$EMImBF_4$–EMIml	150 F g^{-1} (10 mV s^{-1})	36.7	–	116.67% (2500 cycles, 10 mV s^{-1})	[66f]
			33.4	@≈1 000		
			1.89	@≈100 × 10^3		
			≈1	@143 × 10^3		
Porous carbon	EMImTFSI–EMIml	200.6 F g^{-1} (5 mV s^{-1})	175.6	@4994.5	95% (15 000 cycles, 1 A g^{-1})	[64]
AC	CH_3CN–EMImFcNTf	–	23.7	–	–	[16a]
Activated charcoal	TEATFSI–HQ	72 F g^{-1} (0.57 mA cm^{-2})	31.22	–	84.14% (1000 cycles, 4.25 mA cm^{-2})	[61]
Vulcan carbon	PYR14TFSI–p-BQ	70 F g^{-1} (5 mA cm^{-2})	10.3	–	50% (1000 cycles, 10 mA cm^{-2})	[65]
AC	PYR14TFSI–p-BQ	156 F g^{-1} (5 mA cm^{-2})	30	–	–	[65]
Carbon Vulcan	PYR14TFSI–p-BQ	153 F g^{-1} (5 mV s^{-1})	4	–	–	[62]

on the capacitor electrodes when they come into contact with redox electrolytes. Fast and revisable redox reactions are required at the electrode/electrolyte interface to enable fast charging and discharging processes.

3.3.2. Power Density and Energy Density

The power densities and energy densities of reported R-ECs are drawn in the form of Ragone plots (namely, *E* vs. *P*) and compared with those of EDLCs, PCs, capacitors, and batteries. In terms of gravimetric energy and power densities of ECs (Figure 11C) where the masses of active materials were adopted, R-ECs have comparable energy densities to those of batteries but deliver higher power densities (10^2 to 10^4 W kg^{-1}) than Li-ion batteries (10 to 10^2 W kg^{-1}) and Pb–acid and Ni–Cd/Ni–MHs batteries (1 to 10^2 W kg^{-1}). Compared with capacitors, the energy densities of R-ECs are ≈10 to 10^4 times higher, together with slightly lower power densities. Among different ECs (blue circle in Figure 11C), R-ECs occupy

a dominant position with respect to their high energy densities and power densities.

A more obvious prominence of R-ECs in achieving balanced high energy densities and power densities can be seen in their volumetric Ragone plots where the volumes of active materials were applied (Figure 11D). The energy densities of R-ECs are much higher than EDLCs, although they are smaller than those of some batteries. These R-ECs feature a wide range of their power densities. Some R-ECs actually even exhibit higher power densities and energy densities than high-power batteries. In conclusion, the R-ECs can have not only higher power densities than EDLCs and PCs, but also higher energy densities than batteries. Such battery-like ECs or supercapbatteries thus occupy the valuable regions with capacitor-level power densities and battery-level energy densities in the Ragone plot. They are expected to have many practical applications in different fields and for diverse devices.

3.3.3. Self-Discharge Rate

R-ECs are known have the drawbacks of relatively fast self-discharge rates, leading to a quick loss of the stored energy.[129] The main reason was suggested to be the transport of redox-active species between two electrodes or the loss of confined redox electrolytes during the charging/discharging processes.[33] To inhibit the fast self-discharge rates of R-ECs, two strategies have been proposed.[19b,33] The first one is to utilize an ion-exchange membrane to prevent the migration of redox species. The second one is to apply special redox species with solid redox products that can be fixed on the electrode surface during the charging processes. For example, two kinds of R-ECs with suppressed SDPs have been designed and assembled. One was based on an ion-exchange membrane such as a Nafion membrane and the HQ + H_2SO_4 electrolyte. In another case, one special redox electrolyte of $CuSO_4$ + H_2SO_4 with insoluble redox product was selected during the charging process where a porous cellulose acetate membrane was utilized. With the elimination of the shuttle effect of active ions between the electrodes, these two R-ECs featured longer SDPs than the R-EC using the HQ + H_2SO_4 electrolyte and a porous cellulose acetate membrane.[33]

However, the prices of these ion selective membranes are generally high. Moreover, the introduction of these membranes leads to increased internal resistance, and thus decreased power output of the device. Therefore, the artificial adsorption or deposition of charged products of redox couples on the electrode seems to be a more attractive and promising approach to suppress the SDPs of R-ECs. The entrap of an oxidized electrolyte or a reduced electrolyte in the pores of an electrode through the adsorption or a reversible liquid-to-solid phase transformation prevented the cross-diffusion of redox couples, resulting in suppressed SDPs of R-ECs.[31,34,43y,130] It was found that the employment of a porous electrode with an optimized pore volume minimized the diffusion kinetics of the redox ions, suppressed the voltage drop, and eventually slowed down the SDPs of the related R-ECs.[19b] Furthermore, when the reduced/oxidized species are in form of charged ions, they may be electrosorbed at the charged electrode, reducing their free diffusion.[16b] By varying the surface chemistry (e.g., the presence and distribution of acidic groups) of the electrode materials, their ability toward the adsorption of specialized species can be tuned. For example, when $MVBr_2$ and $HVBr_2$ were applied as redox electrolytes for the R-EC construction, the negatively charged oxidation products of Br^{3-} were physically adsorbed on carbon positive electrode, while the positively charged reduction products of MV^+ and HV^+ were adsorbed or participated on carbon negative electrode. The migration of these charged products or their contribution to the SDPs of R-ECs were prevented. A slower self-discharge rate was thus revealed, when compared to that of a cell using an inert electrolyte.[31]

The immobilization of redox products in the electrolytes can also be achieved by the addition of carbon materials in those electrolytes. Conductive CNTs have been introduced into a redox-active GPE of PVA–Li_2SO_4–BMIMBr to suppress the self-discharge rate of an R-EC through the adsorption of redox-active Br^{3-} ions on CNTs. In this case, the diffusion of generated Br^{3-} ions to the negative electrode was prevented. The open-circuit voltage of this R-EC was changed from 1.8 to 1.18 V after a self-discharge test for 5 h. It was still higher than that (0.62 V) of the R-EC using the PVA–Li_2SO_4–BMIMBr electrolyte without the addition of CNTs.[79]

3.3.4. Demonstrators

Several R-EC demonstrators have shown where the designed R-EC devices in the configurations of wire-, planar-, or 3D-shape were connected and used in an electronic circuit. To apply sufficient operating voltages, the R-ECs were often packed in series as a module rather than used directly as a single R-EC cell. These packed R-ECs were generally applied as the power suppliers to light light-emitting diodes (LEDs), drive electric motor fans or to run timers.[25c,28c,35d,39a,43m,52,58,68,69,71,77,78d,79,82–84,101–103,111b,113,114,125,127,131] For example, stand-alone demonstrators (Figure 12A) have been fabricated using the CNF/BDD[25c] and TiC/BDD[43m] based R-ECs. Here, one R-EC was assembled by attaching two electrodes tightly on the both sides of a cell, with a 50 μm thick Nafion membrane inserted in the middle. When several R-ECs were connected in series and controlled with a single board microcontroller, an LED or an LED array was illuminated for a long time. Using redox-active GPEs, solid-state flexible R-EC cells have been constructed.[58,68,79,82–84,103,127] Two cellulose papers coated with functionalized CNTs were example capacitor electrodes. Between them, two GPEs were sandwiched and separated by use of a Nafion membrane (Figure 12B). This demonstrator with two R-ECs connected in series lighted an LED.[127] In addition to these planar R-EC demonstrators, fiber-shaped R-EC demonstrators have been ensembled,[101,102,120,132] for example using two CNT/mesoporous carbon hybrid fiber electrodes and a redox-active GPE of PVA–H_2SO_4–2-mercaptopyridine (Figure 12C).[102] By connecting three R-ECs in series, the demonstrator powered nine red LEDs. It was also easily woven into a fabric. Miniaturized and portable electronic R-EC device has also been developed (Figure 12D).[113] For this device, a graphene/Fe_3O_4 composite material with a 3D interconnected porous structure was used as the electrode and the $Fe(CN)_6^{3-/4-}$ redox pairs were added into the electrolyte. An energy module

Table 3. Performance of quasi-solid-state R-ECs with redox active GPEs (@: the *P*-value is related to *E*; max.: maximum).

Electrode materials	Electrolytes	*C* [F g^{-1} or mF cm^{-2}]	*E* [Wh kg^{-1}]	*P* [W kg^{-1}]	Cycling stability	Ref.
AC	PVA–Li_2SO_4–BMIMI	384.1 F g^{-1} (0.25 A g^{-1})	29.3	–	80.9% (10 000 cycles, 1 A g^{-1})	[83]
AC	PVA–Li_2SO_4–BMIMBr–CNT	392.1 F g^{-1} (0.25 A g^{-1})	43.1	@220.9	87.9% (10 000 cycles, 1 A g^{-1})	[79]
AC	PVA–Li_2SO_4–BMIMBr	353.3 F g^{-1} (0.25 A g^{-1})	38	@232.5	68.3% (10 000 cycles, 1 A g^{-1})	[79]
PEDOT	PMMA–tetraethylammonium tetrafluoroborate ($TEABF_4$)–Fc	363 F g^{-1} (0.5 A g^{-1})	27.4	17.3 × 10^3 (max.)	75% (3000 cycles, 0.5 A g^{-1})	[58]
PEDOT	PMMA–$TEABF_4$–4-oxo TEMPO	275 F g^{-1} (0.5 A g^{-1})	20.8	14.8 × 10^3 (max.)	89% (3000 cycles, 0.5 A g^{-1})	[58]
AC	PVA–KOH–PPD	611 F g^{-1} (0.5 A g^{-1})	82.56	@35.66 × 10^3	83.63% (1000 cycles, 1 A g^{-1})	[72]
AC	PVA–H_2SO_4–indigo carmine	382 F g^{-1} (0.3 A g^{-1})	13.26	–	80.3% (3000 cycles, 1 A g^{-1})	[81]
AC	PVA–H_2SO_4–MB	214.7 F g^{-1} (0.5 A g^{-1})	7.25	@≈245	–	[74]
AC	PVA–PVP–H_2SO_4–MB	334 F g^{-1} (0.5 A g^{-1})	11.2	@246	91% (2000 cycles, 1 A g^{-1})	[78a]
			8.1	@1369		
AC	PVA–H_2SO_4–p-benzenediol	474.29 F g^{-1} (0.83 A g^{-1})	11.31	–	90.77% (3000 cycles, 0.83 A g^{-1})	[70]
AC	PVA–H_3PO_4–2-mercaptopyridine	1128 F g^{-1} (0.5 A g^{-1})	39.17	@250	80% (1000 cycles, 1 A g^{-1})	[78c]
			10.42	@1500		
CNT/mesoporous carbon hybrid fibers	PVA–H_2SO_4–2-mercaptopyridine	507.02 mF cm^{-2} (0.87 mA cm^{-2})	–	–	88% (1000 cycles)	[102]
AC	PVA–H_2SO_4–HQ	941 F g^{-1} (1 mA cm^{-2})	20	@330	83% (400 cycles, 5 mA cm^{-2})	[71]
Partially exfoliated MWCNT	PVA–H_2SO_4–HQ	179 F g^{-1} (20 mA cm^{-2})	17.6	@3.4 × 10^3	89% (2000 cycles, 20 mA cm^{-2})	[119d]
Partially exfoliated MWCNT/PANI	PVA–H_2SO_4–HQ	802.6 F g^{-1} (20 mA cm^{-2})	72.5	@4.9 × 10^3	78% (2000 cycles, 20 mA cm^{-2})	[119d]
PANI	PVA–H_2SO_4–HQ	599 F g^{-1} (20 mA cm^{-2})	60.5	@4.2 × 10^3	69.4% (2000 cycles, 20 mA cm^{-2})	[119d]
CNT- PPy	PVA–H_2SO_4–HQ	55.7 F g^{-1} (0.2 A g^{-1})	4.7	368 (max.)	103% (2000 cycles, 1 A g^{-1})	[120]
AC	PVA–H_2SO_4–HQ	491.3 F g^{-1} (0.5 A g^{-1})	16.3	@≈245	–	[74]
AC	PVA–H_2SO_4–alizarin red S	441 F g^{-1} (0.5 A g^{-1})	39.4	@400	78% (1000 cycles, 1 A g^{-1})	[82]
			20.84	@2404.6		
Polyaniline-based carbon nanosphere	PVA–H_2SO_4–AQSA-Na	430 F g^{-1} (0.8 A g^{-1})	33.4	@600	90% (1000 cycles, 1.5 A g^{-1})	[125]
			26.1	@2250		
AC	PVA–H_2SO_4–1-anthraquinone sulfonic acid sodium	448 F g^{-1} (0.5 A g^{-1})	30.5	@350	91% (1000 cycles, 1 A g^{-1})	[84]
			23.2	@2037		
AC	PVA–H_2SO_4–BAAS	390 F g^{-1} (0.8 A g^{-1})	30.5	@600	90% (1000 cycles, 0.8 A g^{-1})	[68]
AC	PVA–H_2SO_4–Na_2MoO_4	648 F g^{-1} (1.56 A g^{-1})	14.4	@625	93% (3000 cycles, 7.3 A g^{-1})	[103]
AC	PVA–H_2SO_4–Na_2MoO_4	427.4 F g^{-1} (0.5 A g^{-1})	13.9	@≈245	–	[75]
AC	Poly(2-acrylamido-2-methyl-1-propanesulfonic acid)–$(NH_4)_2MoO_4$	530 F g^{-1} (1 A g^{-1})	73	@580	92% (2500 cycles, 1 mA)	[73]
			70	@10 800		
Graphite carbon paper	PVA–H_3PO_4–phosphomolybdic acid	28.65 mF cm^{-2} (0.2 mA cm^{-2})	–	–	50% (2000 cycles, 0.5 mA cm^{-2})	[78d]
AC	PVA–KOH–$K_3[Fe(CN)_6]$	430.95 F g^{-1} (0.5 A g^{-1})	57.94	59.84 × 10^3 (max.)	89.3% (1000 cycles, 1 A g^{-1})	[78b]
AC	PVdF-HFP–BMImTFSI–NaI	334 F g^{-1} (0.84 A g^{-1})	26.1	18 × 10^3 (max.)	–	[69]
AC	PVA–KOH–KI	236.90 F g^{-1} (0.8 A g^{-1})	7.80	15.34 × 10^3 (max.)	95.76% (1000 cycles, 0.8 A g^{-1})	[13]
rGO	PVA–KOH–KI	298 F g^{-1} (0.83 A g^{-1})	–	–	–	[77]
AC	PVA–H_2SO_4–KI	404.6 F g^{-1} (0.5 A g^{-1})	7.85	@≈190	–	[49a]
$BiMn_2O_5$//AC	PVA–H_2SO_4–KI	206 F g^{-1} (1 A g^{-1})	114.4	@990	–	[114]
			85.5	@1990		
			66.6	@3030		

Table 3. Continued.

Electrode materials	Electrolytes	C [F g^{-1} or mF cm^{-2}]	E [Wh kg^{-1}]	P [W kg^{-1}]	Cycling stability	Ref.
AC	PVA–H_2SO_4–$VOSO_4$	585 F g^{-1} (1 mA cm^{-1})	12.83	–	–	[45b]
AC	PVA–H_2SO_4–$VOSO_4$	304.5 F g^{-1} (0.5 A g^{-1})	6.37	@≈190	–	[49a]
AC	PVA–H_2SO_4–$VOSO_4$	249.5 F g^{-1} (0.5 A g^{-1})	7.7	@≈245	–	[75]
AC	Poly(acrylic acid)–H_2SO_4–3-dimethyl (methacryloyloxy-ethyl)ammonium propane sulfonate–BAAS	240 F g^{-1} (0.25 A g^{-1})	8.3	1200 (max.)	89% (5000 cycles)	[126]
AC	PVA–H_2SO_4–KI–VOSO4	1232.8 F g^{-1} (0.5 A g^{-1})	25.4	@=190	93.7% (3000 cycles, 0.5 A g^{-1})	[49a]
AC	PVA–H_2SO_4–HQ | PVA–H_2SO_4–MB	563.7 F g^{-1} (0.5 A g^{-1})	18.7	@≈245	90% (3000 cycles, 0.5 A g^{-1})	[74]
AC	PVA–H_2SO_4–$VOSO_4$ | PVA–H_2SO_4–Na_2MoO_4	543.4 F g^{-1} (0.5 A g^{-1})	17.9	@≈245	80.4% (3000 cycles, 0.5 A g^{-1})	[75]
Functionalized CNT-coated cellulose paper	PVA–BMIMCl–lactic acid–LiBr | PVA–BMIMCl–sodium acetate–LiBr	47 F g^{-1} (2 A g^{-1})	16.3	@932.6	93.4% (10 000 cycles, 10 A g^{-1})	[127]
			7.6	@8342.6		
Mesoporous few-layer carbon	PVA–H_2SO_4–$FeBr_3$	–	40.2	@500	–	[52]

with several micro R-ECs connected in series or in parallel was also fabricated. One example module (that was constructed with two cells connected in series) exhibited a combined voltage of 3.6 V.

4. Perspectives of R-ECs

Up to date, the development of R-ECs using confined inorganic/organic redox electrolytes or redox-active ILs and

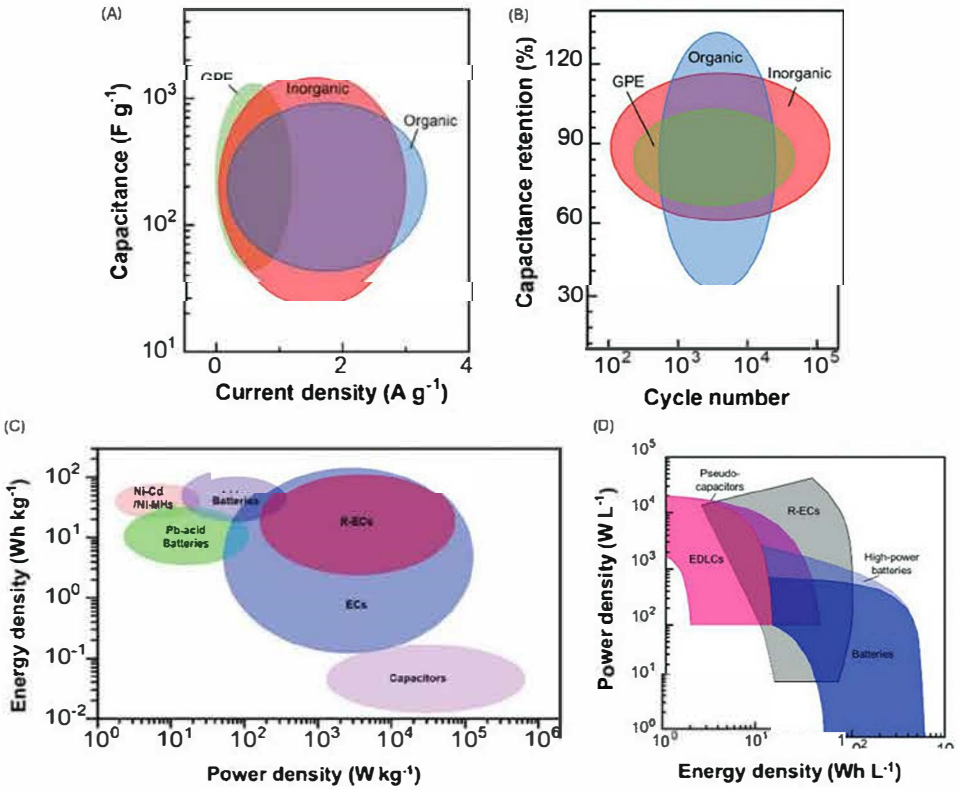

Figure 11. A) Capacitances and B) capacitance retention of different R-ECs when inorganic, organic, and gel-polymer redox electrolytes are applied. C,D) Comparison of gravimetric (C) and volumetric (D) Ragone plots of R-ECs with EDLCs, PCs, batteries, and other capacitors. C) Reproduced with permission.[128] Copyright 2014, American Chemical Society. D) Reproduced with permission.[19c] Copyright 2017, American Chemical Society.

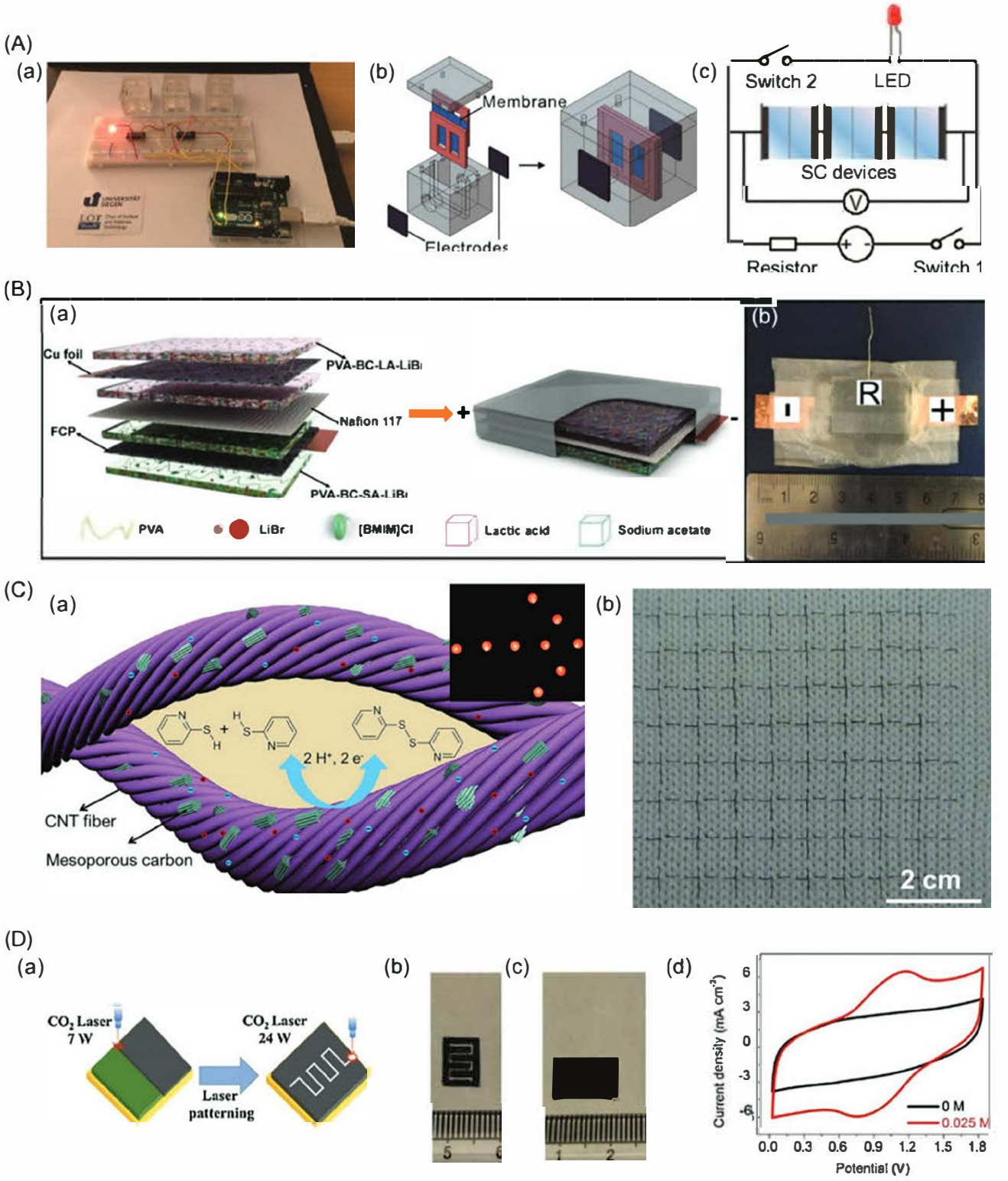

Figure 12. A) A stand-alone SC demonstrator: a) a photograph of the demonstrator consisting of R-ECs in series, a single-board microcontroller connected to the computer using a USB cable, and an LED, b) the design of an R-EC used in the demonstrator, and c) the schematic electrical circuit diagram corresponding to (a). A) Reproduced with permission.[25c] Copyright 2018, Wiley-VCH. B) a) Schematic illustration of a solid-state R-EC made of functionalized CNT-coated cellulose paper (shown as FCP) electrodes and asymmetric redox-active hydrogel polymer electrolytes of acidic PVA–BMIMCl (BC)–lactic acid (LA)–LiBr and neutral PVA–BMIMCl–sodium acetate (SA)–LiBr, separated by a Nafion membrane. b) The corresponding photograph of the R-EC. B) Reproduced with permission.[127] Copyright 2017, American Chemical Society. C) Fiber-shaped R-EC based on

porous capacitor electrodes is still at an early stage. More extensive and throughout investigation on the R-EC construction are desirable, especially with respect to the R-EC fundamentals, such as working mechanism, performance evaluation as well as practical applications of R-ECs. Moreover, the compatibility and interactions between porous electrodes (materials) and individual/multiple redox electrolytes are very crucial for the fabrication of high-performance R-ECs. The interactions of a porous electrode (material) with the designed redox electrolytes, the diffusion kinetics of redox ions in the porous electrode (material) need to be better understood. Additionally, to overcome the disadvantage of short-lived charge storage of R-ECs, the development of low-cost ion exchange membranes that can block the transfer of redox species is highly needed. The development of highly porous electrodes (materials) that can efficiently entrap redox species inside the pores is another solution. In short, a best R-EC must possess the features of a big capacitance, high energy- and power-densities, long-term stability, as well as a low self-discharge rate. To reach this goal, the synthesis of novel electrode materials, design of suitable redox electrolytes, and configuration exploration of new R-EC structures need to be conducted (Figure 13). Universal methods and processes to estimate the performance of these R-ECs need to be developed.

4.1. Materials Synthesis

4.1.1. Development of Porous Electrodes

To attain high performance of an R-EC, an optimal electrode (material) must own a high conductivity, a large surface area, a wide potential window, and good wettability in different solutions. Its nanostructures or nanoscale dimensions should be available or easy to be fabricated since they can improve electron and ion mobility, reduce diffusion lengths as well as enlarge surface areas of as-fabricated capacitor electrodes. Moreover, the surface of used electrode (material) is readily to be functionalized by means of doping with heteroatoms and/or adding surface groups to possess enhanced electrochemical activity[35d,43d,45b] or be involved in the faradaic reactions of redox electrolytes.[28a] For example, a porous structure of an electrode (material) enables ion diffusion in multiple directions. The porous nature of an electrode (material) thus leads to the increase of the contact area between the electrode surface and the electrolyte, although pore structure, pore size, pore distribution need be optimized for the favorable accessibility of electrolyte ions.

Regarding the effect of the pore size of a porous electrode or a porous material-based electrode on the performance of an R-EC, theoretically, the maximal capacitance is possible to be achieved when the pore size matches exactly with the size of the ions in the electrolyte.[12,133] In other words, a suitable pore size inside a porous electrode is much more important than a big surface area to achieve a high capacitance of an R-EC.[134] A suggested ideal porous structure possesses hierarchical pore sizes containing micropores (<2 nm in diameter), mesopores (2–50 nm in diameter) and macropores (>50 nm in diameter). The meso- and micropores play the predominate roles in the achievement of a high E of an R-EC, while the macropores enable the fast transport of the electrolyte ions into/from the meso-/micropores.[43k,135] Numerous activities have been conducted to clarify the pore size distribution (or the SSA in some cases) of the R-EC capacitor electrodes on the R-EC performance.[136] Unfortunately, a solid conclusion about such an effect is still missing. One challenge to be overcome is that an electrode (material) with a changed pore size contribution means that it owns different pore structures, defects, and functionality. The impacts of different pores on the R-EC performance are thus difficult to be separated. Another challenge is the development of new experimental techniques for the accurate measurement of pore size distribution of a porous electrode (material). Since various approaches (e.g., template-assisted growth and selective etching with activating agents[137] are available to produce porous electrodes (materials) with abundantly different morphologies and controlled pore sizes, such an effect is expected to be revealed.

Note that surface properties of a porous electrode (material) directly determine the surface wettability and compatibility of the electrode to the electrolytes, they thus affect the performance of as-formed R-ECs. To vary the surface properties of a porous electrode (material), wet-chemical treatment, thermal treatment, electrochemical treatment, and plasma treatment of a porous electrode (material) under different gas atmosphere[51a,138] can be applied. In addition to these approaches, the doping of heteroatoms into a porous electrode (material) can also vary its surface properties.[57a,139]

To design and employ composite electrodes is another efficient way to improve the R-EC performance in that composite electrodes combine advantages of different components of the composite materials and meanwhile overcome the disadvantages of individual components.[110b,140] For instance, an electrode based on a composite of carbon materials and pseudocapacitive materials are expected to feature a higher capacitance than related carbon materials, and better cycling stability compared to corresponded pseudocapacitive materials.[15a,113] This is because pseudocapacitive electrode materials are known to possess high capacitances. Meanwhile, carbon materials can act as the host materials and buffer the volume changes during the charging/discharging processes. In addition of design and synthesis of these composite electrodes, efforts must also be given to reinforce the binding between different components

CNT/mesoporous carbon hybrid fiber electrodes and redox active gel electrolyte: a) schematic illustration regarding its working mechanism, the inset shows nine red LED lighted by three such R-ECs connected in series and b) a fabric woven from these R-ECs. C) Reproduced with permission.[102] Copyright 2015, Royal Society of Chemistry. D) a) Schematic illustration demonstrating the fabrication process for a micro R-EC consisting of the synthesis of laser-scribed graphene/Fe_3O_4 plain electrode and the formation interdigitated pattern via laser irradiation; b,c) photographs of laser-scribed graphene/Fe_3O_4 interdigitated micro R-ECs in forms of an individual cell (b) and an energy module with two cells connected in series (c); d) CVs of a single symmetric laser-scribed graphene/Fe_3O_4 micro R-EC at a scan rate 100 mV s^{-1} with and without the addition of redox species. D) Reproduced with permission.[113] Copyright 2017, Elsevier.

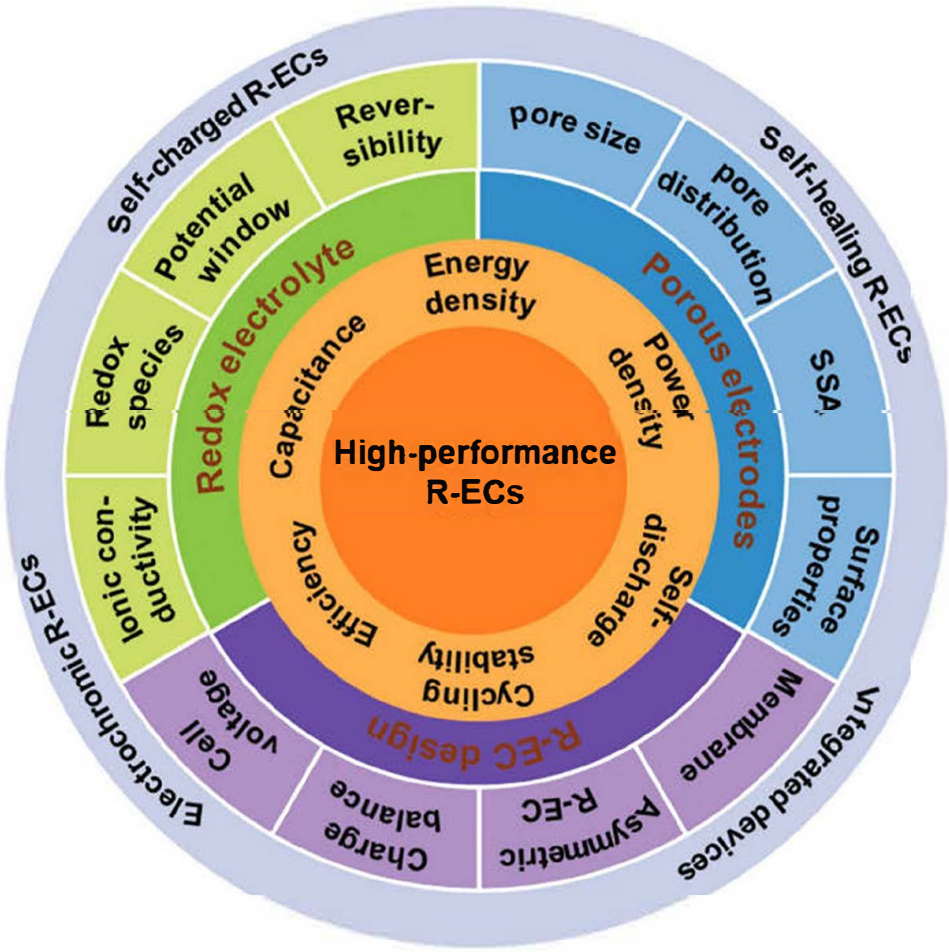

Figure 13. Future perspectives for the design and development of high-performance R-ECs.

in the composite materials, namely to improve the stability of these porous capacitor electrodes and the resultant R-ECs.

Although the reactions of redox couples in the electrolytes are known to determine the charge storage mechanisms of the R-EC capacitor electrodes,[46a,47a] there are few reports addressing the relationship between the charge storage mechanisms of R-EC systems and the polarization of the porous electrodes (materials). In this context, more fundamental studies are required to clarify the kinetics of redox electrolytes on the porous electrodes (materials), especially these porous composite electrodes when they have altered pore structures and surface functionalities as well as when they are polarized.

In short, to eventually achieve the best performance of an R-EC, a porous electrode material with an optimal structure is a must. Namely, the pore size, pore distribution, and the SSA of the used capacitor electrode material need to be optimized. In addition, the surface chemistry of the porous electrode (material) needs to be varied to feature good wettability favoring the affinity and adsorption of electrolyte ions.

4.1.2. Design and Selection of Redox Electrolytes

To construct high-performance R-ECs, suitable redox electrolytes are extremely important. The features of a suitable redox electrolyte include its high ionic conductivity, high solubility, a wide operating potential window, perfect reversibility, and long-term stability.[3b,41,141] For example, to obtain a maximal cell voltage, the potential range of used redox electrolytes is better to be as close as possible to the electrolyte-decomposition window, namely the potential ranges of selected solvent(s) and supporting electrolyte(s). The use of organic electrolytes and ionic liquids is another solution to bring in higher cell voltages, when compared to aqueous solutions. However, a lower ionic conductivity and higher viscosity of the nonaqueous electrolytes, especially ILs will result in a higher equivalent series resistance, eventually resulting in decreased R-EC performance.

Note that the intermixture of redox couples may result in worsened cycling stability and short-lived charge storage (or fast self-discharge rates) of as-formed R-ECs,[5c,19b,33] due to the migration of redox species or increased internal self-discharge rates. The design and synthesis of redox electrolytes with multiple redox centers are thus more worth to be conducted. Such redox electrolytes can react on one electrode at different potentials or possess different centers that react simultaneously on both positive and negative electrodes. The employment of multiple redox electrolytes, namely, the mixtures of different redox species is the alternative to above redox electrolytes. They then enhance total concentrations of redox species in solutions as well as balance the energy storage capacities at both positive

and negative electrodes. The design and synthesis of these redox electrolytes that are soluble in either aqueous/organic solutions or in both media thus need to be conducted.

In general, the properties of redox electrolytes (e.g., ion size, affinity, potential window) should match the properties of porous electrodes (e.g., pore size, wettability, surface chemistry) to achieve high performance R-ECs.

4.2. Assembly of R-EC Devices

The R-EC construction can be realized with the employment of different electrolytes and/or different materials as the positive and negative electrodes. The cell capacitance is determined by the smaller capacitance among two capacitor electrodes. In this regard, it is of great importance to simultaneously improve the capacitances of both electrodes. An optimal or a high performance SC cell must possess balanced charges stored between the positive electrode and the negative one. Surprisingly, the set of such balance has not been done for most of reported R-ECs.

An R-EC is better to provide a wide cell voltage, which is known to be limited by the instability of the electrolytes and electrode materials at high anodic or cathodic potentials. Strategies have been proposed to construct special electrodes and electrolyte systems, where oxygen and hydrogen evolution reactions in aqueous solutions were suppressed.[40b,46c,123,127] By using two electrode materials with different potential windows, the operating cell voltage has significantly widened and the energy densities of as-fabricated R-ECs have been significantly enhanced.[40d,44b,109,111b,112,114,122,124]

In terms of redox electrolytes, the faradaic reactions of redox electrolytes take place at a certain potential only on the positive or negative electrode, resulting in different capacitances and also varied potential distribution of both electrodes. In this case, they can be confined in the positive and negative compartments, and separated with an ion-selective membrane to achieve high cell voltage and prevent immigration of the electrolyte ions.[142] Varied performance and charge balance of the R-ECs can be obtained by tuning the concentrations of used redox electrolytes, especially those containing dual or multiple redox electro lytes.[19a,37a,49b] It is worth mentioning that most of ion-selective membranes are expensive. The cost for the manufacture of an R-EC must be then considered since the development of inexpensive or cost-effective membranes is still challenging.

Consequently, the overall R-EC performance is ultimately dependent on all components included. During the design of an R-EC, the following has to be considered: i) porous electrodes (materials) with respect to their pore sizes, pore size distribution, specific surface areas, and surface properties, ii) redox electrolytes with respect to their electrochemical potential windows and redox activities, iii) the separator with respect to ion permeable or selective ability, iv) the interaction between electrodes and electrolytes, and v) the used current collector.

4.3. Suggestions for Performance Evaluation

The R-EC performance, namely capacitance, capacitance retention, energy density and power density of an R-EC, has been evaluated under different conditions using different methods. Unfortunately, standardized or universal methods to characterize the R-EC performance are still missing. For example, the specific capacitances, energy densities and power densities of reported R-ECs were usually estimated based on the active masses of used electrodes or electrode materials, so-called as dry-masses. However, the redox electrolytes are usually accumulated inside porous electrodes during the energy storage processes. Therefore, wet-masses that include the active masses of a porous electrode (material) and redox electrolytes should be utilized.[5c,21a,143] Since redox electrolyte is an important part of the total weight of an R-EC, the calculated performance values might be different when the dry- or wet-masses are selected. In addition, gravimetric values are commonly chosen to describe the R-EC performance.[5h,21a] Compared to the total masses of packaged R-ECs, especially for carbon materials with low packing densities, the active-masses of used electrodes are extremely low. Additionally, a porous electrode (material) possesses a low amount but a large volume. However, a whole R-EC device consists of current collector(s), binder(s), active electrode(s), electrolyte(s), separator(s), and packaging(s). Consequently, the calculated gravimetric values cannot reflect the real performance of the corresponding R-EC devices in most cases.[144] Therefore, the characterization of both volumetric[19c] and gravimetric[21a] performance of an R-EC is of great importance in that they will provide more intuitive information for scale-up production of the R-EC devices.

Besides, the R-EC performance must be expressed based on the whole cell, not on a single electrode. Only in a whole cell, performance values are realistic for further practical applications and for comparison with the performance of other energy storage systems. This is because in an R-EC the capacitor electrodes generally exhibit varied potential ranges, capacitances, stored energies, and even storage mechanisms. Prior to them, it is worth to check the charging/discharging processes of each capacitor electrode in the cell to understand better electrochemical storage mechanisms of these electrodes. Moreover, capacitance is used in most papers reported in literature for the evaluation of R-ECs. In this review, it has also been used for the description and comparison of the performance of R-ECs. However, R-ECs generally exhibit GCD curves with nonlinear behavior and CVs with sharp peaks, the calculated capacitance may deviate from the actual data and is also highly dependent on the selected cell voltage window. A more proper and accurate way to evaluate R-ECs is to use capacity Q_{GCD}.

The self-discharge of an R-EC is another important aspect to indicate the efficiency of an R-EC. Since its self-discharge is mainly caused by ion migration and the leakage current, an SDP is thus commonly characterized, simply by motoring the voltage decay of the cell at open circuit as a function of time. Recently, the loss of stored energy under an open-circuit condition has also been used to describe the SDP.[31,34] Unfortunately, the study of self-discharge behavior has been ignored in many reported studies.

In conclusion, standard methods and universal rules are highly needed for the evaluation of the R-EC performance in a more accurate and right way. Such an approach can then allow the direct assessment and comparison of different R-ECs, in

turns facilitating the development and benchmarking of high-performance R-ECs.

4.4. Possible Integrated Devices Based on R-ECs

An excellent EESS is expected to feature high energy and power densities, long life-expectancy, easy implementation for different needs, low fabrication and operation cost, and lightweight. For example, hybrid/integrated devices combining an EDLC with a battery integrate the advantages of an EDLC (e.g., long lifespan, high power density, and fast charging ability) and a battery (e.g., high energy density).[145] These systems thus store a large amount of energy, but also response to instantaneous charging and discharging conditions, and expand lifespan. They are thus possible to overcome the shortcomings of the renewable energies, and to be used for the microgrid to compensate the power change, for uninterrupted power suppliers in case of power interruption, and for electric vehicles during a start-stop process to improve the regenerative braking response. However, a complicated topological structure, control methods (mainly the distribution of input and output power flow of both devices) are required to meet the properties of two storage devices and the dynamic external conditions, as well as to improve the power quality and lifespan of the system.[146] Note that some of reported R-ECs already provided higher gravimetric (Figure 11C) and volumetric (Figure 11D) energy densities and power densities as well as high stability (Figure 11D). However, further optimization of the R-EC devices or further improvement of R-EC performance is still required since R-ECs are still in their infancy. For example, the cycling stability of the R-ECs needs to be improved to be comparable with that of EDLCs (>20 000 cycles). The fast self-discharge rates of the R-ECs have to be solved. With these further improvement and optimization, these newly ensembled R-ECs are expected to feature higher energy densities and power densities than batteries, longer stability than EDLCs (>20 000 cycles) and batteries, as well as slow or comparable self-discharge rates with batteries. These high-performance R-ECs can be filled in the gap between SCs and batteries. In other words, these newly ensembled R-ECs can simultaneously meet the energy and power demands, while maintain their efficiencies and lifetime. We have to highlight here that the technique of combining batteries and EDLCs is simple and matured. As another simple but not-well established technique to ensemble high-performance energy devices, the R-ECs are also needed since they are in the right way to reach the end goal of high energy and power quality, high efficiency, fast response to instantaneous load, easy accessibility, feasibility, reduced size, and low cost. Consequently, these R-ECs have the potential to be utilized as the hybrid battery-SC storage systems as the alternative energy storage devices for different applications (e.g., for electric vehicles), of which market is continuously expanding.

Furthermore, self-charged or multifunctional R-ECs are possible to be fabricated with the integration of other devices such as solar cells, piezoelectric, and thermal heaters. For example, photoinduced (or light-driven) R-EC devices couple solar cells with R-ECs; piezoelectric-driven self-charging R-ECs integrate a piezoelectric material as the separator for the direct conversion of mechanical energy into electrochemical energy; thermal self-charging R-ECs store electric energy that is converted from low grade thermal energy; electrochromic R-ECs feature bifunctions of energy storage and electrochromic effect; self-healing R-ECs possess capability to repair mechanical failures and recover their inherent performance.[126,147] In this way, the R-ECs can expand their applications in different areas as attractive power suppliers, ranging from public transportation, industrial equipment, memory backup, and portable electronics devices. Among them, the rapid development of portable and smart R-EC devices claims higher requirements of these power sources in terms of their volume, weight, flexibility, and functions.[148] These demands prompt to develop R-ECs with flexible, stretchable, bendable, foldable, and wearable properties, with micro- or nanodimensions, as well as multifunctions.[149]

5. Summary

An R-EC replaces the inert electrolyte with redox-active electrolyte(s). The introduction of such an additional faradaic charge storage mechanism leads to a big and stable capacitance of an R-EC as well as its significantly enhanced energy density, while its intrinsic characteristics of high power density and cycling stability are maintained. This is thus an easy and facile way to construct high-performance ESSs. In the past few years considerable efforts have been made on the selection of redox electrolytes and porous electrodes or porous material-based electrodes, the performance evaluation, the study of the storage mechanisms, and practical applications of R-ECs.

There are still many challenges that need to be overcome to develop high-performance R-ECs. Several future research directions of R-ECs are thus suggested. First, the storage mechanism, the electrochemical process, and the interaction between the porous capacitor electrode(s) and redox electrolyte(s) of an R-EC need to be understood in a better and deeper way. Second, standards methods are required to evaluate the R-EC performance in a more reliable and comparable way, with respect to specific capacitance (or capacity), energy density, power density, cycling stability, self-discharge rate of an R-EC. In short, a high maximal voltage, a stable capacitance (or capacity), a high energy density, a high power density, and a low self-discharge rate are the general requirements for a high-performance R-EC. Although more activities are required, the R-EC is a new generation of ECs or EESSs and a quite promising alternative energy storage device for our future society. With the possibility to simultaneously achieve high energy densities and high power densities, as well as high stability, high-performance R-ECs are expected to occupy a dominant position among different EESSs. They are thus potential to be employed as power suppliers for various applications such as for sustainable energy storage, public transport, power suppliers of emergency systems, and flexible electronics.

Acknowledgements

N.Y. thanks the financial support from the Deutsche Forschungsgemeinschaft (DFG, German Research Foundation) under the project of 457444676. S.Y. acknowledges the financial support from National

Natural Science Foundation of China (Grant No. 21905235), Fundamental Research Funds for the Central Universities (Grant No. SWU-KT22030), and the Innovation Program for Chongqing's Overseas Returnees (Grant No. cx2019121).

Open access funding enabled and organized by Projekt DEAL.

Note: Figure 3b was revised on August 25, 2022, after initial publication online. The ranges for redox potential for ferrocene, anthraquinone-2,7-disulphonate, heptyl viologen, calcon carboxylic acid sodium, and ethyl viologen were corrected. In addition, some labels were moved to make the ranges clearer.

Conflict of Interest

The authors declare no conflict of interest.

Keywords

confined redox electrolytes, electrochemical capacitors, energy storage, performance evaluation, porous electrodes

Received: March 15, 2022
Revised: April 8, 2022
Published online: July 14, 2022

[1] a) M. A. Hannan, M. M. Hoque, A. Mohamed, A. Ayob, *Renewable Sustainable Energy Rev.* **2017**, *69*, 771; b) F. Béguin, V. Presser, A. Balducci, E. Frackowiak, *Adv. Mater.* **2014**, *26*, 2219; c) L. Yu, G. Z. Chen, *J. Power Sources* **2016**, *326*, 604; d) C. Zhan, C. Lian, Y. Zhang, M. W. Thompson, Y. Xie, J. Wu, P. R. C. Kent, P. T. Cummings, D.-E. Jiang, D. J. Wesolowski, *Adv. Sci.* **2017**, *4*, 1700059; e) J. Liu, J. Wang, C. Xu, H. Jiang, C. Li, L. Zhang, J. Lin, Z. X. Shen, *Adv. Sci.* **2018**, *5*, 1700322.

[2] a) Q. Ke, J. Wang, *J. Materiomics* **2016**, *2*, 37; b) W. K. Chee, H. N. Lim, Z. Zainal, N. M. Huang, I. Harrison, Y. Andou, *J. Phys. Chem. C* **2016**, *120*, 4153; c) R. Raccichini, A. Varzi, S. Passerini, B. Scrosati, *Nat. Mater.* **2014**, *14*, 271; d) S. Fleischmann, J. B. Mitchell, R. Wang, C. Zhan, D.-e. Jiang, V. Presser, V. Augustyn, *Chem. Rev.* **2020**, *120*, 6738.

[3] a) Y. Wang, Y. Xia, *Adv. Mater.* **2013**, *25*, 5336; b) C. Zhong, Y. Deng, W. Hu, J. Qiao, L. Zhang, J. Zhang, *Chem. Soc. Rev.* **2015**, *44*, 7484; c) W. Zuo, R. Li, C. Zhou, Y. Li, J. Xia, J. Liu, *Adv. Sci.* **2017**, *4*, 1600539; d) J. Liu, Z. Huang, T. Ma, *Small Struct.* **2020**, *1*, 2000020.

[4] a) C. Xu, B. Xu, Y. Gu, Z. Xiong, J. Sun, X. S. Zhao, *Energy Environ. Sci.* **2013**, *6*, 1388; b) F. Zhang, T. Zhang, X. Yang, L. Zhang, K. Leng, Y. Huang, Y. Chen, *Energy Environ. Sci.* **2013**, *6*, 1623; c) R. Wang, Q. Zhao, W. Zheng, Z. Ren, X. Hu, J. Li, L. Lu, N. Hu, J. Molenda, X. Liu, C. Xu, *J. Mater. Chem. A* **2019**, *7*, 19909.

[5] a) S. Roldán, C. Blanco, M. Granda, R. Menéndez, R. Santamaría, *Angew. Chem., Int. Ed.* **2011**, *50*, 1699; b) S. T. Senthilkumar, R. K. Selvan, J. S. Melo, *J. Mater. Chem. A* **2013**, *1*, 12386; c) B. Akinwolemiwa, C. Peng, G. Z. Chen, *J. Electrochem. Soc.* **2015**, *162*, A5054.

[6] a) P. V. Braun, J. Cho, J. H. Pikul, W. P. King, H. Zhang, *Curr. Opin. Solid State Mater. Sci.* **2012**, *16*, 186; b) J. Wang, S. Dong, B. Ding, Y. Wang, X. Hao, H. Dou, Y. Xia, X. Zhang, *Natl. Sci. Rev.* **2017**, *4*, 71.

[7] P. J. Hall, M. Mirzaeian, S. I. Fletcher, F. B. Sillars, A. J. R. Rennie, G. O. Shitta-Bey, G. Wilson, A. Cruden, R. Carter, *Energy Environ. Sci.* **2010**, *3*, 1238.

[8] H. I. Becker U.S. 2800616, **1957**.

[9] V. Augustyn, P. Simon, B. Dunn, *Energy Environ. Sci.* **2014**, *7*, 1597.

[10] I. Tanahashi, *Electrochem. Solid-State Lett.* **2005**, *8*, A627.

[11] L.-H. Su, X.-G. Zhang, C.-H. Mi, B. Gao, Y. Liu, *Phys. Chem. Chem. Phys.* **2009**, *11*, 2195.

[12] G. Sun, K. Li, C. Sun, *Microporous Mesoporous Mater.* **2010**, *128*, 56.

[13] S. Roldán, Z. González, C. Blanco, M. Granda, R. Menéndez, R. Santamaría, *Electrochim. Acta* **2011**, *56*, 3401.

[14] G. Lota, G. Milczarek, *Electrochem. Commun.* **2011**, *13*, 470.

[15] H. Yu, J. Wu, L. Fan, K. Xu, X. Zhong, Y. Lin, J. Lin, *Electrochim. Acta* **2011**, *56*, 6881.

[16] J. Zhou, Y. Yin, A. N. Mansour, X. Zhou, *Electrochem. Solid-State Lett.* **2011**, *14*, A25.

[17] a) W. Chen, R. B. Rakhi, H. N. Alshareef, *Nanoscale* **2013**, *5*, 4134; b) W. Chen, R. B. Rakhi, H. N. Alshareef, *J. Phys. Chem. C* **2013**, *117*, 15009.

[18] a) H. J. Xie, B. Gélinas, D. Rochefort, *Electrochem. Commun.* **2016**, *66*, 42; b) E. Mourad, L. Coustan, P. Lannelongue, D. Zigah, A. Mehdi, A. Vioux, Stefan A. Freunberger, F. Favier, O. Fontaine, *Nat. Mater.* **2017**, *16*, 446.

[19] a) J. Lee, B. Kruner, A. Tolosa, S. Sathyamoorthi, D. Kim, S. Choudhury, K.-H. Seo, V. Presser, *Energy Environ. Sci.* **2016**, *9*, 3392; b) J. Lee, S. Choudhury, D. Weingarth, D. Kim, V. Presser, *ACS Appl. Mater. Interfaces* **2016**, *8*, 23676; c) B. Evanko, S. W. Boettcher, S. J. Yoo, G. D. Stucky, *ACS Energy Lett.* **2017**, *2*, 2581.

[20] a) R. Narayanan, P. R. Bandaru, *J. Electrochem. Soc.* **2014**, *162*, A86; b) P. R. Bandaru, H. Yamada, R. Narayanan, M. Hoefer, *Mater. Sci. Eng., R* **2015**, *96*, 1.

[21] a) J. Lee, P. Srimuk, S. Fleischmann, X. Su, T. A. Hatton, V. Presser, *Prog. Mater. Sci.* **2019**, *101*, 46; b) A. J. Bard, L. R. Faulkner, *Electrochemical Methods: Fundamentals and Applications*, John Wiley & Sons, Inc, New York **2001**.

[22] J. M. Cameron, C. Holc, A. J. Kibler, C. L. Peake, D. A. Walsh, G. N. Newton, L. R. Johnson, *Chem. Soc. Rev.* **2021**, *50*, 5863.

[23] a) J. Lee, A. Tolosa, B. Krüner, N. Jäckel, S. Fleischmann, M. Zeiger, D. Kim, V. Presser, *Sustainable Energy Fuels* **2017**, *1*, 299; b) L. F. Arenas, C. Ponce de León, F. C. Walsh, *AIChE J.* **2018**, *64*, 1135.

[24] S. Gentil, D. Reynard, H. H. Girault, *Curr. Opin. Electrochem.* **2020**, *21*, 7.

[25] a) K. Chen, D. Xue, *Chem. Rec.* **2018**, *18*, 282; b) M. Kim, J. Kim, *Electrochim. Acta* **2018**, *260*, 921; c) S. Yu, N. Yang, M. Vogel, S. Mandal, O. A. Williams, S. Jiang, H. Schönherr, B. Yang, X. Jiang, *Adv. Energy Mater.* **2018**, *8*, 1702947; d) S. Yu, N. Yang, H. Zhuang, S. Mandal, O. A. Williams, B. Yang, N. Huang, X. Jiang, *J. Mater. Chem. A* **2017**, *5*, 1778.

[26] A. Laheäär, P. Przygocki, Q. Abbas, F. Béguin, *Electrochem. Commun.* **2015**, *60*, 21.

[27] Y. Shao, M. F. El-Kady, J. Sun, Y. Li, Q. Zhang, M. Zhu, H. Wang, B. Dunn, R. B. Kaner, *Chem. Rev.* **2018**, *118*, 9233.

[28] a) L.-Q. Mai, A. Minhas-Khan, X. Tian, K. M. Hercule, Y.-L. Zhao, X. Lin, X. Xu, *Nat. Commun.* **2013**, *4*, 2923; b) Y. F. Nie, Q. Wang, X. Y. Chen, Z. J. Zhang, *Phys. Chem. Chem. Phys.* **2016**, *18*, 2718; c) Q. Wang, F. N. Yong, Z. H. Xiao, X. Y. Chen, Z. J. Zhang, *J. Electroanal. Chem.* **2016**, *770*, 62; d) X. Huang, Q. Wang, X. Y. Chen, Z. J. Zhang, *Phys. Chem. Chem. Phys.* **2016**, *18*, 10438.

[29] a) G. Xiong, C. Meng, R. G. Reifenberger, P. P. Irazoqui, T. S. Fisher, *Electroanalysis* **2014**, *26*, 30; b) X.-L. Wu, A.-W. Xu, *J. Mater. Chem. A* **2014**, *2*, 4852.

[30] T. Brousse, D. Bélanger, J. W. Long, *J. Electrochem. Soc.* **2015**, *162*, A5185.

[31] S.-E. Chun, B. Evanko, X. Wang, D. Vonlanthen, X. Ji, G. D. Stucky, S. W. Boettcher, *Nat. Commun.* **2015**, *6*, 7818.

[32] E. Frackowiak, K. Fic, M. Meller, G. Lota, *ChemSusChem* **2012**, *5*, 1181.

[33] L. Chen, H. Bai, Z. Huang, L. Li, *Energy Environ. Sci.* **2014**, *7*, 1750.

[34] S. J. Yoo, B. Evanko, X. Wang, M. Romelczyk, A. Taylor, X. Ji, S. W. Boettcher, G. D. Stucky, *J. Am. Chem. Soc.* **2017**, *139*, 9985.

[35] a) E. Frackowiak, M. Meller, J. Menzel, D. Gastol, K. Fic, *Faraday Discuss.* **2014**, *172*, 179; b) C. Zhao, W. Zheng, X. Wang, H. Zhang,

X. Cui, H. Wang, *Sci. Rep.* **2013**, *3*, 2986; c) W. Han, L.-B. Kong, M.-C. Liu, D. Wang, J.-J. Li, L. Kang, *Electrochim. Acta* **2015**, *186*, 478; d) Z. Gao, L. Zhang, J. Chang, Z. Wang, D. Wu, F. Xu, Y. Guo, K. Jiang, *Chem. Eng. J.* **2018**, *335*, 590.

[36] Z. J. Zhang, S. S. Sun, *J. Electroanal. Chem.* **2016**, *778*, 80.

[37] a) Y.-C. Chen, L.-Y. Lin, *J. Colloid Interface Sci.* **2019**, *537*, 295; b) S. T. Senthilkumar, R. K. Selvan, Y. S. Lee, J. S. Melo, *J. Mater. Chem. A* **2013**, *1*, 1086.

[38] a) D. Gastol, J. Walkowiak, K. Fic, E. Frackowiak, *J. Power Sources* **2016**, *326*, 587; b) J. Wu, H. Yu, L. Fan, G. Luo, J. Lin, M. Huang, *J. Mater. Chem.* **2012**, *22*, 19025; c) Y. Yan, T. Kuila, N. H. Kim, S. H. Lee, J. H. Lee, *Carbon* **2015**, *85*, 60.

[39] a) X. N. Sun, W. Hu, D. Xu, X. Y. Chen, P. Cui, *Ind. Eng. Chem. Res.* **2017**, *56*, 2433; b) H. Yu, L. Fan, J. Wu, Y. Lin, M. Huang, J. Lin, Z. Lan, *RSC Adv.* **2012**, *2*, 6736.

[40] a) D. Jain, J. Kanungo, S. K. Tripathi, *Mater. Chem. Phys.* **2019**, *229*, 66; b) X. Wang, R. S. Chandrabose, S.-E. Chun, T. Zhang, B. Evanko, Z. Jian, S. W. Boettcher, G. D. Stucky, X. Ji, *ACS Appl. Mater. Interfaces* **2015**, *7*, 19978; c) L. Su, L. Gong, H. Lü, Q. Xü, *J. Power Sources* **2014**, *248*, 212; d) A. Singh, M. A. Akhtar, A. Chandra, *Electrochim. Acta* **2017**, *229*, 291; e) D. Jain, J. Kanungo, S. K. Tripathi, *Appl. Phys. A* **2018**, *124*, 397.

[41] B. Pal, S. Yang, S. Ramesh, V. Thangadurai, R. Jose, *Nanoscale Adv.* **2019**, *1*, 3807.

[42] a) J. Park, B. Kim, Y.-E. Yoo, H. Chung, W. Kim, *ACS Appl. Mater. Interfaces* **2014**, *6*, 19499; b) L. Hu, T. Zhai, H. Li, Y. Wang, *ChemSusChem* **2019**, *12*, 1118.

[43] a) G. Wang, R. Liang, L. Liu, B. Zhong, *Electrochim. Acta* **2014**, *115*, 183; b) I. C. Monge-Romero, M. F. Suárez-Herrera, *Synth. Met.* **2013**, *175*, 36; c) A. Dekanski, J. Stevanović, R. Stevanović, B. Nikolić, V. Jovanović, *Carbon* **2001**, *39*, 1195; d) Z. Gao, X. Liu, J. Chang, D. Wu, F. Xu, L. Zhang, W. Du, K. Jiang, *J. Power Sources* **2017**, *337*, 25; e) Y. Tian, R. Xue, X. Zhou, Z. Liu, L. Huang, *Electrochim. Acta* **2015**, *152*, 135; f) H. Ju, J. Zhou, C. Cai, H. Chen, *Electroanalysis* **1995**, *7*, 1165; g) S. Roldán, M. Granda, R. Menéndez, R. Santamaría, C. Blanco, *Electrochim. Acta* **2012**, *83*, 241; h) A. S. N. Murthy, K. S. Reddy, *J. Chem. Soc., Faraday Trans. 1* **1984**, *80*, 2745; i) A. M. Bond, F. Marken, E. Hill, R. G. Compton, H. Hügel, *J. Chem. Soc., Perkin Trans. 2* **1997**, *2*, 1735; j) Z. J. Zhang, Y. Q. Zhu, X. Y. Chen, Y. Cao, *Electrochim. Acta* **2015**, *176*, 941; k) Z. J. Zhang, X. Y. Chen, *J. Electroanal. Chem.* **2016**, *764*, 45; l) A. Mukhopadhyay, J. Hamel, R. Katahira, H. Zhu, *ACS Sustainable Chem. Eng.* **2018**, *6*, 5394; m) J. Xu, N. Yang, S. Heuser, S. Yu, A. Schulte, H. Schönherr, X. Jiang, *Adv. Energy Mater.* **2019**, *9*, 1803623; n) W. E. Geiger, *J. Chem. Educ.* **2018**, *95*, 1648; o) I. Noviandri, K. N. Brown, D. S. Fleming, P. T. Gulyas, P. A. Lay, A. F. Masters, L. Phillips, *J. Phys. Chem. B* **1999**, *103*, 6713; p) J. Yang, H. Wang, Y. Yang, J. Wu, P. Hu, L. Guo, *Nanoscale* **2017**, *9*, 9879; q) T. Wang, S. Hu, D. Wu, W. Zhao, W. Yu, M. Wang, J. Xu, J. Zhang, *J. Mater. Chem. A* **2021**, *9*, 11839; r) A. Turcanu, T. Bechtold, *Dyes Pigm.* **2011**, *91*, 324; s) Y. Liu, S. Lu, S. Chen, H. Wang, J. Zhang, Y. Xiang, *ACS Appl. Energy Mater.* **2019**, *2*, 2469; t) X. N. Sun, D. Xu, W. Hu, X. Y. Chen, *ACS Sustainable Chem. Eng.* **2017**, *5*, 5972; u) M. A. Haque, M. M. Rahman, M. A. B. H. Susan, *J. Solution Chem.* **2011**, *40*, 861; v) S. Sathyamoorthi, M. Kanagaraj, M. Kathiresan, V. Suryanarayanan, D. Velayutham, *J. Mater. Chem. A* **2016**, *4*, 4562; w) T.-W. Hui, M. D. Baker, *J. Phys. Chem. B* **2002**, *106*, 827; x) M. Heyrovský, *J. Chem. Soc., Chem. Commun.* **1987**, 1856; y) B. Evanko, S. J. Yoo, S.-E. Chun, X. Wang, X. Ji, S. W. Boettcher, G. D. Stucky, *J. Am. Chem. Soc.* **2016**, *138*, 9373.

[44] a) Q. Li, K. Li, C. Sun, Y. Li, *J. Electroanal. Chem.* **2007**, *611*, 43; b) P. Díaz, Z. González, R. Santamaría, M. Granda, R. Menéndez, C. Blanco, *Electrochim. Acta* **2015**, *168*, 277.

[45] a) Y. Tian, J. Yan, R. Xue, B. Yi, *J. Electrochem. Soc.* **2011**, *158*, A818; b) S. T. Senthilkumar, R. K. Selvan, N. Ponpandian, J. S. Melo, Y. S. Lee, *J. Mater. Chem. A* **2013**, *1*, 7913; c) M. Sandhiya, Vivekanand, S. Suresh Balaji, M. Sathish, *J. Phys. Chem. C* **2021**, *125*, 8068.

[46] a) G. Lota, E. Frackowiak, *Electrochem. Commun.* **2009**, *11*, 87; b) G. Lota, K. Fic, E. Frackowiak, *Electrochem. Commun.* **2011**, *13*, 38; c) K. Fic, M. Meller, E. Frackowiak, *J. Electrochem. Soc.* **2015**, *162*, A5140.

[47] a) S. Roldán, M. Granda, R. Menéndez, R. Santamaría, C. Blanco, *J. Phys. Chem. C* **2011**, *115*, 17606; b) X. Tang, Y. H. Lui, B. Chen, S. Hu, *J. Power Sources* **2017**, *352*, 118.

[48] D. Xu, W. Hu, X. N. Sun, P. Cui, X. Y. Chen, *J. Power Sources* **2017**, *341*, 448.

[49] a) L.-Q. Fan, J. Zhong, J.-H. Wu, J.-M. Lin, Y.-F. Huang, *J. Mater. Chem. A* **2014**, *2*, 9011; b) B. Wang, J. A. Maciá-Agulló, D. G. Prendiville, X. Zheng, D. Liu, Y. Zhang, S. W. Boettcher, X. Ji, G. D. Stucky, *J. Electrochem. Soc.* **2014**, *161*, A1090.

[50] a) L. Ren, G. Zhang, Z. Yan, L. Kang, H. Xu, F. Shi, Z. Lei, Z.-H. Liu, *Electrochim. Acta* **2017**, *231*, 705; b) T.-t. Liu, Y.-h. Zhu, E.-h. Liu, Z.-y. Luo, T.-t. Hu, Z.-p. Li, R. Ding, *Trans. Nonferrous Met. Soc. China* **2015**, *25*, 2661.

[51] a) S. Yu, J. Xu, H. Kato, N. Yang, A. Schulte, H. Schönherr, X. Jiang, *ChemElectroChem* **2019**, *6*, 1088; b) S. Yu, K. J. Sankaran, S. Korneychuk, J. Verbeeck, K. Haenen, X. Jiang, N. Yang, *Nanoscale* **2019**, *11*, 17939.

[52] Y. Wang, Z. Chang, M. Qian, Z. Zhang, J. Lin, F. Huang, *Carbon* **2019**, *143*, 300.

[53] D. Xu, X. N. Sun, W. Hu, X. Y. Chen, *J. Power Sources* **2017**, *357*, 107.

[54] D. Vonlanthen, P. Lazarev, K. A. See, F. Wudl, A. J. Heeger, *Adv. Mater.* **2014**, *26*, 5095.

[55] K. Sun, Z. Zhang, H. Peng, G. Zhao, G. Ma, Z. Lei, *Mater. Chem. Phys.* **2018**, *218*, 229.

[56] H. Luo, G. Wang, J. Lu, L. Zhuang, L. Xiao, *ACS Appl. Mater. Interfaces* **2019**, *11*, 41215.

[57] a) S.-M. Li, S.-Y. Yang, Y.-S. Wang, H.-P. Tsai, H.-W. Tien, S.-T. Hsiao, W.-H. Liao, C.-L. Chang, C.-C. M. Ma, C.-C. Hu, *J. Power Sources* **2015**, *278*, 218; b) X. Wang, Y. Li, F. Lou, M. E. Melandsø Buan, E. Sheridan, D. Chen, *RSC Adv.* **2017**, *7*, 23859.

[58] H. Zhang, J. Li, C. Gu, M. Yao, B. Yang, P. Lu, Y. Ma, *J. Power Sources* **2016**, *332*, 413.

[59] a) H. Yu, J. Wu, L. Fan, S. Hao, J. Lin, M. Huang, *J. Power Sources* **2014**, *248*, 1123; b) J. Fang, X. Zhang, X. Miao, Y. Liu, S. Chen, Y. Chen, J. Cheng, W. Wang, Y. Zhang, *Electrochim. Acta* **2018**, *273*, 495.

[60] Y. Niu, J. Niu, Y. Ma, L. Zhi, *Sci. China Mater.* **2021**, *64*, 329.

[61] S. Sathyamoorthi, V. Suryanarayanan, D. Velayutham, *J. Power Sources* **2015**, *274*, 1135.

[62] P. Navalpotro, M. Anderson, R. Marcilla, J. Palma, *Electrochim. Acta* **2018**, *263*, 110.

[63] S. Yamazaki, T. Ito, M. Yamagata, M. Ishikawa, *Electrochim. Acta* **2012**, *86*, 294.

[64] D.-J. You, Z. Yin, Y.-k. Ahn, S.-H. Lee, J. Yoo, Y. S. Kim, *RSC Adv.* **2017**, *7*, 55702.

[65] P. Navalpotro, J. Palma, M. Anderson, R. Marcilla, *J. Power Sources* **2016**, *306*, 711.

[66] a) L. Siinor, C. Siimenson, K. Lust, E. Lust, *Electrochem. Commun.* **2013**, *35*, 5; b) C. Siimenson, L. Siinor, K. Lust, E. Lust, *ECS Electrochem. Lett.* **2015**, *4*, H62; c) C. Siimenson, M. Lembinen, O. Oll, L. Läll, M. Tarkanovskaja, V. Ivaništšev, L. Siinor, T. Thomberg, K. Lust, E. Lust, *J. Electrochem. Soc.* **2016**, *163*, H723; d) L. Siinor, J. Poom, C. Siimenson, K. Lust, E. Lust, *J. Electroanal. Chem.* **2014**, *719*, 133; e) C. Siimenson, L. Siinor, K. Lust, E. Lust, *J. Electroanal. Chem.* **2014**, *730*, 59; f) T. Tooming, T. Thomberg, L. Siinor, K. Tõnurist, A. Jänes, E. Lust, *J. Electrochem. Soc.* **2014**, *161*, A222; g) E. Lust, L. Siinor, H. Kurig, T. Romann,

V. Ivaništšev, C. Siimenson, T. Thomberg, J. Kruusma, K. Lust, P. Pikma, E. Anderson, V. Grozovski, R. Palm, L. Lall, A. Ruzanov, T. Tooming, O. Oll, A. Janes, *ECS Trans.* **2016**, *75*, 161.
[67] a) X. Cheng, J. Pan, Y. Zhao, M. Liao, H. Peng, *Adv. Energy Mater.* **2018**, *8*, 1702184; b) S. Alipoori, S. Mazinani, S. H. Aboutalebi, F. Sharif, *J. Energy Storage* **2020**, *27*, 101072; c) N. A. Choudhury, S. Sampath, A. K. Shukla, *Energy Environ. Sci.* **2009**, *2*, 55; d) J. Ding, P. Chen, B. Wang, X. Chen, K. Guo, *Small Struct.* **2021**, *2*, 2100073.
[68] E. Feng, G. Ma, K. Sun, F. Ran, H. Peng, Z. Lei, *New J. Chem.* **2017**, *41*, 1986.
[69] N. Yadav, N. Yadav, M. K. Singh, S. A. Hashmi, *Energy Technol.* **2019**, *7*, 1900132.
[70] H. Yu, J. Wu, L. Fan, Y. Lin, K. Xu, Z. Tang, C. Cheng, S. Tang, J. Lin, M. Huang, Z. Lan, *J. Power Sources* **2012**, *198*, 402.
[71] S. T. Senthilkumar, R. K. Selvan, N. Ponpandian, J. S. Melo, *RSC Adv.* **2012**, *2*, 8937.
[72] G. Ma, E. Feng, K. Sun, H. Peng, J. Li, Z. Lei, *Electrochim. Acta* **2014**, *135*, 461.
[73] E. Cevik, A. Bozkurt, M. Hassan, M. A. Gondal, T. F. Qahtan, *ChemElectroChem* **2019**, *6*, 2876.
[74] J. Zhong, L.-Q. Fan, X. Wu, J.-H. Wu, G.-J. Liu, J.-M. Lin, M.-L. Huang, Y.-L. Wei, *Electrochim. Acta* **2015**, *166*, 150.
[75] L.-Q. Fan, J. Zhong, C.-Y. Zhang, J.-H. Wu, Y.-L. Wei, *Int. J. Hydrogen Energy* **2016**, *41*, 5725.
[76] S.-E. Hyeon, J. Y. Seo, J. W. Bae, W.-J. Kim, C.-H. Chung, *Electrochim. Acta* **2019**, *319*, 672.
[77] K. V. Sankar, R. K. Selvan, *Carbon* **2015**, *90*, 260.
[78] a) F. Yu, M. Huang, J. Wu, Z. Qiu, L. Fan, J. Lin, Y. Lin, *J. Appl. Polym. Sci.* **2014**, 131; b) G. Ma, J. Li, K. Sun, H. Peng, J. Mu, Z. Lei, *J. Power Sources* **2014**, *256*, 281; c) K. Sun, M. Dong, E. Feng, H. Peng, G. Ma, G. Zhao, Z. Lei, *RSC Adv.* **2015**, *5*, 22419; d) Y. Xie, J. Wang, *J. Sol-Gel Sci. Technol.* **2018**, *86*, 760.
[79] L.-Q. Fan, Q.-M. Tu, C.-L. Geng, J.-L. Huang, Y. Gu, J.-M. Lin, Y.-F. Huang, J.-H. Wu, *Electrochim. Acta* **2020**, *331*, 135425.
[80] K. S. Ngai, S. Ramesh, K. Ramesh, J. C. Juan, *Ionics* **2016**, *22*, 1259.
[81] G. Ma, M. Dong, K. Sun, E. Feng, H. Peng, Z. Lei, *J. Mater. Chem. A* **2015**, *3*, 4035.
[82] K. Sun, F. Ran, G. Zhao, Y. Zhu, Y. Zheng, M. Ma, X. Zheng, G. Ma, Z. Lei, *RSC Adv.* **2016**, *6*, 55225.
[83] Q.-M. Tu, L.-Q. Fan, F. Pan, J.-L. Huang, Y. Gu, J.-M. Lin, M.-L. Huang, Y.-F. Huang, J.-H. Wu, *Electrochim. Acta* **2018**, *268*, 562.
[84] E. Feng, G. Ma, K. Sun, Q. Yang, H. Peng, Z. Lei, *RSC Adv.* **2016**, *6*, 75896.
[85] S. F. Kiew, L. V. Kiew, H. B. Lee, T. Imae, L. Y. Chung, *J. Controlled Release* **2016**, *226*, 217.
[86] D. Deng, *Energy Sci. Eng.* **2015**, *3*, 385.
[87] D. Yadav, F. Amini, A. Ehrmann, *Eur. Polym. J.* **2020**, *138*, 109963.
[88] Q. Yuan, C.-T. Lin, K. W. A. Chee, *APL Mater.* **2019**, *7*, 030901.
[89] V. V. Mitrofanov, M. M. Slepchenkov, G. Zhang, O. E. Glukhova, *Carbon* **2017**, *115*, 803.
[90] T.-H. Lu, C.-J. Chen, M. Basu, C.-G. Ma, R.-S. Liu, *Chem. Commun.* **2015**, *51*, 17012.
[91] M. Jana, P. Sivakumar, M. Kota, M. G. Jung, H. S. Park, *J. Power Sources* **2019**, *422*, 9.
[92] C. Zhang, J. Ma, F. Han, H. Liu, F. Zhang, C. Fan, J. Liu, X. Li, *J. Mater. Chem. A* **2018**, *6*, 17982.
[93] S. Zhu, W. Huo, X. Liu, Y. Zhang, *Nanoscale Adv.* **2020**, *2*, 37.
[94] D. P. Dubal, P. Gomez-Romero, B. R. Sankapal, R. Holze, *Nano Energy* **2015**, *11*, 377.
[95] C. Xu, K. Bao, S. Ma, D. Li, D. Duan, H. Yu, X. Jin, F. Tian, B. Liu, T. Cui, *RSC Adv.* **2018**, *8*, 14479.
[96] Y. Wang, D. Chao, Z. Wang, J. Ni, L. Li, *ACS Nano* **2021**, *15*, 5420.
[97] S. Mondal, U. Rana, P. Das, S. Malik, *ACS Appl. Polym. Mater.* **2019**, *1*, 1624.
[98] A. de Izarra, C. Choi, Y. H. Jang, *J. Phys. Chem. B* **2021**, *125*, 8601.
[99] F. Wasim, N. Kosar, T. Mahmood, K. Ayub, *J. Mol. Model.* **2018**, *24*, 308.
[100] H. Yu, J. Wu, J. Lin, L. Fan, M. Huang, Y. Lin, Y. Li, F. Yu, Z. Qiu, *ChemPhysChem* **2013**, *14*, 394.
[101] G. K. Veerasubramani, K. Krishnamoorthy, P. Pazhamalai, S. J. Kim, *Carbon* **2016**, *105*, 638.
[102] S. Pan, J. Deng, G. Guan, Y. Zhang, P. Chen, J. Ren, H. Peng, *J. Mater. Chem. A* **2015**, *3*, 6286.
[103] S. T. Senthilkumar, R. K. Selvan, J. S. Melo, C. Sanjeeviraja, *ACS Appl. Mater. Interfaces* **2013**, *5*, 10541.
[104] K. Sun, E. Feng, H. Peng, G. Ma, Y. Wu, H. Wang, Z. Lei, *Electrochim. Acta* **2015**, *158*, 361.
[105] T. Guo, N. Yang, B. Yang, A. Schulte, Q. Jin, U. Koch, S. Mandal, C. Engelhard, O. A. Williams, H. Schönherr, X. Jiang, *Carbon* **2021**, *178*, 19.
[106] S. Yu, N. Yang, H. Zhuang, J. Meyer, S. Mandal, O. A. Williams, I. Lilge, H. Schönherr, X. Jiang, *J. Phys. Chem. C* **2015**, *119*, 18918.
[107] C. Guo, Y. Zhang, T. Zeng, D. Huang, Q. Wan, N. Yang, *Carbon* **2020**, *157*, 298.
[108] B. Krüner, J. Lee, N. Jäckel, A. Tolosa, V. Presser, *ACS Appl. Mater. Interfaces* **2016**, *8*, 9104.
[109] S. Yamazaki, T. Ito, Y. Murakumo, M. Naitou, T. Shimooka, M. Yamagata, M. Ishikawa, *J. Power Sources* **2016**, *326*, 580.
[110] a) Poonam, K. Sharma, A. Arora, S. K. Tripathi, *J. Energy Storage* **2019**, *21*, 801; b) J. Shi, B. Jiang, C. Li, F. Yan, D. Wang, C. Yang, J. Wan, *Mater. Chem. Phys.* **2020**, *245*, 122533; c) S. Najib, E. Erdem, *Nanoscale Adv.* **2019**, *1*, 2817; d) T. Nguyen, M. d. F. Montemor, *Adv. Sci.* **2019**, *6*, 1801797.
[111] a) H. Yu, J. Wu, L. Fan, Y. Lin, S. Chen, Y. Chen, J. Wang, M. Huang, J. Lin, Z. Lan, Y. Huang, *Sci. China Chem.* **2012**, *55*, 1319; b) N. R. Chodankar, D. P. Dubal, A. C. Lokhande, A. M. Patil, J. H. Kim, C. D. Lokhande, *Sci. Rep.* **2016**, *6*, 39205.
[112] A. Singh, A. Chandra, *Sci. Rep.* **2016**, *6*, 25793.
[113] J. Y. Hwang, M. F. El-Kady, M. Li, C.-W. Lin, M. Kowal, X. Han, R. B. Kaner, *Nano Today* **2017**, *15*, 15.
[114] J. Bhagwan, B. Ramulu, J. S. Yu, *Inorg. Chem. Front.* **2019**, *6*, 2061.
[115] L. Qian, X. Tian, L. Yang, J. Mao, H. Yuan, D. Xiao, *RSC Adv.* **2013**, *3*, 1703.
[116] K. Chen, S. Song, D. Xue, *RSC Adv.* **2014**, *4*, 23338.
[117] W. Shi, W. Yu, R. Ding, Z. Jia, Y. Li, Y. Huang, C. Tan, X. Sun, E. Liu, *J. Mater. Chem. A* **2021**, *9*, 9624.
[118] a) Y. Wang, Y. Ding, X. Guo, G. Yu, *Nano Res.* **2019**, *12*, 1978; b) I. Shown, A. Ganguly, L.-C. Chen, K.-H. Chen, *Energy Sci. Eng.* **2015**, *3*, 2; c) M. A. A. Mohd Abdah, N. H. N. Azman, S. Kulandaivalu, Y. Sulaiman, *Mater. Des.* **2020**, *186*, 108199; d) Y. Han, L. Dai, *Macromol. Chem. Phys.* **2019**, *220*, 1800355.
[119] a) W. Chen, C. Xia, R. B. Rakhi, H. N. Alshareef, *J. Power Sources* **2014**, *267*, 521; b) H. Xie, Y. Zhu, Y. Wu, Z. Wu, E. Liu, *Mater. Res. Bull.* **2014**, *50*, 303; c) Y. Zhu, E. Liu, Z. Luo, T. Hu, T. Liu, Z. Li, Q. Zhao, *Electrochim. Acta* **2014**, *118*, 106; d) D. D. Potphode, L. Sinha, P. M. Shirage, *Appl. Surf. Sci.* **2019**, *469*, 162; e) K. Pandey, P. Yadav, I. Mukhopadhyay, *Phys. Chem. Chem. Phys.* **2015**, *17*, 878; f) A. Shanmugavani, S. Kaviselvi, K. V. Sankar, R. K. Selvan, *Mater. Res. Bull.* **2015**, *62*, 161.
[120] R. Xu, F. Guo, X. Cui, L. Zhang, K. Wang, J. Wei, *J. Mater. Chem. A* **2015**, *3*, 22353.
[121] Z. Hu, L. Zu, Y. Jiang, H. Lian, Y. Liu, Z. Li, F. Chen, X. Wang, X. Cui, *Polymers* **2015**, *7*, 1939.
[122] S. T. Senthilkumar, R. K. Selvan, M. Ulaganathan, J. S. Melo, *Electrochim. Acta* **2014**, *115*, 518.
[123] Q. Li, M. Haque, V. Kuzmenko, N. Ramani, P. Lundgren, A. D. Smith, P. Enoksson, *J. Power Sources* **2017**, *348*, 219.
[124] B. Ye, C. Gong, M. Huang, Y. Tu, X. Zheng, L. Fan, J. Lin, J. Wu, *RSC Adv.* **2018**, *8*, 7997.

[125] E. Feng, H. Peng, Z. Zhang, J. Li, Z. Lei, *New J. Chem.* **2017**, *41*, 9024.
[126] E. Feng, W. Gao, J. Li, J. Wei, Q. Yang, Z. Li, X. Ma, T. Zhang, Z. Yang, *ACS Sustainable Chem. Eng.* **2020**, *8*, 3311.
[127] X. Tang, Y. H. Lui, A. R. Merhi, B. Chen, S. Ding, B. Zhang, S. Hu, *ACS Appl. Mater. Interfaces* **2017**, *9*, 44429.
[128] V. Aravindan, J. Gnanaraj, Y.-S. Lee, S. Madhavi, *Chem. Rev.* **2014**, *114*, 11619.
[129] I. S. Ike, I. Sigalas, S. Iyuke, *J. Electron. Mater.* **2018**, *47*, 470.
[130] Q. Abbas, F. Béguin, *Prog. Nat. Sci.: Mater. Int.* **2015**, *25*, 622.
[131] E. Cevik, A. Bozkurt, M. Dirican, X. Zhang, *Int. J. Hydrogen Energy* **2020**, *45*, 2186.
[132] H. Sun, X. You, J. Deng, X. Chen, Z. Yang, P. Chen, X. Fang, H. Peng, *Angew. Chem., Int. Ed.* **2014**, *53*, 6664.
[133] a) J. Huang, B. G. Sumpter, V. Meunier, *Angew. Chem., Int. Ed.* **2008**, *47*, 520; b) J. Huang, B. G. Sumpter, V. Meunier, *Chem. - Eur. J.* **2008**, *14*, 6614; c) J. Chmiola, G. Yushin, Y. Gogotsi, C. Portet, P. Simon, P. L. Taberna, *Science* **2006**, *313*, 1760.
[134] a) E. Raymundo-Piñero, K. Kierzek, J. Machnikowski, F. Béguin, *Carbon* **2006**, *44*, 2498; b) C. Largeot, C. Portet, J. Chmiola, P.-L. Taberna, Y. Gogotsi, P. Simon, *J. Am. Chem. Soc.* **2008**, *130*, 2730; c) L. Zhang, X. Yang, F. Zhang, G. Long, T. Zhang, K. Leng, Y. Zhang, Y. Huang, Y. Ma, M. Zhang, Y. Chen, *J. Am. Chem. Soc.* **2013**, *135*, 5921.
[135] Y. Zhai, Y. Dou, D. Zhao, P. F. Fulvio, R. T. Mayes, S. Dai, *Adv. Mater.* **2011**, *23*, 4828.
[136] a) I. Yang, D. Kwon, J. Yoo, M.-S. Kim, J. C. Jung, *Curr. Appl. Phys.* **2019**, *19*, 89; b) S. Kondrat, C. R. Pérez, V. Presser, Y. Gogotsi, A. A. Kornyshev, *Energy Environ. Sci.* **2012**, *5*, 6474; c) C. Zhou, T. Liu, T. Wang, S. Kumar, *Polymer* **2006**, *47*, 5831; d) C. Young, J. Lin, J. Wang, B. Ding, X. Zhang, S. M. Alshehri, T. Ahamad, R. R. Salunkhe, S. A. Hossain, J. H. Khan, Y. Ide, J. Kim, J. Henzie, K. C.-W. Wu, N. Kobayashi, Y. Yamauchi, *Chem. - Eur. J.* **2018**, *24*, 6127.
[137] a) Z. Li, L. Li, H. Zhu, H. Liao, H. Zhang, *Mater. Lett.* **2016**, *172*, 179; b) N. Talreja, S. Jung, L. T. H. Yen, T. Kim, *Chem. Eng. J.* **2020**, *379*, 122332; c) S. Yang, X. Song, P. Zhang, L. Gao, *ACS Appl. Mater. Interfaces* **2015**, *7*, 75; d) A. R. Mohamed, M. Mohammadi, G. N. Darzi, *Renewable Sustainable Energy Rev.* **2010**, *14*, 1591.
[138] L.-Z. Fan, S. Qiao, W. Song, M. Wu, X. He, X. Qu, *Electrochim. Acta* **2013**, *105*, 299.
[139] a) Y. Li, G. Wang, T. Wei, Z. Fan, P. Yan, *Nano Energy* **2016**, *19*, 165; b) Y. Deng, Y. Xie, K. Zou, X. Ji, *J. Mater. Chem. A* **2016**, *4*, 1144.
[140] a) A. Borenstein, O. Hanna, R. Attias, S. Luski, T. Brousse, D. Aurbach, *J. Mater. Chem. A* **2017**, *5*, 12653; b) X. Wang, D. Wu, X. Song, W. Du, X. Zhao, D. Zhang, *Molecules* **2019**, *24*, 2263.
[141] L. Zhang, X. Hu, Z. Wang, F. Sun, D. G. Dorrell, *Renewable Sustainable Energy Rev.* **2018**, *81*, 1868.
[142] B. Gorska, E. Frackowiak, F. Beguin, *Curr. Opin. Electrochem.* **2018**, *9*, 95.
[143] W. Qin, N. Zhou, C. Wu, M. Xie, H. Sun, Y. Guo, L. Pan, *ACS Omega* **2020**, *5*, 3801.
[144] Y. Gogotsi, P. Simon, *Science* **2011**, *334*, 917.
[145] H. Zhou, T. Bhattacharya, D. Tran, T. S. T. Siew, A. M. Khambadkone, *IEEE Trans. Power Electron.* **2011**, *26*, 923.
[146] a) B. Yang, J. Wang, X. Zhang, J. Wang, H. Shu, S. Li, T. He, C. Lan, T. Yu, *J. Power Sources* **2020**, *448*, 227444; b) L. Kouchachvili, W. Yaïci, E. Entchev, *J. Power Sources* **2018**, *374*, 237.
[147] a) J. Liang, G. Zhu, C. Wang, Y. Wang, H. Zhu, Y. Hu, H. Lv, R. Chen, L. Ma, T. Chen, Z. Jin, J. Liu, *Adv. Energy Mater.* **2017**, *7*, 1601208; b) R. Song, H. Jin, X. Li, L. Fei, Y. Zhao, H. Huang, H. Lai-Wa Chan, Y. Wang, Y. Chai, *J. Mater. Chem. A* **2015**, *3*, 14963; c) A. Kundu, T. S. Fisher, *Electrochim. Acta* **2018**, *281*, 357; d) P. Zhang, F. Zhu, F. Wang, J. Wang, R. Dong, X. Zhuang, O. G. Schmidt, X. Feng, *Adv. Mater.* **2017**, *29*, 1604491.
[148] a) R. Wang, M. Yao, Z. Niu, *InfoMat* **2020**, *2*, 113; b) D. P. Dubal, N. R. Chodankar, D.-H. Kim, P. Gomez-Romero, *Chem. Soc. Rev.* **2018**, *47*, 2065.
[149] a) J. Wang, F. Li, F. Zhu, O. G. Schmidt, *Small Methods* **2019**, *3*, 1800367; b) C. Gao, K. Chen, Y. Wang, Y. Zhao, L. Qu, *ChemSusChem* **2020**, *13*, 1255; c) X. Li, Y. Wang, Y. Zhao, J. Zhang, L. Qu, *Small Struct.* **2022**, *3*, 2100124; d) J. Ma, S. Zheng, P. Das, P. Lu, Y. Yu, Z. Wu, *Small Struct.* **2020**, *1*, 2000053.

Nianjun Yang is group leader of nanomaterials at the University of Siegen, Germany. He works on the growth and electrochemical applications of advanced carbon materials. He has published more than 170 journal papers, edited 1 book series and 4 books, contributed 9 book chapters, organized 10 European Materials Research Society symposiums and acted as the guest-editor of 10 journals. He is working as the associated editor of Materials Lab, editor board member of the journals of Scientific Reports, Diamond and Related Materials, and Materials Futures as well as the program committee member of several diamond-related international conferences.

Siyu Yu obtained her Ph.D. in engineering on June 2018 from University of Siegen (Siegen, Germany). She is now an associate professor at the Southwest University (Chongqing, China). Her current research interests are the chemical vapor deposition of advanced carbon materials, the construction of high-performance supercapacitors by use of these advanced carbon capacitor electrodes as well as the redox-active species contained electrolytes.

Wenjun Zhang is now a chair professor in the Department of Materials Science and Engineering of City University of Hong Kong, and he is also the deputy director of the Center of Super Diamond and Advanced Films (COSDAF). His research interests and areas cover thin film technology, diamond and superhard materials, surface and interface analysis, and nanomaterials and nanodevices. He has published over 380 peer reviewed journal papers and contributed 4 book chapters. He has served as guest editor of Advanced Materials, associate editor of Nano-Micro Lett. (Springer), and editorial board member of Scientific Reports.

Hui-Ming Cheng is a Professor and the Director of Advanced Carbon Research Division of Shenyang National Laboratory for Materials Science, Institute of Metal Research, the Chinese Academy of Sciences. His research activities mainly focus on the synthesis, properties, and applications of carbon, energy storage materials, and photocatalytic semiconducting materials. He published over 350 peer-reviewed papers and received several international and national awards. He is the editor-in-chief of Energy Storage Materials, editorial member for several journals, and the co-chairman of several international conferences. He has given more than 60 plenary/keynote/invited talks in international conferences and symposia.

Patrice Simon is distinguished professor at Université Toulouse III – Paul Sabatier (France) and member of the French Academy of Sciences (2019). His work focuses on the synthesis and electrochemical characterization of materials for electrochemical energy storage applications (supercapacitors, high power batteries). In particular, his interests are directed toward the mechanistic understanding of the charge storage processes at the electrode–electrolyte interface. He is co-editor in Chief of Energy Storage Materials and editorial member for several journals. He has published about 250 papers in peer-reviewed journals, delivered more than 80 plenary/keynote lectures and contributed to 9 books and book chapters.

Xin Jiang has been a professor and the chair holder of Surface and Materials Technology at University of Siegen (Siegen, Germany) since 2003. He received the award "State Specially Recruited Expert" of China in 2013. He was a Changjiang-Visiting Chair Professor at Dalian University of Science and Technology, China. His current research fields cover the growth and applications of diamond thin films, nanomaterials as well as materials characterization. He has published over 360 peer reviewed journal papers and contributed 8 books and book chapters. He has delivered numerous invited talks/lectures at international conferences.